OPTIMIZATION OF DOSE DISTRIBUTION FOR THE SYSTEM OF LINEAR ACCELERATOR BASED STEREOTACTIC RADIOSURGERY

BY

TAE-SUK SUH

A DISSERTATION PRESENTED TO THE GRADUATE SCHOOL
OF THE UNIVERSITY OF FLORIDA IN PARTIAL FULFILLMENT
OF THE REQUIREMENTS FOR THE DEGREE OF
DOCTOR OF PHILOSOPHY

UNIVERSITY OF FLORIDA

1990

UNIVERSITY OF FLORIDA LIBRARIES

ACKNOWLEDGEMENTS

I would like to express my sincere thanks to the members of my supervisory committee for their help and guidance throughout this work. I would like to give special thanks to my committee chairman, Dr. Francis Bova, for his sincere help and guidance all through this work. I would also like to thank Dr. Lawrence Fitzgerald, my committee member, for his helpful suggestions and discussions regarding my research. I would like to thank Drs. Genevieve Roessler, David Hintenlang, George Sandor, Robert Marcus and Rodney Million for their suggestions and corrections through the several meetings.

I would like to give my special thanks to Dale Moss for his excellent job in preparing and reviewing the draft of this manuscript.

Finally I would like to give thanks to my wife, Myung-hae, for her patience and encouragement during my research work.

TABLE OF CONTENTS

Page

ACKNOWLEDGEMENTS ii

ABSTRACT v

CHAPTERS

1 INTRODUCTION 1

Patient Data 5
Optimum Variables 6
3-D Dose Calculational Model 8
Optimization Criteria 9
Guidelines for Optimum Parameters 10
The Optimization with Constraints Problem 12
Optimization with Nonlinear Programming 12

2 REVIEW OF LITERATURE 15

Photon Beam Dose Model 15
    Historical Overview 15
    Contemporary Related Studies 18
Optimization in Radiation Therapy 20

3 DESCRIPTION OF STEREOTACTIC RADIOSURGERY 26

Localization 26
Dose Planning 28
Radiation Treatment 29
    Three Bearing System 31
    The Collimator System 31
    Head Support and Target Positioning System 33

4 DOSE MODEL FOR A FIXED SINGLE BEAM 34

Circular Field 34
    Dose Model 34
    Tissue-Maximum-Ratio 40
    Off-Axis-Ratio 52
    Relative Output Factor 64

Rectangular Field.... 66
    Dose Model 66
    Tissue-Maximum-Ratio 67
    Off-Axis-Ratio 68

5 THREE-DIMENSIONAL DOSE MODEL FOR MULTIPLE MOVING BEAMS.. 70

Exact Dose Model... 71
    Circular Field. 71
    Rectangular Field... 99
Fast Approximate Dose Model..... 105
    Spherical Dose Model.. 106
    Cylindrical Dose Model.. 114

6 EXPERIMENTAL OPTIMIZATION..... 151

Multiple Isocenter Approach.. 152
Field Shaping Approach. 175
    Beam's Eye View Projection 178
    Optimization Using BEV and Field Shaping.... 183

7 ANALYTICAL OPTIMIZATION... 200

Computer-Aided Design Optimization. 200
    Hooke and Jeeves Method 204
    Powell Method. 206
    Penalty Function Method. 208
    Rule-Based Search Method 210
Application and Results 214
    Case 1 214
    Case 2 223
    Case 3 240

8 CONCLUSION 261

REFERENCES 265

BIOGRAPHICAL SKETCH 273

Abstract of Dissertation Presented to the Graduate
School of the University of Florida in Partial Fulfillment
of the Requirements for the Degree of Doctor of Philosophy

OPTIMIZATION OF DOSE DISTRIBUTION FOR THE SYSTEM OF LINEAR ACCELERATOR BASED STEREOTACTIC RADIOSURGERY

by

Tae-suk Suh

August, 1990

Chairman: Frank J. Bova, Ph.D.
Major Department: Nuclear Engineering Sciences

The work suggested in this paper addresses a method for obtaining an optimal dose distribution for stereotactic radiosurgery. Since stereotactic radiosurgery utilizes multiple noncoplanar arcs and a three-dimensional dose evaluation technique, many beam parameters and complex optimization criteria are included in the dose optimization. Consequently, a lengthy computation time is required to optimize even the simplest case by a trial and error method.

The basic approach presented here is to use both an analytical and an experimental optimization to minimize the dose to critical organs while maintaining a dose shaped to the target. The experimental approach is based on shaping the target volumes using multiple isocenters from dose experience, or on field shaping using a beam's eye view technique. The analytical approach is to adapt computer-aided design optimization to find optimum parameters automatically.

Three-dimensional approximate dose models are developed to simulate the exact dose model using a spherical or cylindrical coordinate system. Optimum parameters are found much faster with the use of computer-aided design optimization techniques.

The implementation of computer-aided design algorithms with the approximate dose model and the application of the algorithms to several cases are discussed. It is shown that the approximate dose model gives dose distributions similar to those of the exact dose model, which makes the approximate dose model an attractive alternative to the exact dose model, and much more efficient in terms of computer-aided design and visual optimization.

CHAPTER 1
INTRODUCTION

Stereotactic radiosurgery is a technique for obliterating intracranial tumors which are inaccessible or unsuitable for open surgical techniques, using tightly collimated beams of ionizing radiation. The aim of stereotactic radiosurgery is to deliver, with a high degree of spatial accuracy, a large radiation dose to the target volume within the brain, while maintaining the smallest possible dose to the remainder of the brain tissue. At present, there are three types of radiation beams that can be used for radiosurgery: focused beams obtained from specially designed units incorporating several hundred cobalt sources (the Gamma Knife) (Larsson et al., 1974; Dahlin & Sarby, 1975; Leksell, 1983); heavy charged particle beams (protons, deuterons, helium ions, etc.) obtained from cyclotrons or synchrocyclotrons (Lyman & Howard, 1977; Lyman et al., 1986); and x-rays obtained from medium energy (4 to 10 MV) isocentrically mounted linear accelerators (LINAC) (Heifetz et al., 1984; Colombo et al., 1985; Hartmann et al., 1985; Houdek et al., 1985; Pike et al., 1987; Lutz et al., 1988; Friedman & Bova, 1989). LINAC-based stereotactic radiosurgery is a less expensive alternative to the two proven radiosurgical techniques. The LINAC method is based on the combination of multiple isocentric arc irradiation with small fields centered in the stereotactic target. This optimizes the dose falloff outside the target volume.

Radiosurgical treatment of the brain requires a detailed three-dimensional (3-D) treatment planning system, and intervening and surrounding tissues must be protected from unwanted irradiation while a high dose which conforms to the shape of the target is produced. The design of an optimal radiosurgery planning system which uses 3-D patient data and treatment parameters represents a significant challenge. This is in part due to the lack of 3-D information about target volumes and anatomic structures, and also by the many beam parameters involved in treatment planning.

With the availability of computed tomography (CT) and magnetic resonance (MR) imaging devices, the ability to visualize anatomic structures has been greatly enhanced. Many new tools have been developed and evaluated which permit the generation of 3-D displays of these structures, the accurate specification of beam direction and size, the display of dose distribution in three dimensions, and the evaluation of treatments for optimization. These improvements, however, have also added to the complexity of evaluating a given plan. The full 3-D extent of the tumor, the neighboring anatomy, their relationship to the planned radiation fields, and the resulting dose distribution must all be considered.

The use of graphic displays to present the information obtained from improved 3-D planning can be helpful in acquiring an overall impression of the adequacy of a particular plan. However, 3-D planning uses a large volume of patient data and many beam parameters, which may vary with the treatment. Furthermore, since 3-D calculations take a very long time, interactive modification of treatment using graphic displays may not be practical. Another alternative to complex 3-D optimized treatment is to use an analytical method of handling treatment plans quantitatively. Sufficient information on biologic dose response, tumor control probability, and normal structure complication rate is needed to quantify optimal treatments. Since no detailed information about biologic optimization is available at present, the evaluation method is based on physically optimizing dose distribution.

A possible solution for 3-D treatment plan optimization is to utilize computer-aided design optimization techniques with proper objective functions to represent the physical optimization criteria. The use of analytic formalism as an objective function for automatic optimization has been tried with little clinical success and is still being studied. This effort, however, was limited to optimizing simple linear variables such as beam weights or treatment times, and reflected only two-dimensional considerations. LINAC-based radiosurgery uses many noncoplanar arcs and a 3-D evaluation technique. Accordingly many important nonlinear beam parameters and complex 3-D calculation procedures are included in the dose optimization. Although the most difficult problem is that of specifying the optimization criteria, the full use of 3-D treatment planning for radiosurgery may not be possible without the use of both visual and computer-aided design optimization.

The aim of this work is to investigate the feasibility of planning optimal dose distributions for LINAC-based stereotactic radiosurgery. The basic approach is to use both experimental optimization with visual evaluation of dose distribution, and analytical optimization through computer-aided design optimization. The experimental approach is based on shaping the target volumes through the use of multiple isocenters or field shaping techniques. The analytical approach is to adapt computer-aided design optimization techniques with the use of a fast approximate 3-D dose algorithm to avoid dose to critical organs and find optimum arc positions automatically while maintaining a dose distribution shaped to the target.

In order to study the two approaches, we have investigated some problems associated with a comprehensive 3-D optimization.

Patient Data

The final set of patient data is represented by a series of transverse sectional contours along the patient. This set of 3-D patient data contains external contours, target cross-sections, and relevant normal tissue outlines.

One difficulty in obtaining an optimal dose distribution is due to different patient head geometries and target positions. Another problem originates from the difficulty of outlining the 3-D solid shape of the target and critical organs. It is inconvenient to find the optimum parameters for each patient condition every time. A better approach is to use a general simplified patient model which can simulate accurately the real head shape or target shape without any significant difference between the simplified model and real patient geometry.

A spherical head model with a centered target position is assumed for the experimental optimization study, since it is geometrically simple, and represents a useful result with a RANDO head model. The dose shape is not much changed except in an extreme case (near the surface) as the target position varies. Therefore, useful information such as the isodose shape, or target margin, obtained from this reference model can be used as a guideline for an individual patient model.

The next problem is to identify a 3-D target shape and the critical organs. For simplicity, the target shape and critical organs are approximated by ideal geometries (e.g. cylindrical, spherical, cone, etc.), which sufficiently cover and simulate their physical shapes. The critical organs may be represented by a few discrete points.

This approximation technique can simplify the optimization problem while saving time, and can be used to develop a reference system to prepare standard guidelines. The method yields good results which can then be tailored to the individual case.

Optimum Variables

After defining the target volume and other structures, treatment planning involves selection of beam parameters that reduce the dose to the normal tissues while providing adequate target coverage. It is possible to use all the beam parameters as the optimum variables; however, most recent optimization methods use the most sensitive beam parameters as the optimum variables to obtain favorable results economically. Many noncoplanar arcs are used for stereotactic radiosurgery. Accordingly, many beam parameters (e.g. the position of isocenter, collimator size or shape, arc spacing, and the length and weight for each arc) are included in dose optimization. The problems are how to reduce the variables systematically and choose the optimum variables for the particular situation. Tests were done to find the effects of optimum variables on spatial dose distribution with noncoplanar arcs. The following are some interesting points obtained from the tests:

(1) The shapes of high isodose surfaces were almost spherical with a single fixed isocenter, even with a change in the position of arc and weighting.

(2) The isocenter separation and collimator size with multiple isocenters or collimator shaping were sensitive variables in changing the high isodose shape.

(3) The shape of the beam profile or dose gradient was dependent on the isocenter separation and collimator size.

(4) Different arc weighting for each isocenter shifted all the isodose lines toward the more weighted isocenter.

(5) The shape of low isodose lines changed with a change in arc direction and weighting.

(6) The shape of high isodose lines did not change significantly with a change in patient contour and target position.

The tests stimulated ideas about the proper use of optimum parameters. In order to obtain the corresponding target dose, isocenter position and collimator size must be the active optimum variables. As an alternative, changing the collimator shape could be an effective parameter in obtaining the desired target dose shape. Arc variables could also be useful optimum variables to minimize dose to the surrounding normal tissues after a uniform dose to the target volume is obtained, since those variables change low isodose lines without changing high isodose lines. In Chapter 6 two different methods are discussed about selecting beam parameters for obtaining target corresponding doses using a multiple isocenter approach and a field shaping approach with projection technique.

3-D Dose Calculational Model

After selection of beam parameters, dose distributions are calculated using the exact geometry of the patient and beam configurations. The 3-D dose algorithm is required to calculate doses at any point in the patient for any specified gantry angle, turntable angle, collimator angle and collimator size. Since the dose algorithm operates on a 3-D patient representation stored as set of multiple transverse sectional contours, calculating dose in 3-D space using the exact 3-D dose model is time consuming.

The use of the exact dose model in optimization is not efficient, especially when we utilize mathematical optimization programming. A faster and more efficient dose calculation algorithm is required for the optimization to simulate the exact dose model. This finds the optimum parameters much faster when using computer-aided design optimization. In Chapter 5, a fast approximate dose model is developed for noncoplanar arcs using the exact dose model and a fitting technique.

Optimization Criteria

An essential goal of radiosurgery is to reach the optimum dose distribution within the target volume and surrounding healthy tissue. The most important subject is optimization criteria for the optimal dose distribution. Criteria for optimal external beam radiation therapy can be separated into two stages: clinical optimization and physical optimization. Optimal treatment planning at clinical stages requires a knowledge of the relative response of tumor and normal tissues to irradiation in terms of dosage and fractionation. Physical optimization consists of the development of a treatment plan which will produce a preferred dose distribution. Our concern here is physical optimization, since it is difficult to obtain necessary biologic response information on the single fraction treatments used in radiosurgery at present.

Defining optimization criteria in a mathematical form and determining the relative importance of different criteria are the most serious obstacles to performing automated optimization. Much of physical optimization is the specification of maximum and minimum dose to the target and maximum dose to normal structures at risk. Table 1-1 is a list of some of the quantitative parameters that have been used to evaluate physical dose distributions.

Guidelines for Optimum Parameters

Many variables are used in radiosurgery. It is very important to obtain an optimal dose distribution within a reasonable time. Selection of reasonable optimum variables in the first stage is critical to the success of real time optimization in both visual and computer-aided design optimization.

The pre-study for the selection of optimum variables must be analyzed to find the relationship between dose distribution and optimum variables. This information must be stored so that it can be used to determine the optimized parameters, such as isocenter separation or collimator size, to shape the dose distribution to the target. Furthermore, these guidelines are useful in determining the initial values for the computer-aided design optimization. A useful relationship between optimum isocenter separation and collimator size is used to fit an elongated target within the 80% isodose surface in Chapter 6.

Table 1-1 Quantitative Evaluation of Physical Dose Assessment

- Target volume shape
- 80 or 90% dose volume
- Degree of overlap between volumes,
  i.e., target volume vs. 90% isodose volume
- Maximum dose, minimum dose, mean dose in target
- Dose gradient
- Dose volume histogram
- Treatment volume
- Integral dose
- Therapeutic ratio,
  i.e., target volume dose over treatment volume dose

The Optimization with Constraints Problem

The main limitations in planning are tolerance doses of neighboring tissues and critical organs as well as the tolerance dose of the normal connective tissue within the tumor region. Most earlier optimization methods were based on least square fitting to minimize the variance of dose distributions within the applied target volume, subject to constraining doses at nearby critical structures.

Radiosurgeons may be more interested in minimizing dose to the critical organ with constraining points for the desired dose to the target, since it is always possible to deliver a lethal dose to the tumor, and a large amount of dose is delivered to the brain within a short time. An additional constraint is the limit on variables, which must be specified with reason after consideration of mechanical limitations or other parameters.

Optimization with Nonlinear Programming

Some optimization techniques, such as linear or quadratic programming, have been applied to deal with specific classes of optimization with constraints problems in radiation therapy. However, all of these optimization attempts have incorporated a fairly limited set of linear variables such as beam weights and dose rates because of lengthy recalculation time and the difficulty of dealing with nonlinear variables. Most of the variables used in radiosurgery are nonlinear parameters such as isocenter position, field size, and arc position, which are very important factors in modifying dose distributions to fit the target shape while avoiding dose to the critical organ. A more general category of algorithms referred to as nonlinear programming must be considered for the solution of the optimization problem in LINAC-based radiosurgery.

Since nonlinear programming shows some disadvantage in time required to find the optimum parameters, and it is sometimes difficult to find the global optimum, using too many variables is not efficient. However, nonlinear programming used with a good estimate of initial variables and a simple objective function could be a very powerful technique in the search for optimum variables. Therefore, the fast 3-D dose algorithm with a proper optimization criteria, which makes the objective function simple, is an important factor. The proper selection of optimum variables which change isodose shape are also important factors. Some cases are discussed for obtaining optimal dose distributions using nonlinear programming with constraints in chapter 7.

In the following chapter we review previous studies on dose modeling and optimization methods used in radiation therapy. In Chapter 3 the system of LINAC-based radiosurgery is briefly described. Dose modeling for single and multiple moving beams is discussed in Chapters 4 and 5. Experimental and analytical optimization techniques are discussed in Chapters 6 and 7.

CHAPTER 2
REVIEW OF LITERATURE

Photon Beam Dose Model

Historical Overview

A central element in any radiotherapy treatment planning system is an algorithm for dose calculation. Tsien (1955) is usually mentioned as the first user of computers in this field. Hand calculation, i.e., adding up isodoses graphically using measured isodose charts, had been the standard method before the possibility of utilizing computers was studied. A wide variety of computational models for the numerical evaluation of dose distributions of photon beams have been developed over the years. The approaches taken by various models can be categorized into three groups: data bases of measured values; empirical or semi-empirical formulae; and analytical method.

The method based on data bases of measured beam data is that of determining, by measurement, the relative dose in a two- or three-dimensional array of points in the field. These arrays of points and the corresponding relative dose measurements are stored and the relative dose at any arbitrary point is arrived at by interpolation. Holmes

(1970) used this method with new equipment, the Programmed Console. Bentley & Milan (1971) also measured beams for a limited number of sizes, and stored the measurements as files on magnetic tape or disc. This method has the advantage of speed and a direct relationship between measured and calculated doses. However, apart from the fact that these methods require an impressive measurement effort and mass data storage facilities, the approach is not applicable to the more complicated treatment beam arrangements.

Because of this, interest has grown in another method using empirical or semi-empirical functions. This method is based on the application of an empirical or semi-empirical function to describe the radiation field. Sterling et al. (1964) developed this type of model for depth dose and cross sections. On the basis of this model, other beam models were developed by many other groups (Kalnaes 1966; Orchard 1964; Kornelson & Young, 1975; Thomas & Haybittle, 1975) The projective beam model, which is more empirically oriented, has been studied by the Van de Geijn group (Van de Geijn, 1965, 1986; Van de Geijn et al., 1984). Another popular model, where primary and secondary radiation are calculated separately, was presented (Worthley & Cooper, 1967; Gupta & Cunningham 1966) and introduced the concept of scatter-air-ratio. The scatter air ratio concept was extended in a study by Cunningham (1972). A less empirical method of representing megavoltage beams was developed by Haywood et al.,(1979). That model paralleled the Cunningham model and took advantage of rectangular beam geometry to simplify calculations. These empirical models have been used with a correction factor to account for inhomogeneity. Before CT, the effective path length approach was widely used. The power law tissue-air-ratio method was developed by Batho (1964) and generalized by Sontag and Cunningham (1977), and Webb and Fox (1980). However,this method does not explicitly calculate the scatter component. The differential scatter-air-ratio method proposed by Cunningham (1972) does explicitly separate primary and scatter but requires more computer time. After the development of CT, pixel-based algorithms were developed by several groups. These are modified Batho power-law methods (Cassel et al., 1981, Yuen et al.,1984), the equivalent tissue-air ratio method (Sontag & Cunningham, 1978) and the delta volume method (Wong et al., 1984 and Wong & Henkelman, 1983). These methods take advantage of the three-dimensional anatomical information from CT scans and provide improvements over the earlier methods.

Analytical methods are based on physical grounds rather than empirically chosen functions. It uses a general form of the transport equation, with various techniques being employed for the solution Boyer and Mok (1984) attempted an approach to the computation of scatter dose by using

Fourier transform techniques to convolve a scatter dose distribution kernel with the primary fluence distribution. Ahnesjo (1984) also described an investigation of the possibility of using Fourier transforms with point-spread functions to calculate the dose distribution in external photon beam therapy. Mackie and Scringer (1984) developed a convolution framework for radiation therapy dose calculations. The dose model using Monte Carlo photon transport has been studied, with particular emphasis on the scatter component of such calculations by Mangios et al., (1987). Many other analytical models are being studied and developed, however analytical models are found to be less useful for treatment planning because elaborate mathematical procedures are involved. There are many papers associated with the photon beam model not mentioned here. This literature was reviewed following the stream of trends.

Contemporary Related Studies

Some experience with the treatment of brain tumors using multiple moving beams shows the necessity and efficiency of a three-dimensional radiotherapy treatment planning system. Noncoplanar beams enter the patient in an arbitrary configuration in stereotactic radiosurgery. This type of treatment technique requires a 3-D planning system. This system must employ calculational techniques for four individual model representations: patient, dose computational, treatment beam setup, and visualization. Three-dimensional planning systems and beam optimization studies are based on 3-D dose computation algorithms, which compute the 3-D dose distribution for multiple beam arrangements by adding the beams and combining the relationship between the four model representations. Several dose algorithms have been described which calculate three-dimensional dose distributions for LINAC-based radiosurgery recently (Hartmann et al., 1984, 1987; Pike et al., 1987). These 3-D algorithms are based on an isocentric model (Khan et al., 1980), which is one of the empirical dose models that describe the dose for a single field, and is used as a basis for superimposed fields. For radiosurgery planning, an algorithm is needed that permits the calculation of dose distribution for any single fixed circular field in any orientation, as well as of a number of superimposed fields.

According to Hartman et al. (1984 and 1985), the dose was considered only near isocenter. The dose model of a single field was represented by a measured relative dose file and a measured depth dose curve in a cylindrical coordinate system. The entire 3-D dose distribution was approximated by that of pencil-like beam. The resulting dose distribution was calculated by superimposing single fields. Rice et al., (1987) used a simple isocentric dose model similar to that used by Hartmann et al., (1985);

however, he used somewhat different measured factors. The scatter correction factor, tissue maximum ratio and off-axis ratio were used as basic beam data by that group. Since those two models actually ignored the inverse square factor, dose computation may not be accurate at points far from the isocenter. Pike et al., (1987) used a dose model based on the 2-D Milan and Bentley algorithm (Milan & Bentley, 1974) which uses measured central axis percentage depth doses and beam profiles at several depths in water. The TMR was calculated from the percentage depth dose data using Khan's expression (Khan, 1980), and renormalized to the isocenter. This model is a more accurate method of obtaining the dose within the single field than the previous three beam models. One disadvantage of this model is the enormous effort for the measurements. Many other groups have mentioned the use of a 3-D dose computational algorithm in their papers; however, they were not described in detail.

Optimization in Radiation Therapy

The concept of optimization as applied to radiotherapy planning is concerned with determining the best possible dose distribution for a given treatment situation. Any method which attempts such optimization must incorporate the criteria which define this ideal dose distribution. A detailed study concerning these criteria was carried out by

Hope et al., (1967). The usual starting point for quantitative optimization was the adoption of score functions as quantitative measures of the quality of the treatment plan. Hope et al., (1967) introduced the concept of calculated judgement which allows a more quantitative comparison of isodose distributions to be made through the score functions. The approach requires a considerable amount of data preparation and computer time and, as it is non-interactive, it does not allow rapid recalculation if resulting plans show undesirable distributions.

Another approach using linear programming was investigated by several workers. Hope et al., (1972) and Orr (1972) attempted to optimize the physical or geometric dose distribution through the use of linear programming, which optimized scores that varied linearly from a desired dose at a selected number of points. Bahr (1968) and Hodes (1974) also used linear programming to minimize the integral dose. Initial results using this technique appear to be encouraging but a problem does arise in the choice of the objective function since this must be linear, by definition.

At that time those workers defined color around the target region, which is associated with the requirement of steep fall off in dose in the color region. The criteria of uniformity of dose to the target region was also defined by setting upper and lower dose constraints at preselected points within the target area. Redpath et al., (1976) developed an optimization method in which the variation in dose over the volume is minimized subject to constraining doses at nearby critical structures. The calculation proceeds by way of a quadratic programming which minimizes a second order objective function subject to linear constraints.

McDonald and Rubin (1977) described an alternative approach using a least square method, which could be one of quadratic programming similar to the method used by Redpath et al., (1976). However, they used different weights per sample point to compensate for distortions due to irregular spacing of sample points along the target contour. Starkschall (1984) developed a constrained least square optimization method incorporating, as constraints, maximum allowable doses delivered to critical organs, as well as the requirement that all beam weights be non-negative.

These earlier methods all differ from one another in either their choice of an objective function, or their means for optimizing the objective, or both. Those efforts, moreover, were limited to optimizing beam weights and reflected only two dimensional considerations. The field sizes and beam orientations, which may require nonlinear programming (NLP), are selected visually by the treatment planner, since it is extremely difficult to quantify all the optimization variables and to find global optimum for non-linear variables such as field size or beam orientation.

Another approach is visual optimization, which has been the most common method. The planner observes the effects of varying any of the parameters affecting the dose distribution and so arrives interactively at an acceptable distribution. However, by a visual interactive procedure alone, the full affect of all these parameters cannot be investigated because of the time involved.

The use of computer controlled systems with the visual technique or, sometimes, with mathematical programming were studied to adjust field direction, width and dose rate. Computer-controlled radiation therapy, or dynamic treatment, is simply an extension of the concept of moving-field radiation therapy. Trumph et al., (1961) expanded this technique. They added such refinements as mechanical devices that change field size and beam direction during the treatment, as well as synchronous shaping and shielding. These concepts were further developed by Takahashi (1962), who used a multileaf collimator with independently movable, multiple pairs of jaws to define unsymmetrical, irregular fields (conformation therapy). Mantel et al., (1978) investigated the possibilities of placing the therapy machine under computer control during treatment. Mantel et al., (1978) discussed some computational methods to determine the values of the field size and dose rate through visual methods using linear programming as functions of the gantry angle. As another feasibility study of computer controlled radiation therapy, its application to produce a wedge-shaped dose distribution by moving collimator jaws was evaluated. More advanced computer controlled radiation therapy techniques were described by Chin et al., (1981, 1983). The parameters varied during treatment included dose rate, gantry rotation, table rotation, table translation, position of the four independently movable collimators, and collimator rotation. They also implemented a least square method for the purpose of automatic optimization (Chin et al., 1981).

While the principles of computer controlled radiation therapy are well established, general application has been slow in coming. One reason for this is the increased complexity of the system and the accompanying increased risk of error. However, computer controlled radiation therapy using multileaf collimators has been developed for optimization of some general moving beam treatments (Takai et al., 1987; Lind & Brahma, 1987; Bower et al., 1985).

In recent years, advances in computer and graphics display technologies have opened a wide range of possibilities for 3-D treatment planning. Conformal therapy using multileaf and beam's eye view display techniques (Frase et al., 1987; Goitein et al., 1983; Mohan et al., 1988) is most effective to shape target volume in 3-D space, as well as in 3-D compensator design, while analytical optimization approaches have been applied in teletherapy or brachytherapy optimization using linear programming (Takai et al., 1987) or quadratic programming (Tolli & Ragnhult, 1987; Chung-bin & Malyala, 1987; Tabush et al., 1988).

Several preliminary studies have been proposed in recent proceeding papers, and research is ongoing to solve more complicated optimization problems. Dynamic treatment (varying treatment parameters) (Schlegel et al., 1987), or treatment under temporal variation of one or more treatment parameters during the irradiation is one of the approaches. A multiaxial treatment technique was suggested by Aoki et al., (1987) in order to overcome the disadvantage of conformal treatment planning with a multileaf collimator. The technique is based on a summation of partially rotated conformal techniques with different iso-axes for multileaf multiple planning objects to which patient volume is divided. Hosoi et al., (1987) described a dose corresponding technique, in which several assumed target volumes were put in one original target volume, and the dose distributions from each planning object were calculated with conformal rotation techniques. A dose distribution nearly corresponding to the shape of the original target volume was obtained by summing up these dose distributions.

At present no detailed method is mentioned in the literature for the optimization of dose distribution for stereotactic radiosurgery.

CHAPTER 3
DESCRIPTION OF STEREOTACTIC PROCEDURES

Stereotactic radiosurgery, in various forms, is in use in numerous countries (e.g. France, Italy, Sweden, United States, USSR, West Germany) for the treatment of a variety of lesions. It's utilization and applications are steadily increasing. In this chapter, the procedure of a stereotactic radiosurgery system is described briefly, including unique mechanical and software features of the University of Florida radiosurgical system (Friedman & Bova, 1989).

In order to explain the stereotactic procedure, the three steps of the procedure (localization, dose planning, and treatment) must be examined separately. The ultimate accuracy of the full procedure is dependent on each of these steps and on the consistency of the approach.

Localization

A localization system is an essential prerequisite for stereotactic radiosurgery. The localization technique includes the stereotactic localization of the target in the brain by using a head frame, and determination of the coordinates of the target point with reference to this frame and adjustment of the target point to the isocenter. This is accomplished by one of two means. Currently, the method of choice is through stereotactic angiography. The procedure begins with the stereotactic ring being fitted to the patient. A specially designed intracranial localizer box (or angiographic localizing device) then rigidly attaches to the Brown-Robert-Well (BRW) Head Ring. This device has been described in other literature (Sidden & Barth, 1987) and consists of four sets of reference alignment markers. The coordinates of the sixteen markers are precisely known with respect to the BRW coordinate system (or stereotactic ring). Two localization films are required for reconstruction of the target position and determination of the target. An analysis of the projected target and radio-opaque markers permits reconstruction of the target position and determination of magnification. While this part of the procedure allows the coordinates of the target relative to the localization ring to be determined, more anatomical information is needed for dosimetry analysis.

The next step replaces the angiographic localizing device with another localizer specially designed for localization in CT. This is the standard BRW CT Localizer. The BRW head ring, with CT localizer attached, is clamped to the CT scanner table such that all scans are parallel to the head ring. Five millimeter consecutive scans are obtained from above to below the head, if we can see the target in CT. Three millimeter scans are obtained from above to below the target while 5 mm scans being done for remaining part of the head, if we can not see the target in CT. If the target volume can be identified in the CT image, then the xyz coordinates of the target volume are again calculated. A simple algorithm that transforms spatial points in CT coordinates to BRW stereotactic frame coordinates has been presented in a recent paper (Saw et al., 1987). With the digitally encoded data from the CT scan and the two angiographic films, the data is then transferred to the dosimetry computer system. The CT scan provides three-dimensional anatomical information of the patient, allowing a solid patient model to be constructed. The coordinates of the target volume from the angiogram and the CT scan data are then merged.

Dose Planning

The next concern is a dosimetry system to evaluate the dose delivered to the target and normal tissues in the patient, while it generates an optimal dose distribution that will satisfy a set of clinical criteria for the patient. Radiosurgery treatment in the brain requires detailed information on three-dimensional dose distribution.

A three-dimensional treatment planning program is a prerequisite for treatment plan optimization. It must cover 3-D methods for representing the patient, the dose distributions, and the beam settings. The method is based upon a patient anatomical representation which is obtained from CT images. The ideal system for administering radiation therapy is to deliver a tumoricidal dose to the target volume, not to irradiate tissues outside that volume, and to do this with relative ease and efficiency. Using the 3-D computation algorithm and an appropriate optimization method (visual or analytical), optimum beam setting parameters can be obtained. The target position, spacing between arcs, the size of the collimator, and the variation in arc length and weight will be parameters used in the optimization. The procedure needed for dose planning in stereotactic radiosurgery is shown in figure 3-1.

Radiation Treatment

After dose planning, the radiation treatment system is assembled and tested after the photographic method of Lutz et al., (1988). A 6 MV isocentric LINAC with a 100 cm source-to-axis distance is used at the University of Florida. The required additions or modifications to the LINAC to make it useful for radiosurgery are extra collimator systems (to define the small circular fields) and

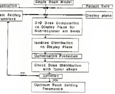
Beam Model
Basic Beam Data
Single Beam Model
Localization
Patient Data
Beam Setting Parameters
Display plane
3-D Dose Computation on Display Plane for Non-coplaner arc beam
Isodose Distribution on Display Plane
Optimization Procedure
Check Dose Distribution with Tumor shape
no
Satisfied
yes
Optimum Beam Setting Parameters

Figure 3-1. The procedure for optimal dose planning in stereotactic radiosurgery.

a three-bearing system (to improve the mechanical accuracy of the LINAC) (Friedman & Bova, 1989).

Three Bearing System

One bearing controls the isocentric accuracy of the collimator. The second bearing controls the rotation of the head of the BRW floorstand. These two bearing systems alone cannot, however, produce the desired accuracy if rigidly attached to the LINAC head. A gimble-type bearing with a sliding collimator mount was developed to avoid any torque transfer from the LINAC head. This allows the radiosurgery mechanical system, and not the LINAC head, to determine the isocentric treatment accuracy (Figure 3-2).

The Collimator System

A series of cerrobend collimators, 15 cm in length and ranging in diameter from 1 to 3 cm in steps of 2 mm (including special sizes of 5 mm and 3.5 cm) were constructed. The collimators have multi-step cylindrical apertures which define, at the machine isocenter, circular fields with the diameters constructed. The multi-step openings are tapered to match beam divergence and minimize penumbra. The accelerator collimator is set to a field size of 5 x 5 cm.

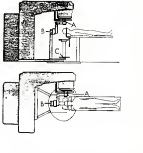

Figure 3-2. The mechanical system illustrated with lateral (upper) and overhead (lower) (From the published paper by Friedman and Bova, 1989). The LINAC head moves around the head. The patient is moved to a new couch position after each individual arc is completed. The rotation of the floor stand (C) and of the LINAC gantry (B) are controlled with precision bearings. The LINAC head is coupled to the arcing bearing via a sliding gimbal bearing (A).

Head Support and Target Positioning System

During treatment the patient's head is positioned and immobilized independently of the radiotherapy couch using the BRW floor stand (Heilbrun et al., 1983). The stand's three orthogonal drives and verniers are used to position the target in the treatment field.

CHAPTER 4
DOSE MODEL FOR A FIXED SINGLE BEAM

Before we discuss the two main approaches for optimization of LINAC-based radiosurgery, we must present some information on dose modeling. In this chapter we discuss the dose model and beam measurement for a fixed single beam. This is basic background for developing an efficient 3-D dose algorithm for multiple moving beams. The 3-D dose algorithm for multiple moving beams will be considered in the next chapter.

A simple empirical isocentric model (Van Panthaleam, 1986; Rice et al., 1987; Khan et al., 1980) will be modified to describe the dose for both circular and rectangular single treatments.

Circular Field

Dose Model

An isocentric model for single circular treatment is given by

$$D_m(C,STD,d,r) = D_{ref} \times ROF(C) \times TMR(w,d) \times (SAD/STD)^2 \times OAR(C,STD,d,r) \qquad (4\text{-}1)$$

where

m = point of interest in a medium

C = collimator size defined at SAD

STD = source to target distance

w = field size at point of interest m expressed by $w = C\ (STD/SAD)$

d = depth of point of interest m

r = off-axis distance

SAD = source to axis distance = 100 cm

D_m = the dose at point of interest m

D_{ref} = the dose for the reference set-up

ROF = relative output factor defined by $D(C,STD=100,d_m,r=0)/D(C_{ref},SSD=100,d_m,0)$

TMR = tissue maximum ratio defined by $D(w,d)/D(w,d_m)$

OAR = off-axis ratio defined by $D(C,STD,d,r)/D(C,STD,d,r=0)$

The measurement data for tissue-maximum-ratio (TMR) and off-axis-ratio (OAR) are the main function data for the dose model developed. These measurements are identified as basic beam data. Early work on basic beam data included two main parts. The first part was to determine the detector system for our small beam measurement. The second part was to formulate basic beam data from our limited measurements.

While we tested many detectors (e.g., iso-octane liquid ion chamber, Markus ion chamber, TLD, film, and diode), the diode detector was chosen as our primary beam measurement device due to the good characteristics and the small size of the sensitive volume (2 mm diameter). Figure 4-1 shows good detector response while representing the linear relationship between diode reading and dose for various x-ray beam energies. Figure 4-2 shows the good agreement between the diode and other detectors (film and TLD) for the OAR measurement.

The effort to formulate the percentage depth dose, output factor, and beam profile was made for the normal rectangular collimator size in the previous reports (Dixon et al., 1977; Van Dyk, 1977; Houdek et al., 1983; Johns & Cunningham, 1983). The formulation of the TMR for the small circular collimator was described in a recent paper (Rice et al., 1987). In order to formulate both the TMR and OAR, a limited number of dose measurements were obtained from the reference set-up. Then the possible empirical formula were used to fit the data. Those formulae were later extended and generalized for any real treatment setup by finding the relationship between fitting parameters and beam parameters. Empirical formulae for 6 MVX at Radiation Therapy at Gainesville Incorporated (RTGI) and 8 MVX at Shands Teaching

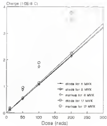

Figure 4-1. Detector response versus dose for a number of energies.

Figure 4-2. Off-axis ratio for field sizes of 1, 2, and 3 cm (SAD=100 cm) scanned at depths of 1.5 (a), 10 (b), and 5 (c) cm in solid water using film, diode, and TLD.

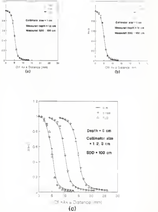
Collimator size = 1 cm
Measured depth = 1.5 cm
Measured SDD = 100 cm
0
5
10
15
20
25
30
0.2
0.4
0.6
0.8
Off Axis Distance (mm)
(a)
Collimator size = 1 cm
Measured depth = 10 cm
Measured SDD = 100 cm
0.2
0.4
0.6
0.8
Off Axis Distance (mm)
(b)
1.2
1
0.8
0.6
0.2
0
5
20
25
30
TLD
Depth = 5 cm
Collimator size
= 1, 2, 3 cm
SDD = 100 cm
Off-Axis Distance (mm)
(c)

Hospital were derived to represent TMR and OAR for any real treatment setup from a limited number of dose measurements.

Tissue-Maximum-Ratio

The TMR was measured from the fixed source to chamber (or source to target) distance, 100 cm with the diode and build-up of solid water. Figure 4-3 shows trends of TMR data measured (data points) for two different X-ray beams. TMR data were fit to a function of the form beyond the build-up region (d_{max}=1.5 cm for 6 MVX or 2 cm for 8 MVX):

$$TMR(STD,C,d) = A(C) \times \exp(-\mu(C) \times d) \qquad (4\text{-}2)$$

where $\mu(C)$ is the effective linear attenuation coefficient in water for collimator field size C, and A(C) allows one to account for the shift in d_{max} with field size. The curves in figure 4-3 represent the fit of TMR data for 1, 2, 3 and 4 cm collimator sizes. Figure 4-4 shows a plot of A and μ values as a function of collimator field size. The values for A and μ are scattered in a linear fashion. Figure 4-5 shows plots of TMR vs. depth for different source-to-target distances. These show a good agreement (to within 1%) between the TMR obtained from the different source-to-target (STD) distances. Since TMR is independent of source to target distance and dependent on field size w_s at depth d, the formula for TMR can be expressed by

Figure 4-3. Tissue-maximum-ratio for 6 MeV X-ray (a) and 8 MeV X-ray (b). The points denote the measured beam data and the curves denote the analytic function.

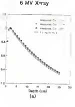
6 MV X-ray
Measured, Col
Measured, Col
Measured, Col
Fitting formula
1.2
1
0.8
0.6
0.4
0.2
0
5
10
15
20
25
30
Depth (cm)

(a)

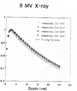
8 MV X-ray
Measured, Col=1cm
Measured, Col=2cm
Measured, Col=3cm
Measured, Col=4cm
Fitting Formula
1.2
1
0.8
0.6
0.4
0.2
0
5
10
15
20
25
30
Depth (cm)

(b)

Figure 4-4. Fitting parameters of TMR function, A and μ vs. collimator settings for 6 MeV X-ray (a) and 8 MeV X-ray (b). Collimator setting define the field size at isocenter (SAD=100 cm).

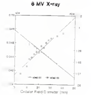
6 MV X-ray
0.048
0.044
0.042
1.08
1.07
0
20
40
50
Circular Field Diameter (mm)

(a)

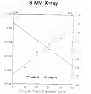
8 MV X-ray
0.04
0.034
0
20
30
50
Circular Field Diameter (mm)

(b)

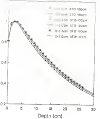

Figure 4-5 Tissue maximum ratio for different source-to-target distance (STD). The points represent the TMR for 100 cm of STD, and the curves represent the TMR for 120 cm of STD.

$$TMR(w,d) = A(w) \times \exp(-\mu(w) \times d) \qquad (4\text{-}3)$$

where

$$A(w) = A_1 + A_2\,w \qquad (4\text{-}4)$$

$$\mu(w) = \mu_1 + \mu_2\,w \qquad (4\text{-}5)$$

$$w = C \times STD / SAD,\ SAD{=}100\ \text{cm} \qquad (4\text{-}6)$$

and A_1, A_2, μ_1 and μ_2 are coefficients of linear regression, and are shown in Table 4-1.

Figure 4-6 shows the TMR trends at or near d_{max} for 6 MVX for both STD=100 and STD=90 using film measurement. The values of TMR for the larger field size are slightly smaller than those for the smaller field size in the region below d_{max}, and vice versa beyond d_{max}. It is possible to derive an empirical formula for TMR within the build-up region. Since the difference of TMR among the different collimator sizes is small, it is desirable to obtain an approximate formula for all the collimators in the build-up region. Figure 4-7 shows the TMR data and cubic polynomial fit within the build-up region.

It is shown that the measurement of TMR for 6 MVX at Shands Teaching Hospital gives trends similar to those of 6 MVX at Radiation Therapy at Gainesville Incorporated (RTGI).

Table 4-1 Table of Fitting Parameters

Tissue Maximum Ratio

Collimator size (cm)	6 MeV		8 MeV	
	A	μ	A	μ
1.0	1.076	0.0462	1.079	0.0398
1.2	1.080	0.0458		
1.4	1.083	0.0459		
1.6	1.066	0.0455		
1.8	1.088	0.0452		
2.0	1.068	0.0448	1.097	0.0380
2.2	1.093	0.0447		
2.4	1.092	0.0445		
2.6	1.096	0.0442		
2.8	1.098	0.0440		
3.0	1.100	0.0437	1.107	0.0370
3.5	1.102	0.0431		
4.0	1.105	0.0427	1.113	0.0361

Energy	A_1	A_2	μ_1	μ_2
6 MeV	1.068	0.0101	0.0478	−0.00135
8 MeV	1.071	0.0112	0.0407	−0.00121

Off Axis Ratio

Collimator size (cm)	Source to Target Distance (cm)	6 MVe		
		a_1	a_2	β
1.2	83	0.252	0.372	0
	100	0.524	0.613	0
	114	0.246	0.953	0
2.0	90	0.496	0.457	0
	100	0.581	0.629	0
	110	0.740	0.773	0
2.8	92	0.523	0.463	0
	100	0.633	0.563	0
	107	0.696	0.643	0

Table 4-1 (continued)

Collimator size (cm)	Source to Target Distance (cm)	6 MVe		
		α_1	α_2	β
1.0	90	0.224	0.562	0.110
	100	0.342	0.680	0.119
	120	0.464	0.100	0.248
1.2	83	0.214	0.372	0.0129
	100	0.392	0.613	0.0533
	114	0.225	0.953	0.197
1.4	85	0.370	0.448	0.0024
	100	0.546	0.696	0.0244
	114	0.552	0.934	0.0862

Collimator size (cm)	Source to Target Distance (cm)	8 MVe		
		α_1	α_2	β
1.0	90	0.358	0.558	0
	100	0.303	0.559	0
	120	0.574	1.030	0
2.0	90	0.413	0.453	0
	100	0.517	0.608	0
	120	0.689	0.792	0
3.0	90	0.347	0.361	0
	100	0.490	0.550	0
	120	0.651	0.806	0
4.0	90	0.377	0.363	0
	100	0.470	0.502	0
	120	0.672	0.681	0

Energy	Q_1	Q_2	Q_3	Q_4	Q_5	Q_6
6 MeV	-0.577	0.0117	-1.005	0.0165		
	-0.0447	0.00359	-1.005	0.0165	-0.433	0.00547
8 Mev	-0.478	0.0099	-0.651	0.0125		

Figure 4-6. Tissue maximum ratio in build-up region for two different of STD, 100 cm (a) and 90 cm (b) using film.

STD = 100 cm

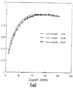

(a)

STD = 90 cm

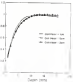

(b)

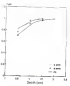

Figure 4-7. Tissue maximum ratio in build-up region for two different energies, 6 and 8 MeV X-ray using diode. The points denote measured data, and curve denotes cubic polinomial fit.

Off-Axis-Ratio

OARs were measured with the diode at d_{max} and at 10 cm depth for 6 MVX and 8 MVX beams while using varying combinations of collimators and source-to-target distances. Figures 4-8 show the result of OAR measurements for different collimator field sizes at d_{max} and 10 cm depth with fixed STD of 100 cm.

Since the difference between OARs at depth at any off-axis distance is small, any profile dependence on depth can be ignored for normal clinical applications. The curves in figures 4-8 represent multi-depth fits for each collimator using the modified Cunningham model:

$$\mathrm{OAR}(\mathrm{STD},C,r) = 1 - 0.5 \times \exp[-\alpha_1 \times (w_d/2 - r)/p - \beta \times (w_d/2 - r)^2/p^2] \quad \text{for } r \le w_d/2 \qquad (4\text{-}7a)$$

$$= t + (0.5 - t) \times \exp[-\alpha_2 \times (r - w_d/2)/p] \quad \text{for } r > w_d/2 \qquad (4\text{-}7b)$$

where w_d is given by Eq. 4-6, and r represents off-axis distance. Penumbra, p, is expressed by

$$p = SS \times (\mathrm{STD}-\mathrm{SCD}) / \mathrm{SCD} \qquad (4\text{-}8)$$

where SS is source size (assumed 2 mm), and SCD is source to collimator distance (70 cm).

Figure 4-8. Off-axis-ratio for 6 MeV X-ray (a) and 8 MeV X-ray (b). The points represent the measured beam data for collimator sizes of 1, 2, and 3 cm at depths of d_{max} and 10 cm with fixed STD of 100 cm. The curves denote fitting formula.

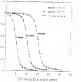

6 MV X-ray

(a)

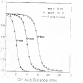

8 MV X-ray

(b)

Figure 4-9 shows OAR beam data at d_{max} and 10 cm depth with the respective formula generated curves for three different STDs with a collimator size of 2 cm. The same accuracy of fit was obtained from fitting formula with other collimators. Since transmission does not change much, the constant value of 0.02 was used for t. Most of the fitting curves agree well with measured data except for smaller collimators. The addition of a quadratic term to the exponent for the inner penumbra description gives an improvement to field sizes smaller than 1.4 cm. This makes it possible to create profiles which have a flat maximum in the center, while maintaining the appropriate gradient in the penumbra region for the small collimator.

Figure 4-10 shows trends of the fitting parameters a_1 and a_2 with the variation of STD and collimator size for two different beam energies. There are several options to determine fitting parameters for any collimator size and STD. One direct method is to interpolate between known parameters. Another is to find the relationship between fitting parameters and beam parameters such as collimator size or STD. Figure 4-11 shows composite linear regression of a_1 and a_2 with STD for multi-collimators ignoring the collimator dependence of a_1 and a_2. Figure 4-12 shows another composite linear regression for multi-collimators for 6 MVX with film measurement. The formula for OAR now can be generalized with new expressions for a_1 and a_2:

Figure 4-9. Off-axis-ratio for 6 MeV X-ray (a) and 8 MeV X-ray (b). The points represent the measured data at d_{max} and 10 cm depth for three different STDs with a collimator size of 2 cm. The curves denote fitting formula.

6 MV X-ray

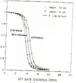

(a)

8 MV X-Ray

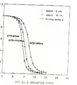

(b)

Figure 4-10. Fitting parameters of OAR function, α_1 and α_2 vs source-to-target distance for different collimator settings (a) α_1 for 6 MeV X-ray, (b) α_1 for 8 MeV X-ray, (c) α_2 for 6 MeV X-ray, (d) α_2 for 6 MeV X-ray.

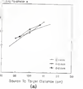
6 MV X-ray
Fitting Parameter a
0
0.2
0.4
0.6
0.8
80
90
100
110
120
130
C=1 4cm
C=2.0cm
C=2.8cm
Source To Target Distance (cm)

(a)

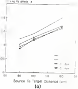
8 MV X-ray
Fitting Parameter a
0
0.2
0.4
0.6
0.8
80
90
100
110
120
130
C 3cm
C 4cm
Source To Target Distance (cm)

(b)

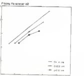
6 MV X-ray
Fitting Parameter a2
0
0.2
0.4
0.6
0.8
1
80
90
100
110
120
130
C= 4 cm
C=2.8 cm
C=2.0 cm
Source To Target Distance (cm)

(c)

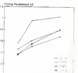
8 MV X-ray
Fitting Parameters a2
0
0.2
0.4
0.6
0.8
1
1.2
80
90
100
Source To Target Distance

(d)

Figure 4-11. Fitting parameters α_1 and α_2 with composite linear regression. The thin solid lines represent the trends of individual fitting parameters, α_1 and α_2 for different collimator sizes and STDs. The thick solid lines denote the composite linear regression for multi-collimators.

6 MV X-ray

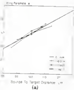

(a)

8 MV X-ray

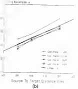

(b)

6 MV X-ray

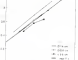

(c)

8 MV X-ray

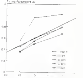

(d)

Figure 4-12 Fitting parameters α_1 and α_2 vs. source-to-target distance for collimator size of 1, 2, 3 cm with a film measurement. (a) α_1 for 6 MeV X-ray, (b) α_2 for 6 MeV X-ray.

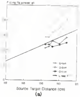
Fitting Parameter a1
0
80
90
100
110
120
Source Target Distance (cm)
D=1cm
D=2cm
D=3cm
Linear Fit

(a)

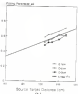
Fitting Parameter a2
0.6
0.6
0.4
0.2
0
80
90
100
110
120
Source Target Distance (cm)
D 1cm
D=2cm
D=3cm
Linear Fit

(b)

$$\alpha_1 = Q_1 + Q_2\ \mathrm{STD} \tag{4-9}$$

$$\alpha_2 = Q_3 + Q_4\ \mathrm{STD} \tag{4-10}$$

with an additional expression for small collimators (C < 1.4 cm):

$$\beta = Q_5 + Q_6\ \mathrm{STD} \tag{4-9a}$$

The coefficients of regression are shown in table 4-1. A formula may be derived from the biquadratic form which includes dependence on both collimator size and STD. However, this is not recommended as more parameters only provide a minimal increase in the accuracy of the expression.

Relative Output Factor

To express the relationship between dose and monitor units for different collimator sizes, relative output factors (ROF) are used. The relative output factor was measured at d_{max} with source-to-chamber distance of 100 cm with the reference setup (source to surface distance of 100 cm at d_{max} for field size of 10 x 10 cm) Figure 4-13 shows the measured ROF for different collimator sizes. The ROF data may be fit to a function of the form:

$$\mathrm{ROF} = S_1 \times C\text{^}S_2 \tag{4-11}$$

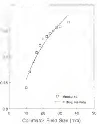

Figure 4-13. Relative output factors vs. collimator settings. Collimator settings define the field size at isocenter. The points denote measured data, the curves denote least square fit.

The final dose model for a single circular field is:

$$D(C,STD,d,r) = D_{Ref} \times ROF(C) \times TMR(w,d) \times (SAD/STD)^2 \times OAR(C,STD,r) \qquad (4\text{-}12)$$

where all function values are explicitly represented by the formulae developed here.

Rectangular Field

Dose Model

An isocentric model for a single rectangular treatment is given by

$$D_R(W_Y,W_Z,STD,d,y_c,z_c) = D_{Ref} \times ROF(W_Y,W_Z) \times TMR(w_Y,w_Z,d) \times (SAD/STD)^2 \times OAR(W_Y,W_Z,STD,d,y_c,z_c) \qquad (4\text{-}13)$$

where W_Y, and W_Z are field sizes measured at isocenter, and w_Y and w_Z are field sizes at the point of interest. The off-axis distance is represented by two off-axis variables, y_c and z_c, in the cartesian collimator coordinate system. Other parameters are the same as those for the circular beam, with circular field size replaced by rectangular field size. The rectangular field is used for the feasibility study of optimal dose distribution associated with conformal optimization using beam's eye view in Chapter 6. The measurement of TMR, OAR and ROF is needed for the rectangular field. Instead of making enormous efforts to obtain the basic beam data for rectangular fields, we used basic beam data for circular fields in representing basic beam data for rectangular fields using equivalent field sizes.

Tissue-Maximum-Ratio

From the relationship between square fields and circular fields (Bjarngard & Siddon, 1982), the equivalent circular field diameter, w, can be represented by

$$w = w_s \;/\; 0.891 \qquad (4\text{-}14)$$

where w_s is a size of the perimeter of the square field. Any rectangular field size can be converted into an equivalent square field by using a conversion expression (Johns & Cunningham, 1983):

$$w_s = 2 \times w_1 \times w_2 \;/\; (w_1 + w_2) \qquad (4\text{-}15)$$

From Eq. 4-14 and 4-15, the equivalent circular diameter, w, is expressed in terms of rectangular field size:

$$w = 2.24 \times w_1 \times w_2 \;/\; (w_1 + w_2) \qquad (4\text{-}16)$$

TMR for rectangular fields can be obtained from TMR for circular fields:

$$\mathrm{TMR}(w_y, w_z, d) = \mathrm{TMR}(w, d) \qquad (4\text{-}17)$$

where w is given by Eq. 4-16, and the analytic form of TMR(w,d) is given by Eq. 4-3 to 4-6.

Off-Axis-Ratio

The OAR can be represented by two separate off-axis ratios as in a primary beam profile [Johns & Cunningham, 1983]:

$$\mathrm{OAR}(W_y, W_z, \mathrm{STD}, d, y_c, z_c)$$
$$= \mathrm{OAR}(W_y, \mathrm{STD}, d, y_c) \times \mathrm{OAR}(W_z, \mathrm{STD}, d, z_c) \qquad (4\text{-}18)$$

For the OAR for each axis of rectangular beam, the OAR expression developed for circular fields may be used approximately, ignoring depth dependence as well as for circular fields:

$$\mathrm{OAR}(W_y, \mathrm{STD}, y_c) = \mathrm{OAR}(C, \mathrm{STD}, r) \qquad (4\text{-}19a)$$

$$\mathrm{OAR}(W_z, \mathrm{STD}, z_c) = \mathrm{OAR}(C, \mathrm{STD}, r) \qquad (4\text{-}19b)$$

The final dose model for single rectangular fields is now given by

$$D_R(W_Y,W_Z,STD,d,y_c,z_c) = D_{ref} \times ROF(W_Y,W_Z) \times TMR(w_Y,w_Z,d) \times (SAD/STD)^2 \times DAR(W_Y,STD,y_c) \times OAR(W_Z,STD,z_c) \quad (4\text{-}20)$$

where all function values are given by Eqs. 4-16, 17, 19a and 19b, and are explicitly represented by the formula developed for circular fields.

CHAPTER 5
THREE-DIMENSIONAL DOSE MODEL FOR MULTIPLE MOVING BEAMS

In chapter 4 we discussed dose models for fixed single beams. Multiple noncoplanar arcs are used for LINAC-based stereotactic radiosurgery. Exact 3-D dose models for non-coplanar arcs were developed using fixed single beam models for both circular fields and rectangular fields. Those exact 3-D dose models will be the bases to evaluate optimal dose distributions through experimental optimization techniques such as the multiple isocenter technique (circular fields) or field shaping (rectangular fields). Fast approximate dose models were also developed using the exact dose model for both coplanar and multiple noncoplanar arcs. These fast 3-D dose models will be used to find the optimum beam parameters through computer based analytical optimization.

Exact Dose Model

Circular Field

Single treatment beam model for angle orientation

From the single isocentric dose model given by Eq. 4-12, the calculation of the dose at each point of interest m requires the depth d, the off-axis distance r, the source to target distance STD, and the collimator size C with gantry and turntable orientation θ_i, ϕ_j. From these parameters the field size w at each point is easily calculated by the relationship: w = C (STD/SAD). When we use different isocenter positions for different arcs, the depth d and off-axis distance r of each point on the dose grid for each increment of gantry rotation θ_i in the algorithm are the only parameters which need to be derived from the patient contour and isocenter position I_j for each arc j. The formula to express the dose at defined point m with two additional variables θ_i, ϕ_j can be written by

$$D(C_j, STD_{ijm}, d_{ijm}, r_{ijm}) = D_{Ref} \times ROF(C_j) \times TMR(w_{ijm}, d_{ijm}) \times (SAD/STD_{ijm})^2 \times OAR(C_j, STD_{ijm}, r_{ijm}) \qquad (5\text{-}1)$$

where

θ_i = gantry angle orientation

ϕ_j = turntable angle orientation

and other parameters are defined as in Eq. 4-1.

Beam setting parameters

The beam setting parameters must be determined first to calculate the dose at the point of interest. They consist of collimator size C, turn table orientation ϕ_j, gantry angle orientation θ_j, the frame coordinates of the isocenter I_j for each arc j, and treatment time t. Using the 3-D computation algorithm and optimization method, optimum beam setting parameters can be obtained.

Dose grid

For dose calculations a matrix of points is established within the image being viewed through the display plane. A cartesian 3-D dose grid is the most popular, however a dose matrix on an oblique line or oblique plane may be desired in certain cases. Three cases of dose grids are discussed: cartesian reference recti-linear BRW coordinates relative to the BRW head ring (axial, sagittal, coronal plane etc.); oblique line dose grids defined by a line passing through two arbitrary points A and B, or defined by angle parameters α and β; and an oblique plane defined by three arbitrary points A, B and C, or defined by a rotation of a cartesian reference coordinate system about a cutting point M by angle parameters, α and β.

Coordinate transformation

If the dose matrix and beam setting parameters are determined, the calculation of the dose on the dose grid requires d_{ija}, r_{ija}, STD_{ija}, and w_{ija} from our dose model in Eq. 5-1. The method is based primarily on the definitions of the coordinate systems and transformations, or vector analysis in three-dimensional space.

Fixed machine coordinate system. The fixed coordinate system is an orthogonal coordinate system which is fixed in the treatment room (Figure 5-1). The origin is at the isocenter. The x_f axis is directed vertically upwards, and the z_f axis is horizontal and directed towards the gantry. The gantry rotates about the z_f axis in x_f-y_f plane. The turntable rotates about the x_f axis in a plane parallel to the y_f-z_f plane. The angles θ_g and ϕ_T define the positive directions of rotation of the gantry and turntable. The unit vectors for three axes x_f, y_f, and z_f are i, j, and k. This coordinate system will be the basic coordinate system for finding the unknown parameters.

Beam coordinate system. The gantry beam coordinate system is a cylindrical coordinate system (Z,r,Φ) which rotates about the z_f axis. The r=0 axis corresponds to the beam axis and the origin is the intersection of the beam axis and the isocenter. The Φ coordinate is actually not required since we can assume symmetry about Φ direction.

Isocentric BRW coordinate system. The isocentric BRW coordinate system (x_p,y_p,z_p) is defined by a rotation of the fixed mathine coordinate system (x_f,y_f,z_f) by ϕ_T about the z_f axis in the fixed coordinate system. The origin is

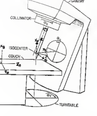

Figure 5-1. Linear accelerator with the three coordinate systems. z_g, x_t and z indicates axis of rotation of the gantry, turntable, and the collimator. These three axis intersect at the center of the target.

isocenter. During rotation of the gantry and turntable, the patient is at rest with respect to the isocentric BRW coordinate system.

BRW coordinate system. The BRW coordinate system (x_s, y_s, z_s) is the stereotactic frame coordinate system. The isocenter positions and dose grid (or display plane) are based on this BRW coordinate system. The BRW coordinate system is the reference coordinate system to represent the individual patient geometry. The CT slices are transferred to the BRW coordinate system.

The coordinate transformation from $[V]_p$ to $[V]_s$ is given by

$$[V]_p = [V]_s - [\mathbf{x}_I]_s \tag{5-2a}$$

where $\mathbf{x}_I$ is the translation vector which translates $[V]_s$ to $[V]_p$, and represents the vector position of the isocenter, I in the $[V]_s$ system. Eq. 5-2a can be written as

$$\begin{vmatrix} x_p \\ y_p \\ z_p \end{vmatrix} = \begin{vmatrix} x_s \\ y_s \\ z_s \end{vmatrix} - \begin{vmatrix} x_I \\ y_I \\ z_I \end{vmatrix} \tag{5-2b}$$

or

$$\begin{aligned} x_p &= x_s - x_I \\ y_s &= y_s - y_I \\ z_p &= z_s - z_I \end{aligned} \tag{5-2c}$$

The coordinate transformation from the isocentric BRW coordinate system to the fixed coordinate system is given by

$$[V]_F = R_x(\phi_T)\ [V]_P \tag{5-3a}$$

where $R_x(\phi_T)$ is the rotation operator which rotates the $[V]_P$ system by the rotation of turntable ϕ_j about x_F or x_P. Using the explicit expression of rotation operator (Siddon, 1981), Eq. 5-3a can be written as:

$$\begin{vmatrix} x_F \\ y_F \\ z_F \end{vmatrix} = \begin{vmatrix} 1 & 0 & 0 \\ 0 & \cos\phi_T & \sin\phi_T \\ 0 & -\sin\phi_T & \cos\phi_T \end{vmatrix} \begin{vmatrix} x_P \\ y_P \\ z_P \end{vmatrix} \tag{5-3b}$$

or

$$\begin{aligned} x_F &= x_P \\ y_F &= y_P \cos\phi_T + z_P \sin\phi_T \\ z_F &= -y_P \sin\phi_T + z_P \cos\phi_T \end{aligned} \tag{5-3c}$$

Determine unknown beam parameters

The unknown parameters must be determined on a defined dose grid for any isocenter position and angle orientation. We will consider three cases of dose grids, cartesian 3-D BRW coordinates; oblique lines; and oblique planes.

On cartesian BRW coordinate dose grid. From geometrical relations in Figure 5-2 between a point M and a line I_jM_j (I_1M_1 or I_2M_2),

Figure 5-2. Geometrical relationship between three coordinate systems with cartesian dose grids (dot line) in recti-linear BRW coordinate system.

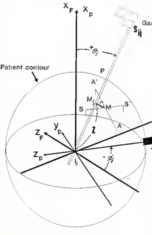
X_F
X_p
Gantry
S_{ij}
$+\theta_\ell$
Patient contour
P
A'
M_j
M
S
S'
A
y_F
y_p
Z
Z_F
Z_p
Table
$-\phi_j$
i_j

$$\overline{I_jM_j} \cdot (\overline{I_jM} - \overline{I_jM_j}) = 0 \qquad (5\text{-}4)$$

where $\overline{I_jM_j}$ and $\overline{I_jM}$ can be expressed in terms of vector units in the fixed coordinate system:

$$\overline{I_jM_j} = Z_{ijm} \cos \theta_i \ i + Z_{ijm} \sin \theta_i \ j + 0 \ k \qquad (5\text{-}5)$$

$$\overline{I\,M} = x_f \ i + y_f \ j + z_f \ k \qquad (5\text{-}6)$$

Rearranging Eq. 5-4 with Eqs. 5-5 and 5-6:

$$Z_{ijm} = |\overline{I_jM_j}| = x_f \cos \theta_i + y_f \sin \theta_i \qquad (5\text{-}7)$$

Eq. 5-7 can be expressed in terms of the isocentric BRW coordinate system with Eq. 5-3:

$$Z_{ijm} = x_p \cos \theta_i + y_p \sin \theta_i \cos \phi_j + z_p \sin \theta_i \sin \phi_j \qquad (5\text{-}8)$$

Eq. 5-8 can be expressed in terms of the BRW coordinate system with Eq. 5-2:

$$\begin{aligned} Z_{ijm} = {} & (x_s - X_j) \cos \theta_i + (y_s - Y_j) \sin \theta_i \cos \phi_j \\ & + (z_s - Z_j) \sin \theta_i \sin \phi_j \end{aligned} \qquad (5\text{-}9)$$

where (X_j, Y_j, Z_j) are the coordinates of the isocenter I_j for arc j in the BRW coordinate system.

Eq. 5-9 is a generalized equation to determine Z_{ijm} in the cartesian BRW coordinate system. The dose grid m can be defined in any cartesian BRW plane (e.g. x_B-y_B for the axial plane, x_B-z_B for the sagittal plane, y_B-z_B for the coronal plane, etc.). If Z_{ijm} is found, unknown parameters such as d, r, STD, and w can be determined from their relationship.

The depth, d_{ijm} is determined by

$$d_{ijm} = P_{ij}M = d_{ijI} - Z_{ijm} \qquad (5\text{-}10)$$

where d_{ijI} is the depth of isocenter, and Z_{ijm} is given by Eq. 5-9.

The problem of finding the depth, d_{ijm} is now reduced to finding the depth of isocenter, d_{ijI} at each increment of the gantry rotation θ_i and turntable rotation ϕ_j about isocenter position I_j. The depth of isocenter is dependent on the individual patient contour, isocenter position, and transformation of CT data to BRW coordinate system, etc. To calculate the depth of the isocenter, d_{ijI}, a simple algorithm has been developed which is based on a database containing a sampling of points on the surface of the patient's head using a ray tracing technique (Siddon, 1985) by the UF research team and other institutes (Fike et al., 1987).

However, for the research purpose of optimization, a spherical head model will be used as our reference patient model, and the coordinate of origin of the sphere will be assumed to be (0,0,0) in the BRW coordinate system. Then, the depth of isocenter will be found for a given gantry angle, turntable angle and isocenter position by their mathematical relationship. The point P on the surface of the spherical head shown in figure 5-3 can be expressed in terms of the BRW coordinate system given by

$$x_s = R \cos \theta_i + X_j \qquad (5\text{-}11)$$

$$y_s = R \sin \theta_i \cos \phi_j + Y_j \qquad (5\text{-}12)$$

$$z_s = R \sin \theta_i \sin \phi_j + Z_j \qquad (5\text{-}13)$$

where R is the depth of isocenter for a given gantry angle θ_i, turntable angle ϕ_j, and isocenter position (X_j, Y_j, Z_j) in BRW coordinates. The square sum of Eqs. 5-11 through 5-13 corresponds to the square of radius of the sphere R_0 and is given by

$$\begin{aligned} & x_s^2 + y_s^2 + z_s^2 = R_0^2 \\ = \; & R^2 + 2\,R\,(X_j \cos \theta_i + Y_j \sin \theta_i \cos \phi_j \\ & + Z_j \sin \theta_i \sin \phi_j) + (X_j^2 + Y_j^2 + Z_j^2) \qquad (5\text{-}14) \end{aligned}$$

If we arrange Eq. (5-14), we obtain a quadratic equation:

$$R^2 + 2\,b\,R + c = 0 \qquad (5\text{-}15)$$

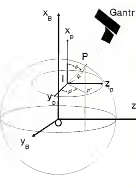

Figure 5-3. The conversion from the BRW coordinate system centered at the origin of sphere head to the cylindrical beam coordinate system to calculate the depth of isocenter.

where

$$b = X_j \cos \theta_i + Y_j \sin \theta_i \cos \phi_j + Z_j \sin \theta_i \sin \phi_j \qquad (5\text{-}16)$$

$$c = (X_j^2 + Y_j^2 + Z_j^2) - R_0^2 \qquad (5\text{-}17)$$

The solution of this quadratic equation may be written in the form:

$$R = d_{ijl} = - b + \sqrt{(b^2 - c)} \quad \text{for } R > 0 \qquad (5\text{-}18)$$

where b and c are given by Eq. 5-16 and 5-17. From the geometrical relationship, the off-axis distance, r_{ijm} is determined by

$$r_{ijm} = \left| \overline{M_jM} \right| = \left| \overline{I_jM} - \overline{I_jM_j} \right| \qquad (5\text{-}19)$$

With Eqs. 5-3c, 5-5 and 5-6, r_{ijm} in Eq. 5-19 can be expressed with some algebra by

$$r_{ijm} = [\, x_p^2 + y_p^2 + z_p^2 - Z_{ijm}^2 \,]^{1/2} \qquad (5\text{-}20)$$

Eq. 5-20 can be expressed in terms of the BRW cartesian coordinates, with Eq. 5-2 as:

$$r_{ijm} = [\, (x_s - X_j)^2 + (y_s - Y_j)^2 + (z_s - Z_j)^2 - Z_{ijm}^2 \,]^{1/2} \qquad (5\text{-}21)$$

where Z_{ijm} is given by Eq. 5-9. The source to target distance, STD_{ijm} is determined by

$$STD_{ijm} = \left|\overline{S_{ij}M}\right| = SAD - Z_{ijm} \qquad (5\text{-}22)$$

where SAD is equal to 100 cm. The field size, W_{ijm} is determined by

$$W_{ijm} = C_j \, (STD_{ijm} \, / \, SAD) \qquad (5\text{-}23)$$

where C_j is the collimator field size defined at isocenter.

Eqs. 5-10, 16, 17, 18, 21, 22, and 23 now constitute an explicit set of algebraic equations for the determination of unknown parameters on the cartesian BRW coordinate dose grid with our spherical model (radius R_0) in terms of the known parameters θ_i, ϕ_j, C, and I_j.

On oblique line dose grid. We may be interested in the dose distribution on any oblique line through any two arbitrary points A and B, especially when we consider using two isocenters to treat the inclined elongated target.

We define a dose grid on the oblique line AB (Fig.5-4a). The first point A will be the origin, and the second point B will determine the direction of the oblique line When A and B are determined in BRW coordinates, the position vector $\underline{x}$ on the line AB can be expressed in terms of two position vectors $\underline{X}_a$ and $\underline{X}_b$:

$$\underline{x} = \underline{X}_a + t \, (\underline{X}_b - \underline{X}_a) \qquad (5\text{-}24)$$

Figure 5-4. Geometrical relationship between BRW coordinate system and oblique line dose grid; (a) defined by a line passing through two arbitrary points A and B, (b) defined by a origin point A and angle parameters α and β.

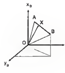
x_B
A
X
B
O
z_B
y_B

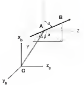
x
B
A
α
Z
x_B
β
y
O
z_B
y_B

$$\underline{x}_a = (x_a, y_a, z_a) \quad \text{in BRW coordinates} \tag{5-25}$$

$$\underline{x}_b = (x_b, y_b, z_b) \quad \text{in BRW coordinates} \tag{5-26}$$

$$\underline{x} = (x_g, y_g, z_g) \tag{5-27}$$

where t is a scalar value representing the distance from the origin A to point X along the line AB. We define the scaled dose grid t' as:

$$t = \frac{t'}{|\underline{x}_b - \underline{x}_a|} \tag{5-28}$$

where

$$|\underline{x}_b - \underline{x}_a| = \sqrt{(x_b - x_a)^2 + (y_b - y_a)^2 + (z_b - z_a)^2} \tag{5-29}$$

The position $\underline{x}$ defined in cartesian BRW coordinates is now redefined in terms of the scaled dose grid t' on the oblique line AB using Eqs. 5-24 to 5-29.

$$x_g = x_a + t' \quad (x_b - x_a)/|\underline{x}_b - \underline{x}_a| \tag{5-30}$$

$$y_g = y_a + t' \quad (y_b - y_a)/|\underline{x}_b - \underline{x}_a| \tag{5-31}$$

$$z_g = z_a + t' \quad (z_b - z_a)/|\underline{x}_b - \underline{x}_a| \tag{5-32}$$

The oblique line can be also defined by an oblique angle α and β from the x_B axis passing through the origin A (Fig.5-4b). Then, the position $\underline{x}$ in the BRW coordinate system is expressed by

$$x_B = x_A + t'' \cos\alpha \qquad (5\text{-}33)$$

$$y_B = y_A + t'' \sin\alpha \cos\beta \qquad (5\text{-}34)$$

$$z_B = z_A + t'' \sin\alpha \sin\beta \qquad (5\text{-}35)$$

where t'' is another dose grid on the oblique line defined as above. Eqs. 5-33 to 5-35 are useful to represent the radial dose distribution in any radial direction defined by α and β about the origin A.

Eqs. 5-9, 10, 16, 17, 18, 21, 22, and 23 now will be used as an explicit set of algebraic equations for the determination of the unknown parameters on the oblique line dose grid, which is defined by Eqs. 5-30 to 5-32 or by Eqs. 5-33 to 5-35 with our spherical model (radius R_0) in terms of the known parameters θ_i, ϕ_j, C, and I_j.

On oblique plane dose grid. We may be interested in dose distributions on any oblique plane through three arbitrary points A, B, and C, especially when we consider more than two isocenters to treat an inclined irregularly shaped target. This is convenient when we consider a plane containing both the target area and critical organ of interest at risk.

When we consider an oblique plane defined by three points A, B and C in figure 5-5, the position X on that plane can be represented in two ways: cartesian reference BRW coordinates, or oblique plane coordinates defined by scalars s and t. Suppose three points A, B and C are determined in the reference BRW coordinate system and represented by vectors **a**, **b** and **c**:

$$\mathbf{a} = (x_a, y_a, z_a) \qquad (5\text{-}36)$$

$$\mathbf{b} = (x_b, y_b, z_b) \qquad (5\text{-}37)$$

$$\mathbf{c} = (x_c, y_c, z_c) \qquad (5\text{-}38)$$

A dose computation algorithm was developed to calculate dose in the reference cartesian coordinate system. With this, oblique plane coordinates should be expressed in terms of cartesian BRW coordinates in order to find unknown beam parameters on the oblique plane defined by the three points. Using vector notation the position X can be expressed in the cartesian BRW coordinate system by

$$\mathbf{x} = \overline{OX} = x_s\, \mathbf{i} + y_s\, \mathbf{j} + z_s\, \mathbf{k} \qquad (5\text{-}39)$$

or can be expressed in the oblique plane coordinates defined by two orthogonal axes s and t by

$$\mathbf{x} = \overline{OA} + \overline{AP} + \overline{PX} = \mathbf{a} + s\, \mathbf{s} + t\, \mathbf{t} \qquad (5\text{-}40)$$

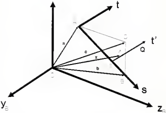

Figure 5-5. Geometrical relationship between BRW coordinate system and oblique plane dose grid defined by three arbitrary points A, B, and C.

where **i**, **j** and **k** are unit vectors of three orthogonal axes in the cartesian BRW coordinate system, and **s** and **t** are unit vectors of two orthogonal axes in the oblique plane coordinate system.

The vectors **s** and **t** are expressed by

$$\mathbf{s} = \frac{\mathbf{b} - \mathbf{a}}{|\mathbf{b} - \mathbf{a}|} \tag{5-41}$$

$$\mathbf{t} = \frac{\overline{OQ} - \overline{OP}}{|OQ - OP|} = \frac{\mathbf{q} - \mathbf{p}}{|\mathbf{q} - \mathbf{p}|} \tag{5-42}$$

The vector **q** can be expressed by

$$\mathbf{q} = \overline{OQ} = \overline{OA} + \overline{AQ} = \mathbf{a} + u\,\mathbf{u} \tag{5-43}$$

where

$$\mathbf{u} = \frac{\mathbf{c} - \mathbf{a}}{|\mathbf{c} - \mathbf{a}|} \tag{5-44}$$

$$u = \sqrt{s^2 + t^2} \tag{5-45}$$

The vector **p** can be expressed by

$$\mathbf{p} = \overline{OP} = \overline{OA} + \overline{AP} = \mathbf{a} + s\,\mathbf{s} \tag{5-46}$$

Simplifying the vector algebra in terms of cartesian BRW coordinates:

$$\mathbf{s} = \frac{\mathbf{b} - \mathbf{a}}{|\mathbf{b} - \mathbf{a}|} = \begin{vmatrix} s_x \\ s_y \\ s_z \end{vmatrix} \tag{5-47}$$

where **a** and **b** are given in Eqs. 5-36 and 37, and $|\mathbf{b} - \mathbf{a}|$ is represented by

$$|\mathbf{b} - \mathbf{a}| = \sqrt{(x_b-x_a)^2 + (y_b-y_a)^2 + (z_b-z_a)^2} \tag{5-48}$$

$$\mathbf{u} = \frac{\mathbf{c} - \mathbf{a}}{|\mathbf{c} - \mathbf{a}|} = \begin{vmatrix} u_x \\ u_y \\ u_z \end{vmatrix} \tag{5-49}$$

where **a** and **c** are given in Eqs. 5-36 and 38, and $|\mathbf{c} - \mathbf{a}|$ is represented by

$$|\mathbf{c} - \mathbf{a}| = \sqrt{(x_c-x_a)^2 + (y_c-y_a)^2 + (z_c-z_a)^2} \tag{5-50}$$

$$\mathbf{q} = \overline{OQ} = \overline{OA} + \overline{AQ} = \mathbf{a} + u\,\mathbf{u} = \begin{vmatrix} q_x \\ q_y \\ q_z \end{vmatrix} \tag{5-43a}$$

where **a** is given by Eq. 5-51, and u and **u** are given by 5-44 and 45.

$$\mathbf{p} = \overline{OP} = \overline{OA} + \overline{AP} = \mathbf{a} + s\,\mathbf{a} = \begin{vmatrix} p_x \\ p_y \\ p_z \end{vmatrix} \qquad (5\text{-}46a)$$

where **a** is given by Eq. 5-36, and **a** is given by 5-47.

$$t = \frac{\overline{OQ} - \overline{OP}}{|OQ - OP|} = \frac{\mathbf{q} - \mathbf{p}}{|\mathbf{q} - \mathbf{p}|} = \begin{vmatrix} t_x \\ t_y \\ t_z \end{vmatrix} \qquad (5\text{-}42a)$$

where **q** and **p** are given in Eqs. 5-43a and 46a, and $|\mathbf{q} - \mathbf{p}|$ is represented by

$$|\mathbf{q} - \mathbf{p}| = \sqrt{(q_x-p_x)^2 + (q_y-p_y)^2 + (q_z-p_z)^2} \qquad (5\text{-}51)$$

The components of all vectors are now expressed in terms of cartesian BRW coordinates. From Eqs. 5-39 and 5-40 the position X expressed by the s-t coordinate system on the oblique plane defined by three points A, B and C is now redefined in terms of the cartesian BRW coordinate system (x_g, y_g, z_g):

$$x_g = x_a + s\,a_x + t\,t_x \qquad (5\text{-}52)$$

$$y_g = y_a + s\,a_y + t\,t_y \qquad (5\text{-}53)$$

$$z_g = z_a + s\,a_z + t\,t_z \qquad (5\text{-}54)$$

Eqs. 5-9, 10, 16, 17, 18, 21, 22, 23 and Eqs. 5-52, 53, 54 now will be used as an explicit set of algebraic equations for the determination of unknown beam parameters (depth of isocenter Z_{ijm}, depth of point of interest d_{ijm}, off-axis distance r_{ijm}, source to target distance STD_{ijm} and field size at point of interest w_{ijm}) on the oblique plane dose grid (s-t) defined by three points A, B and C from known parameters (isocenter position, collimator size, turntable rotation and gantry rotation).

However, a more convenient way to represent the direction of the oblique plane might be to use two angle parameters, α and β, as described in the oblique line dose grid. The oblique plane dose grid is defined in the rotated BRW coordinate system $[V]_R$, which is defined by a rotation of the BRW coordinate system by α about any x_B line passing the origin point A to an intermediate system, followed by β about its own y axis (Fig.5-6).

First, we define the translated BRW coordinate system, $[V]_T$ from the BRW coordinate system, $[V]_B$ with translation vector X_a (or OA):

$$[V]_T = [V]_B - [X_a]_B \qquad (5\text{-}55)$$

The T and B systems are parallel. The origin of the T system is A, ie. X_a (X_a, Y_a, Z_a) in the BRW coordinate system.

Second, we define a rotating BRW coordinate system, $[V]_R$ from the $[V]_T$ coordinate system with the rotation angle

Figure 5-6. Geometrical relationship between four coordinate systems with oblique plane dose grid defined by a cutting point A and angle parameters α and β.

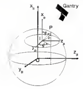

x_B
Gantry
x_p
P
I
z_p
y_p
z_B
O
y_B

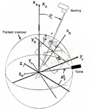

x_F x_p
Gantry
θ_c
Patient contour
x_R
y_R
P
y_F
z_F
y_p
z_p
Table
ϕ_t
I

parameters α and β. Using rotation operators, the transformation from $[V]_T$ to $[V]_R$ is therefore

$$[V]_R = R_Y(\beta)\ R_X(\alpha)\ [V]_T \tag{5-56}$$

Eq. 5-56 can be also expressed using the unitary operator property by

$$[V]_T = R_X(-\alpha)\ R_Y(-\beta)\ [V]_R \tag{5-57}$$

where $R_X(\alpha)$ and $R_Y(\beta)$ are given by

$$R_X(\alpha) = \begin{vmatrix} 1 & 0 & 0 \\ 0 & \cos\alpha & \sin\alpha \\ 0 & -\sin\alpha & \cos\alpha \end{vmatrix} \tag{5-58}$$

$$R_Y(\beta) = \begin{vmatrix} \cos\beta & 0 & -\sin\beta \\ 0 & 1 & 0 \\ \sin\beta & 0 & \cos\beta \end{vmatrix} \tag{5-59}$$

The dose grid is now defined on the x_R-y_R plane in the $[V]_R$ system, which is rotated from the x_T-y_T plane in the $[V]_T$ system by α about the x_T axis and β about the y_T axis. The position $\underline{x}$ defined in cartesian SRW coordinates is now redefined in terms of the dose grid x_R-y_R on the rotated oblique plane with Eqs. 5-55 to 5-59:

$$[V]_S = R_X(-\alpha)\ R_Y(-\beta)\ [V]_R + [X_o]_S \tag{5-60}$$

Simplifying the matrix algebra,

$$x_s = x_\ell \cos \beta + X_s \qquad (5\text{-}61)$$

$$y_s = y_\ell \cos \alpha + x_\ell \sin \alpha \sin \beta + Y_s \qquad (5\text{-}62)$$

$$z_s = y_\ell \sin \alpha + x_\ell \cos \alpha \sin \beta + Z_s \qquad (5\text{-}63)$$

Eqs. 5-9, 10, 16, 17, 18, 21, 22, and 23 now will be used as an explicit set of algebraic equations for the determination of unknown parameters on the oblique plane dose grid, which is defined by Eqs. 5-61 to 5-63 with our spherical model (radius R_0) in terms of the known parameters θ_i, ϕ_j, C, and I_j.

The final algorithm to express dose at the point of interest m in the defined dose grid for a noncoplanar arc j which may have different isocenter positions is expressed in the form given by

$$D_m = \sum_j \sum_i D_{ijm} \qquad (5\text{-}64)$$

where D_{ijm} is given by Eq.(5-2).

The unknown beam parameters for one gantry (θ_i) and turntable orientation (ϕ_j) of each arc j are determined in the cartesian reference BRW coordinate system, or the oblique plane coordinate system. TMR and OAR values are then obtained by empirical fitting formulae developed in Eqs. 4-2 through 4-11 with the beam parameters determined here.

Rectangular Fields

Single treatment beam model for angle orientation

From the single isocentric dose model given by Eq 4-13, the calculation of the dose at each point of interest m requires the depth d, the off-axis distances y_c and z_c, the source to target distance STD, the collimator size W_Y and W_Z, and field size w_y and w_z with gantry, turntable, and collimator orientation θ_i, ϕ_j and r_k. The field size w_y and w_z at each point is easily calculated by the relationship, $w_y = W_Y$ (STD/SAD). When we use different isocenter positions for different arcs, the depth d and off-axis distance y_c and z_c of each point on the dose grid for each increment of gantry rotation θ_i in the algorithm are the only parameters which need to be derived from the patient contour and isocenter position I_j for each arc j. The formula to express the dose at defined point m with three additional variables θ_i, ϕ_j, and r_k can be written by

$$\begin{aligned} &D(W_{Y(j)}, W_{Z(j)}, STD_{ijm}, d_{ijm}, Y_{c(ijkm)}, Z_{c(ijkm)}) = \\ &\quad D_{Ref} \times ROF(W_{Y(j)}, W_{Z(j)}) \times TMR(W_{Y(ijm)}, W_{Z(ijm)}, d_{ijm}) \\ &\quad \times (SAD/STD_{ijm})^2 \times OAR(W_{Y(j)}, W_{Z(j)}, STD_{ijm}, Y_{c(ijkm)}, Z_{c(ijkm)}) \end{aligned} \tag{5-65}$$

where

θ_i = gantry angle orientation

ϕ_j = turntable angle orientation

r_k = collimator angle orientation

and the other parameters are defined as in the rectangular field in Chapter 4.

Beam setting parameters

The beam setting parameters consist of collimator size $W_{Y(j)}$, $W_{Z(j)}$, turn table orientation ϕ_j, gantry angle orientation θ_i, collimator angle orientation τ_k, the frame coordinates of the isocenter I_j for each arc j, and arc weighting.

Dose grid

Three cases of dose grids can be used as defined in the circular field: cartesian reference BRW coordinates; oblique line dose grids; and oblique plane dose grids.

Coordinate transformation

The calculation of the dose at the dose grid requires $W_{Y(j)}$, $W_{Z(j)}$, STD_{ijm}, d_{ijm}, $y_{c(ijm)}$, and $z_{c(ijm)}$ from our dose model in Eq. 5-65. Four coordinate systems were considered to determine unknown beam parameters for the circular field. The cylindrical beam coordinate system with the rectangular field can be replaced by the cartesian gantry coordinate system and collimator system (Figure 5-7).

The gantry system $[V]_G$ is defined by a rotation of the fixed machine coordinate system by θ_i about the z_f axis. The origin is at the isocenter. The transformation from $[V]_f$ to $[V]_G$ is given by

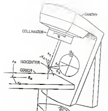

Figure 5-7. Linear accelerator with the four coordinate system.

$$[V]_G = R_z(\theta_i)\ [V]_T \qquad (5\text{-}66)$$

The collimator system $[V]_C$ is defined by a rotation of the gantry coordinate system by τ_k about the x_G axis. The origin is at the isocenter. The treatment field size W_Y and W_Z are measured at isocenter. The transformation from $[V]_G$ to $[V]_C$ is given by

$$[V]_C = R_x(\tau_k)\ [V]_G \qquad (5\text{-}67)$$

The isocentric BRW coordinate system $[V]_P$ is defined by a rotation of $[V]_T$ by $-\phi_j$ about the x_T axis. The origin is at the isocenter. The transformation from $[V]_T$ to $[V]_P$ is given by

$$[V]_P = R_x(-\phi_j)\ [V]_T \qquad (5\text{-}66)$$

The reference BRW coordinate system $[V]_B$ is defined by a translation of the $[V]_P$ system by vector $\underline{I}_j$:

$$[V]_B = [V]_P + [\underline{I}_j]_B \qquad (5\text{-}69)$$

From Eqs. 5-66 to 5-69, $[V]_B$ can then be transformed to the $[V]_C$ system by the combined transformation:

$$[V]_C = R_x(\tau_k)\ R_z(\theta_i)\ R_x(\phi_j)\ (\ [V]_B - [\underline{I}_j]_B\ ) \qquad (5\text{-}70)$$

where

$$R_X(\tau_k) = \begin{vmatrix} 1 & 0 & 0 \\ 0 & \cos\tau_k & \sin\tau_k \\ 0 & -\sin\tau_k & \cos\tau_k \end{vmatrix} \tag{5-71}$$

$$R_Y(\theta_l) = \begin{vmatrix} \cos\theta_l & \sin\theta_l & 0 \\ -\sin\theta_l & \cos\theta_l & 1 \\ 0 & 0 & 0 \end{vmatrix} \tag{5-72}$$

$$R_X(\phi_j) = \begin{vmatrix} 1 & 0 & 0 \\ 0 & \cos\phi_j & \sin\phi_j \\ 0 & -\sin\phi_j & \cos\phi_j \end{vmatrix} \tag{5-73}$$

Determine unknown beam parameters

The unknown parameters must be determined on a defined dose grid for any isocenter position and angle orientation. From Eq. 5-70 the points of interest expressed in BRW coordinates are represented by the collimator coordinate system, where the treatment field is specified. Now unknown beam parameters are found from the coordinates (x_c, y_c, z_c) determined in the collimator coordinate system.

x_c represents the distance between the isocenter and the point of interest, and is expressed in terms of the BRW coordinate system.

The depth of the point of interest is determined by

$$d_{ijm} = d_{ijl} - x_c \tag{5-74}$$

where x_c can be expressed with the help of Eq. 5-70:

$$x_c = (x_s - X_j) \cos \theta_i + [(y_s - Y_j) \cos \phi_j + (z_s - Z_j) \sin \phi_j] \sin \theta_i \qquad (5\text{-}75)$$

With the spherical head model, depth of isocenter, d_{ijk} is given by Eqs. 5-16 to 5-18:

$$d_{ijk} = R = - b + \sqrt{(b^2 - c)} \text{ for } R > 0 \qquad (5\text{-}18)$$

$$b = X_j \cos \theta_i + Y_j \sin \theta_i \cos \phi_j + Z_j \sin \theta_i \sin \phi_j \qquad (5\text{-}16)$$

$$c = (X_j^2 + Y_j^2 + Z_j^2) - R_0^2 \qquad (5\text{-}17)$$

and y_c and z_c represent off-axis distance from the center of the beam:

$$y_c = [-(x_s - X_j) \sin \theta_i + \{ (y_s - Y_j) \cos \phi_j + (z_s - Z_j) \sin \phi_j\} \cos \theta_i] \cos \tau_k + \{-(y_s - Y_j) \sin \phi_j + (z_s - Z_j) \cos \phi_j \} \sin \tau_k \qquad (5\text{-}76)$$

$$z_c = - [-(x_s - X_j) \sin \theta_i + \{ (y_s - Y_j) \cos \phi_j + (z_s - Z_j) \sin \phi_j\} \cos \theta_i] \sin \tau_k + \{-(y_s - Y_j) \sin \phi_j + (z_s - Z_j) \cos \phi_j \} \cos \tau_k \qquad (5\text{-}77)$$

The source to target distance is determined by

$$STD_{ijk} = SAD - x_c \qquad (5\text{-}78)$$

where SAD is equal to 100 cm.

The field size, w_y and w_z are determined by

$$w_y = W_y\ (STD_{ijk} / SAD) \qquad (5\text{-}79)$$

$$w_z = W_z\ (STD_{ijk} / SAD) \qquad (5\text{-}80)$$

where W_y and W_z are collimator field sizes defined at isocenter.

Eq. 5-16 to 5-18 and 5-74 to 5-80 now constitute an explicit set of algebraic equations for the determination of unknown parameters on the cartesian BRW coordinate dose grid with the spherical model (radius R_0) in terms of the known parameters θ_i, ϕ_j, r_k, W_y, W_z and I_j.

Fast Approximate Dose Model

Using beam data and the exact dose model, a study of the spatial dose distribution for coplanar and noncoplanar arcs was carried out. The dose distribution generated by the exact dose model could be represented by a simple approximate analytic form which is convenient and very efficient for calculating dose distribution iteratively in the optimization procedure. Two kinds of simple dose models were developed for small collimators to represent the dose in 3-D space in the patient coordinate system. One is a spherical dose model for four noncoplanar arcs about a single isocenter with equal arc spacing (e.g. the standard arcs used in stereotactic radiosurgery), and the other is a cylindrical dose model for full or partial rotational arcs.

Spherical Dose Model

When we use multiple symmetrical arcs with a single isocenter, dose distributions are approximately spherically symmetrical about the isocenter with some differences due to the different angle position (Fig. 5-8). Our approach to finding a closed form result for approximately representing the radial dose distribution is to utilize the nonlinear least square fitting (NLLS) technique. Among the competitive analytic forms, one simple modified gaussian form was chosen for small collimators, which are useful for multiple isocenter treatments. The analytic form for multiple arcs with equal spacing, which are commonly used in stereotactic radiosurgery is given by

$$\text{Dose}_s = p_1 + p_2 \times \exp[-r \times r/(p_3\ C \times C)] \qquad (5\text{-}81)$$

where r is radial distance from the isocenter and C is the collimator diameter (less than 1.6 cm). The p parameters are fitting parameters. The parameters obtained by NLLS for smaller collimators are given in Table 5-1. The fits are shown by the thick lines in Figure 5-9. The thin lines are radial dose distributions for different angle orientations, and are determined by the exact dose model. The gaussian form does not fit well with large collimator sizes. The more general form was found to represent radial dose distribution for any collimator size. Two separate analytic

Figure 5-8. Radial dose profile through various radial directions for four full rotational arcs (a) and four 100° partial rotational arcs (b), with equal arc spacing 45°. The numbers shown in figure represent the angle of radial direction from zero gantry position.

Full Rotational Arc

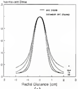

(a)

Partial Rotational Arc

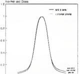

(b)

Table 5-1 Parameters for Approximate Dose Model

	Coll(cm)	P_1	P_2	P_3				
(1)	≤ 1.4	0.071	0.966	0.458				
		S_1	S_2	S_3	S_4	S_5		
(2)	1	0.320	7.430		0.020	2.520		
	2	0.232	7.009		0.032	1.606		
	3	0.257	9.575		0.036	1.071		
	all	0.249	7.019		0.029	1.927		
		q_1	q_2	q_3	q_4	q_5	q_6	q_7
(3)	≤ 1.4	0.387	6.176	1.182	0.395	0.695	2.077	3.551
	all	same value used approximately						

Figure 5-9. Radial dose profile with the analytic fits (thick solid line) and exact dose data (thin solid line and dashed line). The numbers shown in figure represent the angle of radial direction from zero gantry position.

Full Rotational Arc

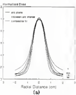

(a)

Partial Rotational Arc

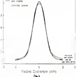

(b)

forms are used to represent the radial dose distribution for both the inner and outer penumbra regions, and are given by

$$\text{Dose}_s = 1 - s_1 \exp[- s_2 \times (C/2 - r) - s_3 \times (C/2 - r)^2] \quad \text{for } r \leq C/2 \qquad (5\text{-}82)$$

$$= s_4 + (1 - s_1 - s_4) \exp[- s_3 \times (r - C/2)] \quad \text{for } r > C/2 \qquad (5\text{-}83)$$

The s parameters are fitting parameters. The parameters obtained by NLLS for collimator sizes are given in Table 5-1. The fits are shown by the thick lines in Figure 5-10. The thin lines represent the steepest and shallowest radial dose distributions, and are determined by the exact dose model. From examining the influence of the simple spherical dose model, it is concluded that it is important to use approximate forms with reasonable limits (probably down to 20 % isodose). Since high dose is required on the target, the spherical dose model is useful to shape the field to the target using the multiple isocenter approach.

For dose calculations a matrix point is established in cartesian BRW coordinates. As an example, using a 1 cm collimator, a dose model for a single isocenter with four standard arcs is given by

$$D_i = 0.071 + 0.985 \times \exp[-r \times r/(0.458\ C \times C)] \qquad (5\text{-}84)$$

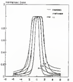

Figure 5-10. Radial dose profile for various collimator size (1, 2 and 3 cm) The dark solid line denote analytic fit. The thin solid line and dashed line represent the exact dose data of the steepest and shallowest.

where radial distance r is expressed in terms of the reference BRW coordinate system (rf. exact dose model) with isocenter position I.

$$r = [(x_g - X_I)^2 + (y_g - Y_I)^2 + (z_g - Z_I)^2]^{1/2} \qquad (5\text{-}85)$$

A dose distribution for multiple isocenters is obtained by simply adding each contribution from each isocenter. A dose model for multiple isocenters is expressed in the form given by

$$D_t = \Sigma D_I \qquad (5\text{-}86)$$

where D_I is given by Eqs. 5-84 and 5-85. Figure 5-11 gives a montage of the spatial contours of dose distribution (on the coronal plane in cartesian BRW coordinates) from single, two and three isocenters with a 1 cm collimator. The beam profile AB and CD in Figure 5-11b and c represents a good result with a beam profile obtained from the exact dose model (Fig. 5-12).

Cylindrical Dose Model

The spherical dose model may not be very useful when we consider the optimization problem with constraints to normal structures. The spherical dose model assumes symmetrically spaced standard arcs without allowing the individual movement of each arc. A more general approach

Figure 5-11. Isodose distributions calculated by a spherical dose model on the plane through the isocenters; single (a), two (b,c), and three (d). The isodose lines displayed are from 20 to 90 in 10 increments and normalized by maximum.

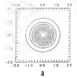
0.0
1.0
2.0
-2.0
-1.0
0.0
1.0
2.0

a

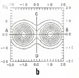
-1.0
0.0
1.0
2.0
C
A
B
D
1.0
0.0
-1.0
-2.0
-2.0
-1.0
0.0
1.0
2.0

b

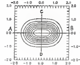
-2.0
-1.0
0.0
1.0
2.0
C
A
B
D
1.0
0.0
-1.0
-2.0
-2.0
-1.0
0.0
1.0
2.0

c

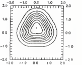
-2.0
-1.0
0.0
1.0
2.0
1.0
0.0
-1.0
-2.0
-2.0
-1.0
0.0
1.0
2.0

d

Figure 5-12. Dose profile through A-B (a) and C-D (b) in Fig. 5-11. The dose profiles were calculated by a exact dose model.

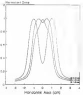
Normalized Dose
2
1
0.8
0.6
0.4
0.2
0
4
3
-2
1
0
1
2
3
4
Horizontal Axis (cm)

(a)

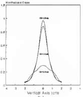
Normalized Dose
1.2
1
0.8
0.6
0.4
0.2
0
4
3
2
0
1
2
3
4
Vertical Axis (cm)

(b)

must allow the movement of individual arcs and different arc weighting to avoid significant dose to the critical organs, which may be located away from the target area. Brahme et al., (1982) developed an analytical approach for a solution of an integral equation encountered in rotation therapy. In the present study we develop an empirical cylindrical dose model which may be used to represent the dose distribution for one full rotation arc and one partial rotational arc. Since the cylindrical dose model does not ignore an angle dependence, that model is more accurate than the spherical dose model over the entire region including both the target area and normal structure area of interest.

Full rotational arc

One simple analytical form was found, which well represents both radial and axial dose distribution for one full rotational arc with small collimators. After a tedious search for fits to a collection of 200 points of exact dose data we found good results with the equation:

$$\begin{aligned} D_j = {} & q_1 \times \exp[(-q_2 \times Z^2 + q_3 \times |Z| - q_4 \times r)/ C] \\ & + q_5 \times \exp[(-q_4 \times r^2 - q_7 \times Z^2)/ C^2] \end{aligned} \qquad (5\text{-}87)$$

where r and Z are radial and axial distances from isocenter in cylindrical geometry and C is collimator diameter (less than 1.6 cm). D_j is the dose contributed from arc j. The q parameters are fitting parameters. The parameters obtained by NLLS for small collimator size are given in Table 5-1. Figure 5-13 represents a series of radial dose distributions for different axial positions with an exact dose model (solid curves) and with the cylindrical dose model (dashed curves) using analytic fits. However, this continuous analytic form does not fit well with large collimator sizes.

The radial distance r and axial distance Z in the cylindrical arc coordinate system are expressed in terms of a fixed machine coordinate system (rf. Figure 5-14).

$$r = [x_F^2 + y_F^2]^{1/2} \qquad (5\text{-}88)$$

$$Z = z_F \qquad (5\text{-}89)$$

The coordinate, which represents angle orientation in the cylindrical coordinate system is not required since radial distribution shows symmetry about the angle direction.

To calculate dose in the patient coordinate (i.e. BRW coordinate) system the dose matrix is transformed from the Fixed coordinate to the Patient coordinate system. As described in the exact dose model, the coordinate transformation from the isocentric BRW coordinate system to the fixed coordinate system is given by

$$[V]_F = R_x(\phi_j)\ [V]_B \qquad (5\text{-}3a)$$

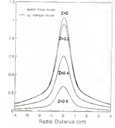

Figure 5-13. Radial dose profiles for various axial planes parallel to centrall arc plane with 1 cm collimator size. The dashed curves represent dose data with an exact model and solid curves denote cylindrical dose model.

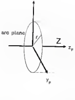

Figure 5-14: The conversion from the fixed machine coordinate system (x_F, y_F, z_F) centered at the isocenter to the cylindrical coordinate system (r, Φ, Z).

where isocentric BRW coordinates (x_p, y_p, z_p) are expressed in terms of the reference BRW coordinate system.

$$[V]_p = [V]_B - [X_j]_B \qquad (5\text{-}89)$$

The transformation from $[V]_f$ to $[V]_B$ is therefore

$$[V]_f = R_x(\phi_j) \; \{ \; [V]_B - [X_j]_B \; \} \qquad (5\text{-}90)$$

A dose distribution for multiple arcs is obtained simply by adding each contribution from each arc. A dose model for multiple arcs is expressed in the form given by

$$D = \sum_j D_j \qquad (5\text{-}91)$$

where D_j is given by Eqs. 5-87. Figure 5-15 gives a montage of the spatial contours of the dose distribution (on the coronal plane in cartesian BRW coordinates) from two arcs with isocenter position (0,0,0) and collimator size 1 cm. The isodose shape in Figure 5-15a shows good agreement with that obtained from the exact dose model (Figure 5-15b).

Figure 5-16a gives a montage of spatial contours of dose distribution on the major arc plane from one full rotation arc with isocenter position (0,0,0) and collimator size 1 cm. The isodose shape in figure 5-16a shows good agreement with that obtained from the exact dose model (Figure 5-16b).

Figure 5-15. Isodose distributions on the coronal plane vertical to two orthogonal arcs (full rotational arcs), calculated by cylindrical dose model (a) and exact dose model (b). The isodose lines displayed are from 10 to 90 in 10 increments.

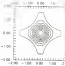
0.00
1.00
0.00
-1.00
-2.00
-2.00
-1.00
0.00
1.00
2.00

a

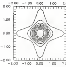
-2.00
-1.00
0.00
1.00
2.00
2.00
1.00
0.00
-1.00
-2.00

b

Figure 5-16. Isodose distributions on the arc plane, calculated by cylindrical dose model (a) and exact dose model (b) with one full rotational arc. The isodose lines displayed are from 20 to 90 in 10 increments.

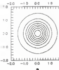
−2.0 −1.0 0.0 1.0 2.0
2.0
1.0
0.0
−1.0
−2.0
2.0
1.0
0.0
−1.0
−2.0
−2.0 −1.0 0.0 1.0 2.0

a

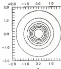
−2.0 −1.0 0.0 1.0 2.0
2.0
1.0
0.0
−1.0
−2.0
2.0
1.0
0.0
−1.0
−2.0
−2.0 −1.0 0.0 1.0 2.0

b

Partial rotational arc

In the previous section a simple approximate form was found for one full rotation arc. When a full 360° rotation arc is used, the isodose curves tend to be circles on the arc plane (Fig.5-17a). If partial rotation is used, this symmetry is lost and the region of highest dose is shifted from the axis of rotation away from the missing sector (Fig.5-17b to 17f). If the missing sector is a small fraction of the 360° rotation, the effect is negligible. As the sector becomes larger the distortion also becomes larger. This is true no matter what the shape of the contour.

We adapted the cylindrical dose model for full rotational arcs to the development of a more useful dose model for a partial rotational arcs. We accomplished this by transforming the cylindrical dose model for full rotation arcs to the modified cylindrical dose model for partial rotation arcs with an arc correction factor, which is dependent on varying the length and position of the arc.

When we consider partial rotation arcs, we obtain an asymmetry factor by comparing the dose distribution obtained from the cylindrical dose model for full rotation with that obtained from the exact dose model for partial rotation arcs. The arc correction factor, g, is now defined by

$$g = \frac{D_p}{D_f} \qquad (5\text{-}92)$$

Figure 5-17. Isodose distributions on the arc plane, calculated by exact dose model with various partial rotational arcs. (a) full rotational, (b) 25°, (c) 50°, (d) 100°, (e) 180°, and (f) 260°. The isodose lines displayed are from 90 to 10 in 10 decrements and normalized by maximum dose.

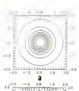
-1.0
-2.0
-2.0
-1.0
0.0
1.0
2.0

a

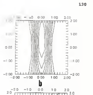
0.00
1.00
2.00
2.00
1.00
0.00
-1.00
-2.00
-2.00
-1.00
0.00
1.00
2.00

b

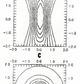
-2.0
-1.0
0.0
1.0
2.0
2.0
1.0
0.0
-1.0
-2.0

c

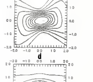
-2.0
-1.0
0.0
1.0
2.0
2.0
1.0
0.0
-1.0
-2.0

d

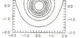
-2.0
-1.0
0.0
1.0
2.0
2.0
1.0
0.0
-1.0
-2.0

e

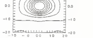
-2.0
-1.0
0.0
1.0
2.0
2.0
1.0
0.0
-1.0
-2.0

f

where D_f is the dose for a full rotation arc and is given by Eqs. 5-87. Here, we consider a 1 cm collimator for the demonstration. D_p is the dose from the exact dose model for partial rotation at the same position. Since it is not practical to find a correction factor at every position, it is desirable to find the approximate correction factor over the major arc plane for the possible partial rotational arcs (100°, 180°, etc.). The arc correction factors for 50°, 100° and 180° partial rotation arcs were found for the different angle positions about five isodose lines (20, 30, 50, 70 and 90) of full rotational arcs (dashed circles in Fig. 5-18a to c).

Figures 5-19a to c show the plot of arc correction factors for five isodose lines. The arc correction factors for 100° and 180° partial rotation arcs are well represented by a simple quadratic form

$$g = g_0 + g_1\,\mu + g_2\,\mu^2 \qquad (5\text{-}93)$$

where

$$\mu = \cos\theta \qquad (5\text{-}94)$$

where θ is defined as the angle from the position of the angle of the bisector of the arc, θ_b (Fig. 5-20). θ_b can be expressed in terms of starting and ending gantry angle θ_{Gs}, θ_{Ge} for the arc by

$$\theta_b = \frac{\theta_{Gs} + \theta_{Ge}}{2} \qquad (5\text{-}95)$$

Figure 5-18. Comparision of isodose distributions between partial rotational arcs (solid isodose lines) and full rotational arc (dashed isodose lines). The isodose displayed by partial rotational arcs are from 90 to 10 in decrements 10. The isodose displayed by full rotational arcs are 20, 30, 50, 70, and 80.
(a) 50° arc (gantry move -25° to 25°)
(b) 100° arc (gantry move 30° to 100°)
(c) 180° arc (gantry move -90° to 90°).

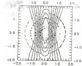
1.0
0.0
1.0
2.0
0
1.0
0.0
−1.0
−2.0
−2.0
−1.0
0.0
1.0
2.0
1.0
0.0
−1.0
−2.0

a

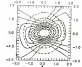
−2.0
−1.0
0.0
1.0
2.0
2.0
1.0
0.0
−1.0
−2.0
−2.0
−1.0
0.0
1.0
2.0
2.0
1.0
0.0
−1.0
−2.0

b

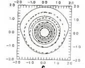
−2.0
−1.0
0.0
1.0
2.0
2.0
1.0
0.0
−1.0
−2.0
−2.0
−1.0
0.0
1.0
2.0
2.0
1.0
0.0
−1.0
−2.0

c

Figure 5-19. Arc correction factors for five isodose lines, 20, 30, 50, 70, and 80 for partial rotational arcs 50° (a), 100° (b), and 150° (c).

50 Arc Length

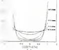

(a)

100 Arc Length

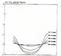

(b)

180 Arc Length

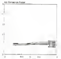

(c)

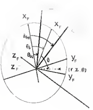

Figure 5-20 The conversion from the fixed machine coordinate system (x_f, y_f, z_f) to the bisector coordinate system ($x_{f'}$, $y_{f'}$, $z_{f'}$).

Figures 5-21a and b show plots of g_0, g_1 and g_2 values as a function of relative dose given by Eq.(5-87). The values for g_0, g_1 and g_2 are scattered in a linear fashion for a 100° rotation arc. The coefficients of linear regression are shown in table 5-2. The arc correction factors for 180° do not change much as relative dose varies. Two separate linear regressions could be used in two different regions (below 30° and above 30°). The arc correction factors about 20% and 80% relative dose were used as the values to represent the arc correction factors below 20° and above 80°. The arc correction factor for a 50° partial rotation arc is not well represented by a simple quadratic form. Another analytic form may be used to represent the arc correction factor for the smaller partial rotation arcs.

The dose for a partial rotation arc can be expressed in terms of a full rotation dose model with an arc correction factor in the cylindrical coordinate system (r, Z and θ) defined in Fig. 5-20.

$$D_p = D_f(C,r,Z)\ g(C,\theta) \qquad (5\text{-}96)$$

where D_f is given by Eq. 5-87 and g is given by Eq. 5-92. The r, Z and θ can be expressed in terms of the Bisector Cartesian coordinate system ($x_{f'}$, $y_{f'}$, $z_{f'}$) defined in Fig. 5-20.

$$r = \sqrt{(x_{f'}^2 + y_{f'}^2)} \qquad (5\text{-}97)$$

Figure 5-21. Fitting parameters of arc correction function g_0, g_1, and g_2 vs. relative dose from full rotational dose model for two partial rotational arcs; (a) 100° and (b) 180°.

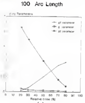
100 Arc Length
Fitting Parameters
g/l parameter
g parameter
gd parameter
0
10
20
30
40
50
60
70
80
90
100
Relative Dose (%)

(a)

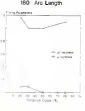
180 Arc Length
Fitting Parameters
1.2
0.8
0.4
g/l parameter
g parameter
0
20
30
40
50
60
70
80
90
Relative Dose (%)

Table 5-2 Coefficients of Linear Regression for g factor

$$g = g_0 + g_1 \mu + g_2 \mu^2$$

$$g_0 = g_{01} + g_{02} D_F$$

$$g_1 = g_{11} + g_{12} D_F$$

$$g_2 = g_{21} + g_{22} D_F$$

g_{01}	g_{02}	g_{11}	g_{12}	g_{21}	g_{22}
-0.327	1.663	0.114	-0.116	2.725	-3.260

$$Z = z_F \quad (5\text{-}98)$$

$$\theta = \tan^{-1}\left(\frac{y_{F'}}{x_{F'}}\right) \quad (5\text{-}99)$$

or

$$\mu = \cos\theta = \frac{x_{F'}}{r} \quad (5\text{-}100)$$

To calculate dose in the reference patient coordinate system (i.e. BRW coordinates), the dose matrix is transformed from the Bisector coordinate system $[V]_{F'}$ to the Fixed Machine coordinate system $[V]_F$, and then, from $[V]_F$ to the Isocentric BRW coordinate system $[V]_P$, and finally, from $[V]_P$ to the reference BRW coordinate system $[V]_B$.

The coordinate transformation from $[V]_{F'}$ to $[V]_F$ is given by

$$[V]_{F'} = R_z(\theta_b)\ [V]_F \quad (5\text{-}101a)$$

where $R_z(\theta_b)$ is the rotation operator which rotates the $[V]_F$ system by the rotation of bisector angle θ_b about z_F. Using the explicit expression of rotation operator, Eq. 5-101a can be written as:

$$\begin{vmatrix} x_{F'} \\ y_{F'} \\ z_{F'} \end{vmatrix} = \begin{vmatrix} \cos\theta_b & \sin\theta_b & 0 \\ -\sin\theta_b & \cos\theta_b & 0 \\ 0 & 0 & 1 \end{vmatrix} \begin{vmatrix} x_F \\ y_F \\ z_F \end{vmatrix} \quad (5\text{-}101b)$$

or

$$x_{f'} = x_f \cos \theta_b + y_f \sin \theta_b$$

$$y_{f'} = -x_f \sin \theta_b + y_f \cos \theta_b$$

$$z_{f'} = z_f \qquad (5\text{-}101c)$$

The coordinate transformation from $[V]_f$ to $[V]_p$ is given by

$$[V]_f = R_x(\phi_j)\ [V]_p \qquad (5\text{-}3e)$$

where $R_x(\phi_j)$ is the rotation operator which rotates the $[V]_p$ system by the rotation of the turntable, ϕ_j about the x_p. The coordinate transformation from $[V]_p$ to $[V]_s$ is given by

$$[V]_p = [V]_s - [x_j]_s \qquad (5\text{-}2e)$$

The transformation from $[V]_{f'}$ to $[V]_s$ is therefore:

$$[V]_{f'} = R_x(\theta_b)\ R_x(\phi_j)\ ([V]_s - x_j) \qquad (5\text{-}102)$$

where rotation operators and translation vectors are given by Eqs. 5-101b, 5-3b and 5-2b.

A dose distribution for multiple arcs is obtained simply by adding each contribution from each arc, and can be represented on dose grids defined (cartesian or oblique). A dose model for multiple arc is expressed in the form given by

$$D = \sum_j D_j \tag{5-91}$$

where j is an arc number and D_j is given by Eq. 5-96.

Figures 5-22a and b give montages of spatial contours of dose distribution from the dose model developed on major arc planes for 100° and 180° partial rotation arcs with isocenter position (0,0,0) and collimator size 1 cm. The isodose shape in figures 5-22a and b is in good agreement with that obtained from the exact dose model (Figures 5-22c and d).

Figures 5-23a,c and e give montages of spatial contours of dose distribution from a modified cylindrical dose model on three orthogonal planes (axial, sagittal and coronal) for four standard arcs (used in routine stereotactic radiosurgery) with isocenter position (0,0,0) and collimator size 1 cm. The isodose shape in figures 5-23a, c and e is in good agreement with that obtained from the exact dose model (Figures 5-23b, d and f).

Figure 5-24b give montages of spatial contours of dose distribution from a modified cylindrical dose model on the coronal plane for eight standard arcs with two isocenters, (0,-0.6,0) and (0,0.6,0) (four arcs about each isocenter) and collimator size 1 cm. The isodose shape in figures 5-24b is in good agreement with that obtained from the exact dose model (Figure 5-24a), and shows more accurate dose distribution than those from dose models previously

Figure 5-22. Isodose distributions calculated by modified cylindrical dose model (a,b) and exact dose model (c,d) for partial rotational arcs. (a) and (c) represent isodose distributions for 100° arc (gantry 30° to 130°). (b) and (d) represent isodose distributions for 180 arc (gantry -90° to 90°). Isodose lines displayed are from 90 to 10 in decrements 10.

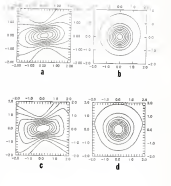
1.00
0.00
-1.00
-2.00
-2.00 -1.00 0.00 1.00 2.00
a
0.0 1.0
-1.0 0.0 1.0 2.0
b
-2.0 -1.0 0.0 1.0 2.0
2.0
1.0
0.0
-1.0
-2.0
c
d

Figure 5-23. Isodose distributions calculated by modified cylindrical dose model (a,c,e) and exact dose model (b,d,f) for four standard arcs (100° arc with turn-table orientation 0°, 45°, -45°, and -90°) with 1 cm collimator size. The distributions are displayed onto the transverse (a,b), sagittal (c,d) and coronal planes (e,f). Isodose lines displayed are from 10 to 90 in increments 10 and normalized by maximum.

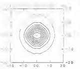
-2.0
-1.0
0.0
1.0
2.0

a

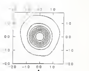
-2.0
-1.0
0.0
1.0
2.0

b

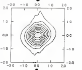
-2.0
-1.0
0.0
1.0
2.0

c

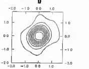
-2.0
-1.0
0.0
1.0
2.0

d

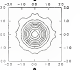
-2.0
-1.0
0.0
1.0
2.0

e

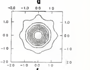
-2.0
-1.0
0.0
1.0
2.0

f

Figure 5-24. Isodose distributions on the coronal plane for eight standard arcs with two isocenters, calculated by (a) exact dose model, (b) modified cylindrical dose model (partial rotational), (c) cylindrical dose model (full rotational), (d) spherical dose model The isodose lines displayed are from 90 to 10 in 10 decrements and normalized by maximum.

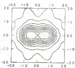

a

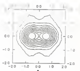

b

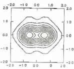

c

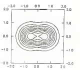

d

developed (i.e. the spherical dose model in Fig.5-24d and the cylindrical dose model for full rotation arcs in Fig.5-24c).

As a consequence, the programs required approximately 30 seconds to calculate dose for four standard arcs on a 20 x 20 matrix (400 points) using the modified cylindrical dose model for partial rotational arcs and an additional 7 minutes to perform grid generation to represent isodose curves with a Zenith 386/16 computer without floating point processor. This is much faster (approximately 20 times) than the exact dose model to calculate dose for four standard arcs. Thus, with the use of a simple dose model optimum parameters can be found 20 times faster than with the exact dose model, which makes it possible to perform real-time optimization during computer dosimetry treatment planning.

CHAPTER 6
EXPERIMENTAL OPTIMIZATION

Since LINAC-based stereotactic radiosurgery uses multiple noncoplanar arcs, three-dimensional dose evaluation and many beam parameters, a lengthy computation time is required to optimize even the simplest case by a trial and error or a computer search method. The basic approach presented in this paper is to use both an experimental optimization and an analytic optimization to solve the problem quickly and efficiently.

An important problem is the utilization of the proper beam parameters, to which dose shape is sensitive, as the optimum variables to obtain a favorable result economically. In comparing optimum variables, multiple isocenter positions and collimator size and shape are most useful for changing the shape and margin of the high isodose surface, which makes it possible to shape the field to the target by varying these parameters. Since arc variables such as length, direction, and weighting do not change much about a high isodose shape within a restricted range of arc variables with fixed isocenter positions and collimator sizes, it is possible to change the low isodose shape encompassing critical organs while maintaining the shape of the target dose.

Experimental optimization is based on two approaches. One is shaping the target volumes through the use of multiple isocenters determined from dose experience and testing. The other method is conformal therapy using a beam's eye view technique and field shaping.

Two exact dose models developed for circular and rectangular fields in chapter 5, are used for experimental or visual optimization. The circular dose model is used for a multiple isocenter approach, while a rectangular dose model is used for the field shaping approach.

Multiple Isocenter Approach

In this section, a brief description of a multiple isocenter approach is given, and a useful rule for optimum isocenter separation and collimator size is developed to shape the target margin uniformly with an 80% isodose surface for an elongated target.

The method is based on the relationship between an isodose shape and optimum variables. The current technique utilizes a single isocenter approach with multiple noncoplanar arcs. This approach results in spherical dose distributions in the target and dose fall-offs outside the target, which depend on the arrangement of the arc system. The method presented here is to use multiple isocenters with standard arcs to shape target volumes through the use of multiple spherical targets. The approximate spherical dose model may be used to see the dose shape immediately.

The test is based on the use of two or three isocenters in parallel for 1-D shape about an elongated target. Dose distributions were inspected for different isocenter separations and collimator sizes. Four standard arcs (three 100° and one 180°) with equal arc spacing (45°,270° 315°, and 0° turntable angle) were used for each isocenter. After checking the dose shape, including field uniformity and dose falloff, the useful combinations of isocenter separations and collimator sizes were considered.

Figures 6-1a to f represent two major beam profiles for three different collimator sizes and different isocenter separations with two isocenters; horizontal axes along two isocenters on the coronal plane; and vertical axes perpendicular to horizontal axes at the mid-point of two isocenters on the coronal plane. Figures 6-2a to d represent isodose distributions on the coronal plane for different isocenter separations with 1 cm collimator size. Figures 6-3a to d show 3-D dose profiles on the same coronal plane.

A reasonable optimization criteria for the target dose is to fit the target margin within the 80% isodose surface. When we use multiple isocenters in parallel, the isodose surface can be elongated-shape. The elongated target shape

Figure 6-1. Dose profiles through horizontal axis (a,c,e) and vertical axis (b,d,f) for three different collimator sizes and four different isocenter separation using two isocenters. The numbers shown in figure represent the isocenter separation in cm. The relative dose is normalized at isocenter.

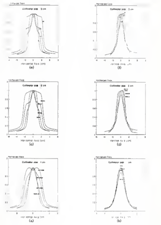
Normalized Dose
Collimator size 3 cm
Horizontal Axis (cm)
(e)
Normalized Dose
Collimator size 3 cm
Vertical Axis (cm)
(f)
Normalized Dose
Collimator size 2 cm
Horizontal Axis (cm)
(c)
Normalized Dose
Collimator size 2 cm
Vertical Axis (cm)
(d)
Normalized Dose
Collimator size 1 cm
Horizontal Axis (cm)
(a)
Normalized Dose
Collimator size
Vertical Axis (cm)
(b)

Figure 6-2. Isodose distributions on the coronal plane with 1 cm collimator size for different isocenter separation; (a) 0 cm, (b) 0.4 cm, (c) 1 cm, (d) 1.2 cm. The isodose lines displayed are from 90 to 10 in 10 decrements and normalized by maximum.

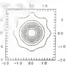
1.0
0.0
-1.0
-2.0
-2.0
-1.0
0.0
1.0
-2.0

a

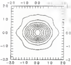
-2.0
-1.0
0.0
2.0
1.0
0.0
-1.0
-2.0
-2.0
-1.0
0.0
1.0
2.0
0.0
-1.0
-2.0

b

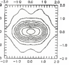
-2.0
-1.0
0.0
1.0
2.0
2.0
1.0
0.0
-1.0
-2.0
-2.0
-1.0
0.0
1.0
2.0
2.0
1.0
0.0
-1.0
-2.0

c

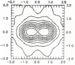
-2.0
-1.0
0.0
1.0
2.0
2.0
1.0
0.0
-1.0
-2.0
-2.0
-1.0
0.0
1.0
2.0
2.0
1.0
0.0
-1.0
-2.0

d

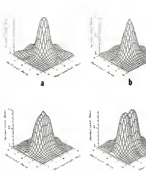

Figure 6-3. 3-D dose profiles on the coronal plane for different isocenter separation in figure 6-2.

can be approximated by a elliptical, a cylindrical or peanut shape with the longest and shortest margin. Figure 6-4 represents longest (L) and shortest distances (S) of the target, which can be fitted to the 80% isodose surface for different isocenter separations and collimator sizes. Although other isodose lines can be used to fit the target volume according to the shape of the dose, the guideline for 80% may give some basic idea to obtain the best target corresponding dose. These guidelines can be used to determine the isocenter positions and collimator sizes for the target of interest.

Figures 6-5a to f represent two major beam profiles for three different collimator sizes and different isocenter separations with three isocenters in parallel: horizontal axes along three isocenters on the coronal plane; and vertical axes perpendicular to horizontal axes at mid-isocenter of three isocenters on coronal plane. Figures 6-6a to i represent isodose distributions on axial, sagittal and coronal planes for the optimum isocenter separations, which are 60% of collimator sizes (1,2,and 3 cm).

Figure 6-7 represents the guidelines for three isocenters. For a more elongated target, we can add another isocenter to obtain the desired height and diameter (Fig. 6-8a). It is possible to use more than three isocenters in parallel, however there is no increased benefit if the

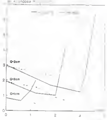

Figure 6-4. Guideline for two isocenters. The solid lines represent the longest margin (L), and dashed lines represent the shortest margin (S) of the elongated target, which can be fitted to the 80 % isodose surface.

Figure 6-3. Dose profiles through horizontal axis (a,c,e) and vertical axis (b,d,f) for different collimator size and isocenter separation using three isocenters in parallel.

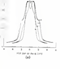
Normalized Dose
Collimator size = 2 cm
Horizontal Axis (cm)
(e)

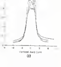
Normalized Dose
Collimator size = 3 cm
Vertical Axis (cm)
(f)

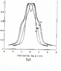
Normalized Dose
Collimator size = 4 cm
1
0.8
0.6
0.4
0.2
0
-6
-4
-2
0
2
4
6
Horizontal Axis (cm)
(c)

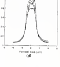
Normalized Dose
Collimator size = 4 cm
0.8
0.6
0.4
0.2
0
-6
-4
-2
0
2
4
6
Vertical Axis (cm)
(d)

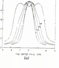
Normalized Dose
Collimator size = 1 cm
0.8
0.6
0.4
0.2
0
Horizontal Axis (cm)
(a)

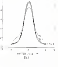
Normalized Dose
Collimator size = 1 cm
0.8
0.6
0.4
0.2
Vertical Axis
(b)

Figure 6-6. Isodose distribution on the three orthogonal planes (axial, sagittal, coronal) using three isocenters in parallel and the optimum isocenter separations to give uniform target dose, which are 60 % of collimator size. (a,b,c) for 1 cm, (d,e,f) for 2 cm, and (g,h,i) for 3 cm collimator size. The isodose lines displayed are from 10 to 90 in increment 10 and normalized by maximum.

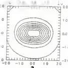
2.0
1.0
0.0
−1.0
−2.0
−2.0 −1.0 0.0 1.0 2.0

a

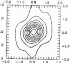
−2.0 −1.0 0.0 1.0 2.0
2.0
1.0
0.0
−1.0
−2.0
−2.0 −1.0 0.0 1.0 2.0

b

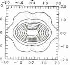
−2.0 −1.0 0.0 1.0 2.0
2.0
1.0
0.0
−1.0
−2.0
−2.0 −1.0 0.0 1.0 2.0

c

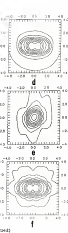

Figure 6-6 (continued)

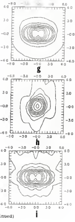

Figure 6-6 (continued)

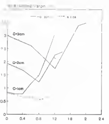

Figure 6-7. Guideline for three isocenters in parallel. The solid lines represent the longest margin (L), and dashed lines represent the shortest margin (S) of the assumed elongated target, which can be fitted to the 80 % isodose surface.

Figure 6-8. Isodose distribution using more than two isocenters in parallel. (a) three isocenters with collimator size of 1 cm and isocenter separation of 1.2 cm, (b) five isocenters with collimator size of 1 cm and isocenter separation of 0.3 cm. The isodose lines displayed are from 10 to 90 in increment 10 and normalized by maximum.

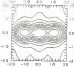
-2.0
-1.0
0.0
1.0
2.0
1.0
0.0
-1.0
-2.0
1.0
0.0
-1.0
-2.0
-2.0
-1.0
0.0
1.0
2.0

a

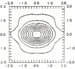
-2.0
-1.0
0.0
1.0
2.0
2.0
1.0
0.0
-1.0
-2.0
2.0
1.0
0.0
-1.0
-2.0
-2.0
-1.0
0.0
1.0
2.0

b

isocenter separation is small (e.g. five isocenters in Fig. 6-8b).

Two potential studies are suggested for the use of multiple isocenters. One is to fit isodoses to the 2-D or 3-D shape of a target such as a thin plate or arbitrary target by constructing multiple isocenters geometrically on coplanar planes or in 3-D space. Figure 6-9a and f represent dose distributions on coplanar planes through three isocenters, which forms a triangular geometry and gives uniform target dose with two possible isocenter separations. This isocenter separation configuration will be a basic unit to fit the 2-D shape of a target by arranging or adding isocenters. Figures 6-10a and f represent dose distributions on the plane through four isocenters whith form a pyramid geometry. This isocenter separation configuration will be a basic unit to fit the 3-D shape of a target by arranging or adding isocenters. However, it may not be desirable to develop guidlines for these asymmetric target shapes, since the benefit of using too many isocenters is small. The other possible study is to utilize the simple spherical dose model developed for the study of multiple isocenters. Since the dose calculation speed using the spherical dose model is much faster than that with the exact dose model, it would be very useful to find the optimum isocenter position and collimator size by a trial and error method or computer-aided design optimization

Figure 5-9. Isodose distribution on the three orthogonal planes (coronal, sagittal, axial) using three isocenters in triangle geometry on the coronal plane with 1 cm collimator size and two different isocenter separations; 1 cm (a,b,c) and 1.2 cm (d,e,f). The isodose lines displayed are from 10 to 90 in increment 10 and normalized by maximum.

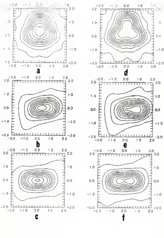
a
d
b
e
c
f
-2.0
-1.0
0.0
1.0
2.0

Figure 6-10. Isodose distribution on the three orthogonal planes (axial, sagittal, coronal) using four isocenters in tetrahedra geometry with 1 cm collimator size and two different isocenter seperations; 1 cm (a,b,c) and 1.2 cm (d,e,f). The isodose lines displayed are from 10 to 90 in increment 10 and normalized by maximum.

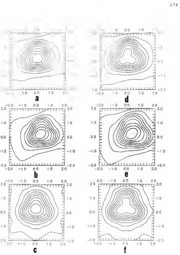
a
d
b
e
c
f
-2.0
-1.0
0.0
1.0
2.0

technique. The use of computer-aided design optimization with a spherical dose model is discussed in chapter 7. Another possible study is to utilize conformal therapy using beam's eye view and field shaping. This technique is discussed in next section.

In conclusion, the guidelines in Figs. 6-4 and 6-7 are useful in determining the optimum isocenter position and collimator size for elongated target shapes, and much more benefit is obtained from the multiple isocenter approach rather than the single isocenter approach to fit the elongated target shape (e.g. within an 80% isodose surface, compare Fig. 6-11a,b with c,d).

Field Shaping Approach

In designing radiation treatment plans, the objective is to conform and confine the high dose regions to the shape of the target as closely as possible. It is necessary to shape the aperture of the beam and compensate for surface irregularities, internal inhomogeneities, and target shape to achieve desirable dose distributions. Since radiosurgery uses a small beam to treat homogeneous brain tissues, the compensation problem is not important. Our concern in this section is field shaping using the beam's eye view projection technique and adjusting of the collimator (rotation and size). Instead of using irregular field

Figure 6-11. Isodose distributions for single isocenter technique (a,b) and two multiple isocenters technique (c,d) with a cylindrical target (length = 1.6 cm, diameter = 0.4 cm) covered by the 80% isodose surface. (a) and (c) represent the isodose distribution on the plane through two isocenters, (b) and (d) represent the isodose distribution on the plane vertical to the planes (a) and (c). (e) and (f) represent isodose distribution for two multiple isocenters and two different collimator sizes (1.0 and 2.4 cm) with a cone shaped target (length = 1.6 cm, diameter = 1.2 cm) covered by the 80% isodose surface. The isodose lines displayed are from 90 to 10 or 20 in decrement 10 and normalized by maximum.

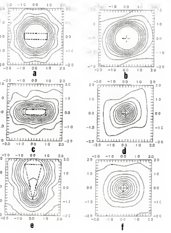
-2.0
-1.0
0.0
1.0
2.0
a
b
c
d
e
f

shapes such as multileaf collimators, the variation of a rectangular field, which seems to be more practical in radiosurgery, is considered in this section.

Beam's Eye View Projection

For practical 3-D treatment planning, one of the most important perspectives to be used is the Beam's Eye View (BEV), since it displays the relationship of the target volume to the proposed radiation beams. Beam's eye view is a display of relevant anatomical, dosimetric and beam data from the perspective of the radiation source, looking down the radiation beam. Discussion of the beam's eye view concept and it's implementation at other sites can be found in the literature (Fraass et al., 1987; Goitein et al., 1982; Purdy et al., 1987; Chin et al., 1985, Mohan et al., 1988). The patient structures which have been defined can be made into wire frame (Houlard & Dutreix, 1984) or shaded 3-D views (Bauer-Kirpes et al., 1987). In this work, BEV is accomplished by displaying a wire-frame diagram of contours outlining the patient's anatomic structures in three dimensions as if being viewed from the source of radiation along the central axis of the beam.

In order to display the defined anatomy in beam's eye view, transformation was performed from the anatomical coordinate systems (i.e. reference BRW) into beam coordinates (i.e. Collimator system). Next, beam coordinates were transformed into screen coordinates. The first is called viewing transformation, and second, perspective transformation.

The viewing coordinate system is affixed to the collimator of the treatment machine with its x_c-axis pointing from the isocenter to the source and y_c and z_c-axes parallel to the jaws defining the field size as discussed in rectangular field in chapter 5. The origin of this collimator system is at isocenter. The contour points defining the structures are given in the reference BRW coordinate system, which are transformed from the original coordinate system of the CT images. These points undergo a series of rotational and translational transformations to be expressed in terms of the collimator system. From Eqs. 5-70 to 5-73, $[V]_s$ can be transformed to the $[V]_c$ system by the combined transformation:

$$[V]_c = R_x(r_k)\ R_z(\theta_i)\ R_z(\phi_j)\ (\ [V]_s - [I_j]_s\ ) \qquad (5\text{-}70)$$

where

$$R_x(r_k) = \left|\begin{array}{ccc} 1 & 0 & 0 \\ 0 & \cos r_k & \sin r_k \\ 0 & -\sin r_k & \cos r_k \end{array}\right. \qquad (5\text{-}71)$$

$$R_Y(\theta_i) = \left|\begin{array}{ccc} \cos\theta_i & \sin\theta_i & 0 \\ -\sin\theta_i & \cos\theta_i & 1 \\ 0 & 0 & 0 \end{array}\right. \qquad (5\text{-}72)$$

$$R_X(\phi_j) = \left|\begin{array}{ccc} 1 & 0 & 0 \\ 0 & \cos\phi_j & \sin\phi_j \\ 0 & -\sin\phi_j & \cos\phi_j \end{array}\right. \qquad (5\text{-}73)$$

The collimator coordinates can be expressed in more detail in terms of BRW coordinates

$$x_c = (x_s - X_j) \cos \theta_i + [(y_s - Y_j) \cos \phi_j + (z_s - Z_j) \sin \phi_j] \sin \theta_i \qquad (5\text{-}75)$$

$$y_c = \{-(x_s - X_j) \sin \theta_i + ((y_s - Y_j) \cos \phi_j + (z_s - Z_j) \sin \phi_j) \cos \theta_i] \cos \gamma_k + \{-(y_s - Y_j) \sin \phi_j + (z_s - Z_j) \cos \phi_j) \sin \gamma_k \qquad (5\text{-}76)$$

$$z_c = - [-(x_s - X_j) \sin \theta_i + ((y_s - Y_j) \cos \phi_j + (z_s - Z_j) \sin \phi_j) \cos \theta_i] \sin \gamma_k + \{-(y_s - Y_j) \sin \phi_j + (z_s - Z_j) \cos \phi_j) \cos \gamma_k \qquad (5\text{-}77)$$

After the viewing transformation, those points are then projected on the defined imager screen. Suppose a point D is chosen, whose collimator coordinates are (d,0,0). The plane x_c=d is the screen perpendicular to the x_c axis. The screen coordinate system is then determined by prescribing its origin to be D and its y_s and z_s-axes to have the same directions as the x_c and y_c-axes, respectively. To take into account the beam divergence, the objects nearer to the source than screen are proportionally magnified and those farther than the screen are demagnified (Ammereal, 1987). In our implementation of the beam's eye view, the isocenter is assumed to be the view point. In Fig. 6-12 the triangles SPI and SP'D are similar. Hence:

$$\frac{P'D}{SD} = \frac{PI}{SI} \tag{6-1}$$

So we have:

$$\frac{y_s}{d} = \frac{y_c}{(SAD - x_c)} \tag{6-2}$$

$$y_s = d \, \frac{y_c}{(SAD - x_c)} \tag{6-3}$$

In the same way we can derive:

$$z_s = d \, \frac{z_c}{(SAD - x_c)} \tag{6-4}$$

The screen distance d can be any distance, however the isocenter can be assumed to be at the center of the screen in practical beam's eye view. A more advanced display method could also be used with the beam visualization algorithm (Reynolds et al., 1988). However, the use of that algorithm is more complicated and is not necessary for our study purpose. Using Eqs. 5-75 to 77, and Eqs. 6-3 and 4, the program was written in BASIC language to display the BEV for any structure.

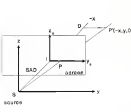

Figure 6-12. The conversion showing viewing transformation.

Optimization Using BEV and Field Shaping

The basic idea of BEV is to determine the optimum directions and field sizes of oblique noncoplanar beams so as to maximize the coverage of the target region while minimizing the inclusion of healthy critical organs in the high dose region. The best arc direction in radiosurgery can be determined among the possible directions by observing the dose distribution through the entire volume in the patient. Another way to determine the arc position is to utilize dose volume histograms (Mohan et al., 1987) or a volume matrix (Myrianthopoulos et al.) through the information obtained from beam's eye view. A dose volume histogram, though less graphic than the isodose plots, can provide a complete summary of the entire 3-D dose matrix relative to the irradiated and unirradiated volume of the patient. This is especially helpful when evaluating how much of a normal organ is receiving an amount of dose. It is invaluable when several plans have to be evaluated and compared. Once directions of incidence of the radiation beams have been selected, the collimator opening is adjusted to the smallest size that covers the target volume. The outline of the aperture should conform to the shape of the target visible from the direction of incidence and provide adequate margins.

In practical cases, it is convenient to automatically specify the shape of the aperture enclosing the target region. This is especially important for moving beam treatments using multi-leaf collimators. In this study, a rectangular collimator is used to fit the target margin instead of multi-leaf collimator, since the use of the rectangular collimator is easy, less time consuming, provides a simpler dose model, and quite accurate for a small target.

Figures 6-13 and 6-14 show the projection of a collimator orientation superimposed on a set of elongated rectangular and cylindrical targets as seen from the source. The targets have a 3-D description including 7 slices using a wire-frame model. The center of a target is located at isocenter in the spherical head model. The dimension of the target and all other geometry are shown in Figure 6-15. The objective in each view is changed as the collimator rotates (at a ten degree angular step) with four different table orientations (0, 45, -45, -90). The fields in Figures 6-13 and 6-14 are selected to encompass the target plus some margin, and are shown as dashed lines. Dose distributions are then calculated using the rectangular dose model developed. Figures 6-16 to 6-17 show three orthogonal dose distributions for cylindrical targets using one arc (table angle 0 or -90) or two arcs (table angle 0 and -90). Dose distributions in figures 6-17a, b, and c show results comparable with that obtained from the multiple isocenter approach (d,e,f in Fig. 6-17). Figure 6-18 shows three

Figure 6-13. Beam's eye view of a rectangular target in Fig. 6-15. The target has a 3-D description including 7 slices using a wire-frame model. (a) table orientation 0°, (b) -90°, (c) 45°, and (d) -45°. The two cross lines represent two central axis of 0° collimator. The dashed line represents rectangular field outline which can shape target projection with the rotation of collimator.

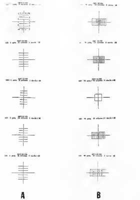
A
B

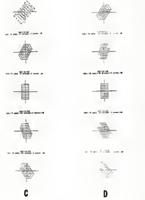

Figure 6-13 (continued)

Figure 6-14. Beam's eye view of a cylindrical target in Fig. 6-15. The target has a 3-D description including 7 slices using a wire-frame model. (a) table orientation 0°, (b) -90°, (c) 45°, and (d) -45°.

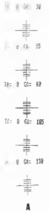
TA= 0 GA= 30
TA= 0 GA= 55
TA= 0 GA= 80
TA= 0 GA= 105
TA= 0 GA= 130
A

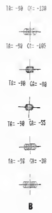
TA= -90 GA= -130
TA= -90 GA= -105
TA= -90 GA= -80
TA= -90 GA= -55
TA= -90 GA= -30
B

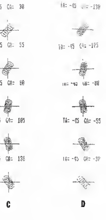

Figure 6-14 (continued)

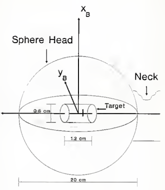

Figure 6-15. The dimensions of the target and sphere head.

Figure 6-16. Isodose curves on the three orthogonal planes (axial, sagittal, coronal) through the target point due to the field shaping technique using beam's eye view from one arc at either (a) table orientation 0° with gantry angle (-80° to 80°) or (b) -90° with gantry angle (30° to 130°). The isodose lines displayed are from 10 to 90 in increment 10 and normalized by maximum.

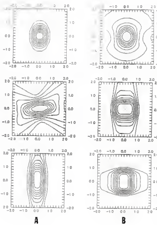
-2.0
-1.0
0.0
1.0
2.0
A
B

Figure 6-17. Isodose curves on the three orthogonal planes (axial, sagittal, coronal) through the target point due to (a) the field shaping technique using beam's eye view from two arcs at table orientation 0° with gantry angle (-80° to 80°) and -90° with gantry angle (30° to 130°), and (b) due to two multiple isocenter technique using standard eight arcs. Both 80 % isodose surfaces covered the same margin of the cylindrical target. The isodose lines displayed are from 10 to 90 in increment 10 and normalized by maximum

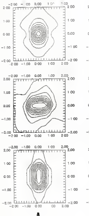

A

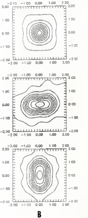

B

orthogonal dose distributions for a rectangular target using angle 0, 45, -45, and -90). The collimator was rotated to achieve proper field matching. Figure 6-19 shows a dose volume histogram for a rectangular target in two cases (4 arc field shaping and 2 multiple isocenter).

Figure 6-18. Isodose curves on the three orthogonal planes (axial, sagittal, coronal) through the center of rectangula target due to the field shaping technique using beam's eye view from four arcs at table orientation 0° with gantry angle (-80° to 80°), -90°, 45° and -45° with gantry angle (30° to 130°). The isodose lines displayed are from 10 to 90 in increment 10 and normalized by maximum.

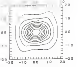
2 0
1 0
0 0
−1 0
−2 0
0 8
1 0
2 0
−2 0
−1 0
0 0
1 0
2 0

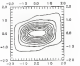
−2 0
−1 0
0.0
1 0
2.0
2.0
1 0
0.0
−1.0
−2 0
2 0
1.0
0.0
−1 0
−2 0
−2 0
−1 0
0.0
1 0
2 0

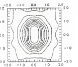
−2 0
−1 0
0.0
1 0
2.0
2 0
1 0
0 0
−1 0
−2 0
2 0
1 0
0 0
−1 0
−2 0
−2 0
−1 0
0 0
1 0
2 0

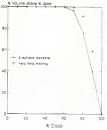

Figure 6-19. Dose Volume Histogram for a rectangular target in Figure 6-15.

CHAPTER 7
ANALYTICAL OPTIMIZATION

The purpose of this approach is to find optimum parameters automatically by using mathematical programming to minimize irradiation outside the target area while maintaining the target dose.

We have adopted a simple dose model to simulate the exact dose model and to find the optimum parameters much faster using computer-aided design optimization. The implementation of computer-aided design algorithms and their application to several cases are discussed.

Computer-Aided Design Optimization

A computer-aided design (CAD) optimization is any use of an algorithmic approach to optimizing a dose distribution using a quantitative evaluation of the optimality of a treatment plan. In this category of optimization methods, one expresses the optimization criteria as some mathematical function of the beam variables. The function which evaluates the relationship of the calculated dose distribution to the optimization criteria is known as the objective function.

The optimization criteria for the objective function in radiosurgery can be either to minimize the dose to critical organs or to maximize the dose gradient between the target boundaries and the normal structures near the target. In addition, the target shape dose must be guaranteed by constraint conditions on the target. The side constraints that require a reasonable range of variables (upper or lower limits) should also be considered.

Since it is not efficient to quantify all the optimization variables in CAD optimization, the better approach is to utilize the most sensitive beam parameters as the variables to obtain a favorable result economically. From the study of the effects of optimum variables, isocenter positions and collimator sizes are useful variables to change the high dose region and arc variables are useful variables to change the low dose region. The method to find optimum parameters is based on three steps. The first step is to find the isocenter position and collimator size with which the high dose region shapes well the target while minimizing the dose to the normal structure around target volume, or maximizing dose grdient between target boundary and normal structure. A spherical dose model with standard arc setting can be utilized with a computer-aided design optimization. The second step is to find optimum arc parameters with which dose to critical organs or normal structures can be further minimized by varying arc spacing or arc weighting while maintaining target dose. A cylindrical dose model with one full rotational or partial rotational arc is used with a computer-aided design optimization technique. The third step is to adjust optimum parameters obtained from the previous two steps by examining the dose distribution using exact dose model. The isocenter position and collimator size, which are easy to optimize experimentally, may be selected by the treatment planner, leaving the set of arc parameters as the variables which are left for the CAD optimization. The objective function is then written as some function of the arc variables, and optimized through CAD optimization technique.

In the present work, the objective function is selected to minimize the weighted dose to the critical organs defined at different positions, or to maximize the dose gradient between target boundary and normal structure around target. We can now write our nonlinear constrained optimization problem mathematically as follows:

$$\text{Minimize:} \quad \Sigma\, W_c\, D_c(\mathbf{x}) \quad \text{Objective function} \quad (7\text{-}1a)$$

or

$$\text{Maximize:} \quad \Sigma\, (D_t(\mathbf{x}) - D_n(\mathbf{x}))^2 \quad (7\text{-}1b)$$

Subject to:

$$D^l \le D_t(\mathbf{x}) \le D^u \quad \text{Constraints} \quad (7\text{-}2)$$

$$\mathbf{x}^l \le \mathbf{x} \le \mathbf{x}^u \quad \text{Side constraints} \quad (7\text{-}3)$$

where

$\mathbf{x}$ = Design vector

$D_c(\mathbf{x})$ = Dose to the critical organ at position c

W_c = weighting factor to evaluate importance of critical organ at position c

$D_t(\mathbf{x})$ = Dose to the target at position t

$D_n(\mathbf{x})$ = Dose to the normal structure position n around target boundary

D^l, D^u = Lower and upper limits of the desired dose

$\mathbf{x}^l$, $\mathbf{x}^u$ = Lower and upper limits of the design variables

A more general category of algorithms, referred to as nonlinear programming (NLP), is needed to solve this general optimization problem (Jacoby et al., 1972; Ben-Israel et al., 1981; Shoup & Mistree, 1987).

Nearly all of the optimization techniques that are currently in use can be categorized as methods for unconstrained minimization or maximization. This means that they find an optimum without regard to any constraints. Since our problems have a number of equality and inequality constraints, the use of an unconstrained optimization algorithm by itself will usually not provide the best approach to finding a usable solution. The penalty function approach is one powerful way to adapt constrained optimization problems for solution by unconstrained methods (Fiacco & McCormick, 1968).

Before we discuss the penalty function approach, we describe briefly two of the most popular optimization algorithms used for unconstrained minimization: Hooke and Jeeves' pattern search method (Hooke & Jeeves, 1961); and Powell's conjugated direction search method (Powell, 1964). Finally, a rule-based search algorithm is developed using well developed idea from experimental dose experience to find optimum isocenter positions and collimator sizes.

Hooke and Jeeves Method

The pattern search technique of Hooke and Jeeves is an easily programmed, climbing technique that does not require the use of derivatives. The algorithm has ridge-following properties and is based on the premise that any set of design moves that have been successful during early experiments will be worth trying again. The method is based on the assumption of unimodality and is used to find the minimum of a multivariable, unconstrained function.

The logic diagram for this method is shown in Fig. 7-1a. The algorithm proceeds as follows. First, a base point in the feasible design space is chosen together with exploration step sizes. Next, an exploration is performed at given increments along each of the independent-variable directions following the logic shown in Fig. 7-1b. Once this exploration is complete, a new base point is established and "pattern move" takes place. The pattern

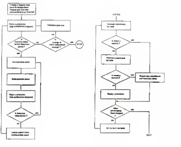
Make exploration
(See exploration diagram)
Decrease step size
Is function value better than base point ?
no
Is change in match value small enough ?
yes
STOP
Set new base point
Make pattern move
Make exploration
(See exploration diagram)
Is function value better ?
Leave search from previous base point
A
ENTER
Increase coordinate by step
Is there a success ?
Decrease coordinate by step
Is there a success ?
Retain new coordinate and function value
Reset coordinate
Have all variables been changed ?
Go to next variable
EXIT
B

Figure 7-1. The Hooke and Jeeve pattern search.

move consists of an extrapolation along a line between the new base point and the previous base point. Once the step decreased below a predetermined value with no substantial change in the objective function, the procedure algorithm terminates. Although this method lacks mathematical elegance, it is a highly efficient optimization algorithm. The relative simplicity of the method has made it one of the most popular for computer implementation.

Powell Method

Powell's method, together with modifications subsequent to it's original development, is one of the most efficient and reliable, and certainly one of the most popular of the zero-order methods. Powell's method is based on the concept of conjugated directions, where directions S^i and S^j are conjugate if

$$(S^i)^T H S^j = 0 \tag{7-4}$$

where H is the Hessian matrix.

The basic concept of Powell's method is to first search in n orthogonal directions (i.e. n design variables), S^i, i=1,n being the coordinate directions, where each search consists of updating the x vector according to

$$x^q = x^{q-1} + \alpha_{q^*} S^q \tag{7-5}$$

where q is the iteration number, $\mathbf{x}$ is the vector of design variables, $\mathbf{S}^q$ is the search direction, and α_q is a scalar multiplier determining the amount of change in $\mathbf{x}$ for q iteration. Having completed the n unidirectional searches, a new search direction is created by connecting the first and last design points. This becomes the n+1 search direction. It is convenient to store the search information in a Hessian array matrix $\mathbf{S}$. We begin with the identity matrix

$$\mathbf{S} = \mathbf{I} = \begin{vmatrix} 1 & & & & \\ & 1 & & 0 & \\ & & 1 & & \\ & 0 & & \cdot & \\ & & & & 1 \end{vmatrix} \tag{7-6}$$

The columns of $\mathbf{S}$ are the unidirectional search vectors $\mathbf{S}^i$, i=1,n. After finding the minimum in each direction (i.e. one dimensional search using golden section or quadratic interpolation), we replace $\mathbf{S}^i$ in matrix $\mathbf{H}$ by $\alpha_i\mathbf{S}^i$ to give, after n iterations:

$$\mathbf{H} = \alpha_1\mathbf{S}^1, \alpha_2\mathbf{S}^2, \ldots, \alpha_n\mathbf{S}^n \tag{7-7}$$

We now create a conjugate direction:

$$\mathbf{S}^{n+1} = \sum_{i=1}^{n}\alpha_i\mathbf{S}^i = \text{sum of columns of } \mathbf{S} \; \ldots\ldots\ldots \tag{7-8}$$

We next search in this direction to determine the move parameter α_{n+1*}. Now shift each column of the H matrix one to the left, eliminating the $\alpha_{1*}S^1$ entry, and store $\alpha_{n+1*}S^{n+1}$ in column n. This provides a new H matrix containing n search directions to start the entire search process over. The algorithm for Powell's method is given in Figure 7-2.

Penalty Function Method

A common approach to solving the constrained minimization problem is based on the penalty function approach with the unconstrained minimization method. The main idea of the penalty function approach is to minimize the objective function as an unconstrained function but to provide some penalty to limit constraint violations. For example, in the event that the dose at the position of a critical organ is outside the constrained arc range, a certain penalty is assessed to the objective function. The classical approach to using the penalty function is to create a pseudo-objective function by summing the penalty function and the previous objective function:

$$\Phi(\mathbf{x},r_p) = F(\mathbf{x}) + r_p\, P(\mathbf{x}) \qquad (7\text{-}5)$$

where F(**x**) is the original objective function, which is represented by Eq. 7-1. P(**x**) is an imposed penalty function, the form of which depends on the penalty function

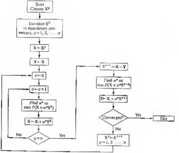
Start
Choose X^0
Initialize S^q to coordinate unit vectors, $q = 1, 2, \ldots, n$
$X \leftarrow X^0$
$Y \leftarrow X$
$q \leftarrow 0$
$q \leftarrow q + 1$
Find α^* to min $F(X + \alpha^* S^q)$
$X \leftarrow X + \alpha^* S^q$
$q = n$
No
Yes
$S^{q+1} \leftarrow X - Y$
Find α^* to min $F(X + \alpha^* S^{q+1})$
$X \leftarrow X + \alpha^* S^{q+1}$
Converged?
Yes
Exit
No
$S^q \leftarrow S^{q+1}$
$q = 1, 2, \ldots, n$

Figure 7-2. The Powell conjugated direction search algorithm.

being employed: an exterior penalty function; an interior penalty function; or an extended interior penalty function. The penalty function is zero for all design points satisfying the constraints. Clearly, if all constraints are satisfied, the minimization of $\Phi(x,r_p)$ is equivalent to the minimization of $F(x)$. The scalar r_p is a multiplier which determines the magnitude of the penalty, and r_p is held constant for a complete unconstrained minimization. The subscript p is the unconstrained minimization number. The vector x represents the optimum variables.

Rule-Based Search Method

Two previous algorithms, the "pattern search" and "conjugated direction search" methods are well suited to finding optimum arc positions using the cylindrical dose model. However, those two algorithms have problems in finding optimum isocenter positions and collimator sizes with the spherical dose model because they find local optima instead of global optima. A simplistic approach is to vary the relevant parameters in suitable increments, and then search for the global maximum or minimum of a suitable objective function. Since the number of variables is too large to compute the radiation isodoses for all possible configurations, a total search method is not desirable. Consider, for example, the very simple situation of four non-isocentric arcs. Suppose we allow the parameters to vary as follows for each arc: (1) table angle 0 - 180° in 10° increments (18 steps); (2) collimator sizes 1.0 - 3.0 cm in 0.2 cm increments (11 steps); (3) isocenter positions in 3D space 5 x 5 x 5 mm cubes in 1 mm increments (125 steps); (4) relative arc weighting from 0.2 to 1.0 in 0.2 increments (5 steps). The number of choices for each arc is then 123,750 (i.e. 18 x 11 x 125 x 5). The total number of plans to be calculated is then $123,750^4$ or 2.345×10^{20}. The calculation of a single plan with four arcs take 2 minutes to compute a 400 point dose matrix using a 386-16 computer, even with a math coprocessor. Then, 8.92×10^{14} years would be required to run through the various options. Even the fast approximate dose model can only speed computations by a factor of 100. Even though the "pattern search" and "conjugated direction search" methods are more sophiscated than the total search method, these two search methods sometimes have problems in finding global minima or maxima.

A rule-based search algorithm was developed to find the optimum isocenter positions and collimator sizes to maximize the dose gradient between the target boundary and normal structures while overcoming the local minimum problem. One or two isocenters are considered in the present study, since the dose gradient using more than two isocenters is not sharper than that using a single isocenter in fitting the dose distribution to a complicated target shape.

The use of this search method consists of two major steps. First is the determination of reasonable initial variables from the imaged target shape, and second is to follow a rule-based search procedure according to the relationship between isocenter separation and collimator sizes, while satisfying constraint conditions. From the patient data obtained from a series of CT or MRI slices, the target can be assumed to be a spherical shape or can be separated into two spherical targets using the same or different collimator sizes. The one isocenter case is simpler than the two isocenter approach, so we will discuss two isocenters. The first step is to determine approximately the initial beam parameters (isocenter positions and collimator sizes) from the 3-D target shape which is generated from a series of target contours. The collimator sizes are initially chosen to be smaller than the estimated target size, so that the target volume will be included in the planner selected isodose surface only by increasing the collimator size. After initial values are given, the second step is to determine a search vector to efficiently find the optimum isocenter positions and collimator size to maximize the dose gradient around the target. Instead of considering an arbitrary search direction (isocenter positions in arbitrary 3-D target area), the direction of a vector through the two initial isocenter positions or two arbitrary positions close to the two initial isocenter positions could be useful assuming initial values are reasonable. The third step is to check the objective function at every movement of the isocenter position in a 1-D search direction determined in step 2 as well as the variation of collimator size. From the relationship between optimum isocenter separation and collimator size for uniform target dose, isocenter separation can be adjusted by choosing two collimator sizes (i.e. optimum isocenter separation = 80 to 120 percent of the average of the two collimator sizes), and two temporary optimum isocenter positions can be determined by moving the initial isocenter positions according to the propotional ratio of collimator sizes. Therefore, instead of checking every point on the search vector determined, a couple of points checked near the experimental optimum isocenters is sufficient. The fourth step is to check whether constraint conditions for the target are satisfied. All selected constraint points along the target outline are checked to ensure that the planner selected isodose surface covers all the constraint points. One of two collimator sizes is increased according to the comparision of isocenter-to-target constraint distance normalized by collimator size until all the target constraints are satisfied. Then, the isocenter positions are readjusted by the change of collimator sizes. The value determined here is optimum for the first iteration. The fifth step is to choose another isocenter positions near the first optimum isocenter position determined on the first iteration to check whether a better optimum can be obtained, while fixing the second optimum isocenter position. The procedure is repeated following steps one through four. The final step is again to fix the first optimum isocenter position while varying the second isocenter position near the initial second isocenter position. The change between first and second isocenter is repeated until the planner is satisfied. However, after better optimum values are obtained after several cycles, it might be better to check isodose distributions visually using the exact dose model, and then readjust slightly. The steps for this method are given in Figure 7-3.

Application and Results

We discussed two main approaches and detailed methods to optimize dose distribution for stereotactic radiosurgery. The implementation of computer-aided design optimization with experimental optimization and it's application is discussed to illustrate the method and the results.

Case 1

Problem chosen

The specific problem is to minimize the dose to the critical organs, which are represented by a few points,

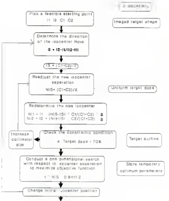
Pick a feasible starting point
I1 I2 C1 C2
Imaged target shape
Determine the direction of the isocenter move
S = I2-I1/|I2-I1|
IS = (C1+C2)/2
Readjust the new isocenter separation
NIS= (C1+C2)/2
Uniform target dose
Redetermine the new isocenter
NI1 = I1 (NIS-IS) C1/(C1+C2) S
NI2 = I2 + (NIS-IS) C2/(C1+C2) S
Increase collimator size
Check the constraints condition
Target dose > 70%
Target outline
Conduct a one dimensional search with respect to isocenter separation to maximize objective function
Store temporary optimum parameters
Change initial isocenter position
Choose the best optimum parameters

Figure 7-3. Rule-based search algorithm.

while giving the desired dose to the target area. The target is assumed to be an elongated cylindrical shape (height=1 cm, diameter=0.5 cm), and is located at the center of the spherical head model (20 cm diameter). The critical organs are assumed to be located at three different positions for two different cases (Figs. 7-4a and b): case 1-1, $C_1(0,0,2)$, $C_2(0,2,0)$, and $C_3(0,2,2)$; case 1-2, $C_1(0,0,2)$, $C_2(0,2,0)$, and $C_3(0,2,0.828)$. We optimize this problem using both experimental and analytical approaches.

Experimental optimization

The isocenter positions and collimator sizes are predetermined experimentally. The test is based on 0-D (sphere), 1-D (elongated shape), 2-D (plate shape), and 3-D (arbitrary shape) target shapes. Usually, four arcs with equal arc spacing (45°) are used for each isocenter. Cases 1-1 and 1-2 simply deal with the 1-D target shape problem. From guidelines shown in Fig. 6-4 developed for sphere and elongated target shapes, the two isocenter positions (0,-0.5,0) and (0,0.5,0) with collimator size 1 cm are chosen for case 1-1 and 2. Now the 80% isodose surface sufficiently covers the target shape for both case 1-1 and case 1-2.

Objective function to be minimized

After the isocenter positions and collimator sizes are determined experimentally with the standard arc system, the

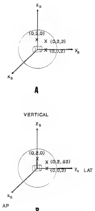

Figure 7-4. Schematic diagram for case 1.

best arrangement of arc orientation and weighting to minimize the dose to the critical organs is searched for by the computer-aided design optimization technique.

In the present work, the objective function is selected to minimize the sum of the weighted dose to the critical organs defined at designated positions. Our aim is now to find optimum parameters (arc orientation and weighting) such that the objective function

$$\Sigma\ W_c\ D_{c(x)} \qquad j = 1,\ 3 \qquad (7\text{-}1a)$$

is minimized subject to the constraint conditions described in Eqs. 7-2 and 7-3, where c's represent positions of critical organs designated for cases 1-1 and 1-2. D_c is relative dose to the critical organ located at position c, and is represented by the approximate cylindrical dose model given by Eq. 5-91. All the arc weights are assumed to be one. The critical organ weights W_c are assumed to be one in case 1-1 , however, much more weight is given to the position $C_3(0,2,0.828)$ in case 1-2.

Constraints chosen

In the course of minimizing the sum of the weighted doses, the constraints (or behavior constraints) and side constraints must be specified and quantified. The major constraint condition for uniform target dose is to assure the delivery to the target volume of a relative dose larger than certain level (e.g. 80% or 70%), which is expressed by Eq. 7-2. The side constraints require a reasonable range of variables due to physical limitations (e.g. upper and/or lower limits), which are expressed by Eq. (7-3).

When we adjust only the shift angle δ of the total arc orientation with equal arc spacing (45°), which would not change the target dose shape, the constraint conditions are simplified to:

$$0 \le \delta_1 \le \pi/4 \tag{7-10}$$

$$\phi_1 = \delta_1 \tag{7-11}$$

$$\phi_2 = \delta_1 + \pi/4 \tag{7-12}$$

$$\phi_3 = \delta_1 + \pi/2 \tag{7-13}$$

$$\phi_4 = \delta_1 + 3\pi/4 \tag{7-14}$$

$$0 \le \delta_2 \le \pi/4 \tag{7-15}$$

$$\phi_5 = \delta_2 \tag{7-16}$$

$$\phi_6 = \delta_2 + \pi/4 \tag{7-17}$$

$$\phi_7 = \delta_2 + \pi/2 \tag{7-18}$$

$$\phi_8 = \delta_2 + 3\pi/4 \qquad (7\text{-}19)$$

where δ_1 and δ_2 are shift angles of two isocenters from the standard arc position and ϕ_1 through ϕ_8 are table angle orientations for eight individual arcs, which can be determined easily by the equality constraint relationship between δ and ϕ (or we may search for ϕ's directly using different constraint conditions and a reasonable arc range).

Penalty function method for constrained minimization

The two main constraint equations (Eq. 7-10 and 7-15) can now be stated in the standard form to be implemented in the penalty function approach:

$$g_1(x) = -\delta_1 \le 0 \qquad (7\text{-}20)$$

$$g_2(x) = \delta_1 - \pi/4 \le 0 \qquad (7\text{-}21)$$

$$g_3(x) = -\delta_2 \le 0 \qquad (7\text{-}22)$$

$$g_4(x) = \delta_2 - \pi/4 \le 0 \qquad (7\text{-}23)$$

The most common penalty function used in the interior method is

$$P(x) = \sum_{j=1}^{4} \frac{-1}{g_j(x)} \qquad (7\text{-}24)$$

where P(m) is an imposed penalty function. The vector m represents the arc variables δ_1 and δ_2 in this problem. Other arc variables, ϕ_1 through ϕ_8, are determined easily from δ_1 and δ_2. Our pseudo-objective function is now expressed explicitly by

$$\Phi(m, r_p) = F(x) + r_p\ P(m) \qquad (7\text{-}25)$$

where F(m) is the original objective function, which is represented by Eq. 7-1a. We optimize this problem using an unconstrained minimization algorithm and penalty function method.

Results

Cases 1-1 and 1-2 were solved using two design variables, δ_1 and δ_2, by the interior penalty function. For the initial values of arc position, a 2° shift angle for δ_1 and δ_2, which is close to standard arc position (0°), was used. In each case, the Hooke and Jeeve method and the Powell method were used for the unconstrained minimization subprogram. The initial design vector (δ_1, δ_2) and optimum dseign for the two cases are given in table 7-1. The values obtained from the computer algorithm seem to be quite reasonable. Initially the arc positions were assigned to hit the critical organs. The final arc positions were rearranged not to hit the critical organs while minimizing the weighted dose to the critical organs in both case 1-1

Table 7-1 Optimum Variable Values

Case	Variable	Initial	Method	
			Hooke and Jeeve	Powell
Case 1-1	δ_1	2°	22.4°	22.4°
	δ_2	2°	22.6°	22.6°
Case 1-2	δ_1	2°	36.2°	36.2°
	δ_2	2°	2.6°	2.6°

and case 1-2. Geometrically, 22.5° is a good shifted angle in case 1-1, which is very close to 22.4° and 22.6° which were obtained from the computer algorithm. In case 1-2 we put a more important critical organ on the 22.5° arc position. Depending upon the weighting factor (i.e. the importance of critical organ), the arc positions (36.2° and 2.6°) were searched to put the more weighted critical organ in the better position while sacrificing the less weighted critical organ.

As a consequence, the programs required approximately 1 minute to find the optimum parameters in this problem using the Powell method with the full rotational cylindrical dose model, and an additional 2 min for the Hooke and Jeeves method with Zenith 386/16 computer without a floating point processor. This speed can be increased with a more advanced computer and floating point processor, which makes it possible to do real-time optimization during computer dosimetry treatment planning.

Case 2

In case 1 only two variables (two shift angles) were considered as design variables while keeping equal arc spacing (45°). Here we allow the individual arcs to vary within a reasonable restricted range, which changes arc spacing and may give a more desirable dose distribution under certain conditions. In the following examples, we consider this situation and discuss specific cases to implement the CAD optimization technique.

Problem chosen

Case 2-1: The target is assumed to be a spherical shape (radius=0.8 cm) located at the center of the spherical head (diameter = 20 cm). The critical organs are located at two different positions, $C_1(0,-0.2,1.0)$ and $C_2(0,0.4,-0.8)$ in the reference BRW coordinate system (Fig. 7-5a).

Case 2-2: The target is assumed to be an elongated cylindrical shape (height=2.0 cm, diameter=0.4 cm) located at the center of the spherical head (diameter=20 cm). The critical organs are located at two different positions, $C_3(0,-0.6,1.0)$ and $C_4(0,0.6,-1)$ in the reference BRW coordinate system (Fig. 7-5b).

We optimize case 2-1 and case 2-2 using both an experimental approach and an analytical approach. The isocenter positions and collimator sizes are predetermined to shape to the target experimentally, and are followed by an analytic optimization technique to search for the best arc parameters (arc spacing or arc weighting) to minimize dose at the critical points chosen.

Experimental optimization

The isocenter positions and collimator sizes are predetermined experimentally. Case 2-1 and 2-2 simply dealt with the 0-D and 1-D target shape problems. From guidelines

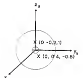

CASE 2-1

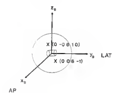

CASE 2-2

Figure 7-5. The schematic diagram for case 2.

with the 0-D and 1-D target shape problems. From guidelines shown in Fig. 6-4, developed for spherical and elongated target shapes, the single isocenter position (0,0,0) with collimator size 1 cm is chosen for case 2-1. Two isocenter positions (0,-0.6,0) and (0,0.6,0) with collimator size 1 cm are chosen for case 2-2. Now the 80% isodose surface sufficiently fits the target shape for both case 2-1 and case 2-2.

Objective function to be minimized

Our aim is now to find optimum parameters (arc orientation and weighting) such that the objective function:

$$\Sigma\ W_c\ D_{c(x)} \qquad c = 1,2 \qquad (7\text{-}1a)$$

is minimized subject to the constraint conditions described in Eqs. 7-2 and 7-3, where c's represent positions of critical organs designated for case 2-1 and case 2-2. D_c is relative dose to the critical organ located at position c, and is represented by the approximate dose model given by Eq. 5-91. All the arc weights are assumed to be one, and the critical organ weights W_c are assumed to be one in both case 2-1 and 2-2.

Constraints chosen

Instead of using Eq. 7-2 as constraints to maintain target dose shape, it may be simpler and more desirable to create a few constraint conditions that can search for the optimal result by varying parameters in a restricted range about the starting point values. Initially, four arcs with equal spacing (45°) are used for the standard plan. From experience, four arcs with a small variation from equal arc spacing (up to 30°) does not significantly change the high isodose shape. Now the constraint conditions given by Eq. 7-2 are simplified for case 2-1 by

$$-\pi/2 \le \phi_1 \le 0 \qquad (7\text{-}26)$$

$$\phi_2 \ge \phi_1 + \pi/6 \qquad (7\text{-}27)$$

$$\phi_3 \ge \phi_2 + \pi/6 \qquad (7\text{-}28)$$

$$\phi_3 + \pi/6 \le \phi_4 \le \pi/3 \qquad (7\text{-}29)$$

with additional conditions for case 2-2:

$$-\pi/2 \le \phi_5 \le 0 \qquad (7\text{-}30)$$

$$\phi_6 \ge \phi_5 + \pi/6 \qquad (7\text{-}31)$$

$$\phi_7 \ge \phi_6 + \pi/6 \qquad (7\text{-}32)$$

$$\phi_7 + \pi/6 \le \phi_8 \le \pi/3 \qquad (7\text{-}33)$$

where ϕ_1 to ϕ_8 are turntable angle orientations for eight arcs. These simplified constraints can quickly solve the problems chosen. The speed of this approach would allow the treatment planner to explore unusual treatment options that might yield better results than more standard techniques.

Given the physical limitation of turntable rotation, the side constraints for design variables are given by

$$-\pi/2 \leq \phi_j \leq \pi/2 \ , \ j=1,2\ldots8 \qquad (7\text{-}34)$$

Since all the constraint conditions given by Eqs. 7-26 to 7-33 satisfy side constraints given by Eq. 7-34, side constraints can be deleted in this problem.

Penalty function method for constrained minimization

The constraint conditions for case 2-1 and case 2-2 shown in Eqs. 7-26 to 7-33 can now be stated in the standard form to be implemented in the penalty function approach:

$$g_1(\mathbf{x}) = \phi_1 \leq 0 \qquad (7\text{-}35)$$

$$g_2(\mathbf{x}) = -\phi_1 - \pi/2 \leq 0 \qquad (7\text{-}36)$$

$$g_3(\mathbf{x}) = \phi_1 - \phi_2 + \pi/6 \leq 0 \qquad (7\text{-}37)$$

$$g_4(\mathbf{x}) = \phi_2 - \phi_3 + \pi/6 \leq 0 \qquad (7\text{-}38)$$

$$g_5(\mathbf{x}) = \phi_3 - \phi_4 + \pi/6 \leq 0 \qquad (7\text{-}39)$$

$$g_6(\mathbf{x}) = \phi_4 - \pi/3 \leq 0 \qquad (7\text{-}40)$$

with additional conditions for case 2-2:

$$g_7(\mathbf{x}) = \phi_5 \le 0 \qquad (7\text{-}41)$$

$$g_8(\mathbf{x}) = -\phi_5 - \pi/2 \le 0 \qquad (7\text{-}42)$$

$$g_9(\mathbf{x}) = \phi_5 - \phi_6 + \pi/6 \le 0 \qquad (7\text{-}43)$$

$$g_{10}(\mathbf{x}) = \phi_6 - \phi_7 + \pi/6 \le 0 \qquad (7\text{-}44)$$

$$g_{11}(\mathbf{x}) = \phi_7 - \phi_8 + \pi/6 \le 0 \qquad (7\text{-}45)$$

$$g_{12}(\mathbf{x}) = \phi_8 - \pi/3 \le 0 \qquad (7\text{-}46)$$

The penalty function used in the interior method is:

$$P(\mathbf{x}) = \sum_{j=1}^{J} \frac{-1}{g_j(\mathbf{x})} \qquad (7\text{-}47)$$

where $J = 6$ for case 2-1, and $J = 12$ for case 2-2. The vector $\mathbf{x}$ represents the arc variables ϕ_1 to ϕ_4 in case 1 and ϕ_1 to ϕ_8 in case 2. Our pseudo-objective function is now expressed explicitly by Eqs. 7-25, 7-1a and 7-24, and can be minimized through the unconstrained optimization algorithm programmed.

Feasible starting values of design vector

Because of the nature of the inverse function from the interior penalty function method, the pseudo objective function $\Phi(\mathbf{x}, r_p)$ will approach infinity on the constraint boundaries. The solution method using interior penalty functions proceeds as follows. First, a feasible design point in the allowable space is chosen inside the constrained set. Once the starting point is inside the constrained area, the optimum found will also be within this area. Once the minimum is achieved, it's location becomes the starting point for a new pseudo-objective function in which the value of r_p is reduced. The optimization process is repeated for a sequence of decreasing r_p values.

In addition to the requirement of feasible starting values, good estimated starting values within the feasible range saves iteration time to reach the optimum. In the present problem we may choose standard arc positions as starting values of arc variables. However, when the standard arc hits the critical organ, it is desirable to use as starting values the arc positions which do not hit the critical organ. This speeds reaching for the optimum.

Suppose we know the coordinates of four corners of the rectangle which sufficiently covers the critical organ on a series of CT slices, and the coordinate of the isocenter position in the BRW coordinate system. The purpose is to find the critical arc ranges which hit the critical organ defined by a series of rectangles. Using the geometrical relationship between spherical and cartesian BRW coordinate systems:

$$R = \sqrt{[(x_s - X_j)^2 + (y_s - Y_j)^2 + (z_s - Z_j)^2]} \qquad (7\text{-}49)$$

$$R \sin \theta \cos \phi = y_s - Y_j \qquad (7\text{-}49)$$

$$R \sin \theta \sin \phi = z_s - Z_j \qquad (7\text{-}50)$$

$$R \cos \theta = x_s - X_j \qquad (7\text{-}51)$$

From Eqs. 7-48 and 7-51:

$$\theta = \cos^{-1} \left[\frac{(x_s - X_j)}{R} \right] \qquad (7\text{-}52)$$

From Eqs. 7-49 and 7-50:

$$\phi = \tan^{-1} \left[\frac{(z_s - Z_j)}{(y_s - Y_j)} \right] \qquad (7\text{-}53)$$

A series of sets, (ϕ,θ), can be determined for the coordinates of the rectangular corners from Eqs. 7-52 and 7-53. Then, the critical arc range (lower and upper limits of turntable angle ϕ and gantry angle θ) in figure 7-6 are determined from this information. The critical arc range (θ^l-θ^u and ϕ^l-ϕ^u) determined can be constraint conditions or may be useful to determine the starting arc positions in computer-aided design optimization.

Result

Case 2-1 and case 2-2 were solved using four and eight design variables by the interior penalty function method. For the starting values of arc position, turntable angles

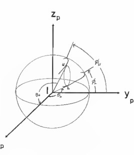

Figure 7-6. Geometrical relationship between critical arc range and isocentric NRW coordinate system.

-85°, -40°, 3° and 44°, which are close to the standard arc positions (-90°, -45°, 0°, 45°), were used. The "Hooke and Jeeves" and "Powell" methods were used for the unconstrained minimization subprogram in both case 2-1 and case 2-2. The starting design values and final design values for the two cases are given in table 7-2.

The values obtained from the computer algorithm represent useful results. The initial arc positions were assigned to hit the coordinates of critical organs. The final arc positions were searched not to hit the coordinates of critical organs while minimizing the weighted dose to the critical organs in both case 2-1 and 2-2. The number of iterations depends on termination criteria and kinds of algorithm used. The "Powell" method usually converges faster than the "Hooke and Jeeves" method, since we have adapted the efficient quadratic interpolation for 1-D search with the Powell method unlike the tedious step search used in the Hooke and Jeeves method.

As a consequence, the programs required approximately two minutes to search optimum parameters for four design variables using the Powell method and a modified cylindrical dose model with the Zenith 386/16 computer, and five minutes using the Hooke and Jeeves method. It took ten minutes to search optimum parameters for eight design variables using the Powell method, and more than one hour using the Hooke and Jeeves method.

Table 7-2 Optimum Variable Values

Case	Variable	Initial	Method	
			Hooke and Jeeve	Powell
Case 2-1	ϕ_1	-86°	-78°	-79°
	ϕ_2	41°	-28°	-11°
	ϕ_3	2°	12°	19°
	ϕ_4	44°	48°	50°
Case 2-2	ϕ_1	-86°	-60°	-56°
	ϕ_2	41°	-16°	-7°
	ϕ_3	2°	18°	20°
	ϕ_4	44°	52°	55°
	ϕ_5	-86°	-62°	-59°
	ϕ_6	41°	-17°	-11°
	ϕ_7	2°	18°	26°
	ϕ_8	44°	53°	56°

Figure 7-7a gives a montage of spatial contours of dose distribution on the coronal plane from a modified cylindrical dose model and the four optimum arc positions searched by the Powell method for case 2-1. The isodose shape in figure 7-7a shows a comparable result with that obtained from the exact dose model near low isodose line (Figure 7-7b). The dose distribution obtained with final search values in Fig. 7-7b gives improved distribution compared to the dose distribution obtained with the starting design in Fig. 6-4a, while keeping the target margin and minimizing dose near the critical organs. The search doesn't seem to be complete because of a rough termination criteria or local minimization.

Figure 7-8a gives a montage of spatial contours of dose distribution on the coronal plane from a modified cylindrical dose model and the eight optimum arc positions searched by the Powell method for case 2-2. The isodose shape in figure 7-8a shows a nearly comparable result with that obtained from the exact dose model near the critical area in low isodose line (Figure 7-8b). The dose distribution with the final search values in Fig. 7-8b gives a more optimum distribution than that obtained with the starting design values in Fig. 7-8c, while keeping the target margin and minimizing dose near the critical organs (lowered from 25% to 15%).

Figure 7-7. Isodose distribution on the coronal plane from a modified cylindrical dose model (a) and exact dose model (b), with the four optimum arc positions searched. The isodose lines displayed are from 10 to 90 in increment 10 and normalized by maximum.

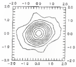
-2.0 -1.0 0.0 1.0 2.0
2.0 1.0 0.0 -1.0 -2.0
-2.0 -1.0 0.0 1.0 2.0
2.0 1.0 0.0 -1.0 -2.0

A

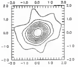
-2.0 -1.0 0.0 1.0 2.0
2.0 1.0 0.0 -1.0 -2.0
-2.0 -1.0 0.0 1.0 2.0
2.0 1.0 0.0 -1.0 -2.0

B

Figure 7-8. Isodose distribution on the coronal plane from a modified cylindrical dose model (a), and exact dose model (b) with the eight optimum arc positions searched. (c) represents the isodose distribution with the standard arcs and experimentally determined isocenter positions and collimator sizes. The isodose lines displayed are from 10 to 90 in increment 10 and normalized by maximum.

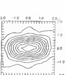
-2.0
-1.0
0.0
1.0
2.0
2.0
1.0
0.0
-1.0
-2.0
-2.0
-1.0
0.0
1.0
2.0
2.0
1.0
0.0
-1.0
-2.0

a

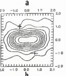
-2.0
-1.0
0.0
1.0
2.0
2.0
1.0
0.0
-1.0
-2.0
-2.0
-1.0
0.0
1.0
2.0
2.0
1.0
0.0
-1.0
-2.0

b

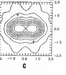
-2.0
-1.0
0.0
1.0
2.0
2.0
1.0
0.0
-1.0
-2.0
-2.0
-1.0
0.0
1.0
2.0
2.0
1.0
0.0
-1.0
-2.0

c

It is concluded that the modified cylindrical dose model is useful in calculating dose quickly for partial rotational arcs, which are generally used in arc-based radiosurgery, and gives dose distributions similar to those of the exact dose model except on high isodose lines, which makes this approximate dose model an attractive alternative to the exact dose model and much more efficient in finding optimum arc parameters to further minimize the dose to the critical organ through computer-aided design optimization after determining optimum isocenter positions and collimator sizes either experimentally or by computer-aided design optimization.

Case 3

In the previous two cases the isocenter positions and collimator sizes were determined experimentally to shape the dose distribution to the target, and were followed by an analytic optimization technique to search for the best arc parameters to further minimize the dose at critical points chosen. In this case computer-aided design optimization is used to find all the optimum parameters involved. The first step is to determine the isocenter positions and collimator sizes which fit the target shape with a high isodose surface while maximizing dose gradient between target and surrounding normal structures. A rule based search method with a spherical dose model is used to shape the target using multiple isocenters and multiple collimators. The second step is to find optimum arc parameters, with which the selected critical points can be further minimized by varying arc parameters while maintaining target dose. Two previous zero order search algorithms or a new rule-based search method could be used with the cylindrical dose model. The second step may be deleted, if further minimization to the critical points is not necessary. In the following examples, we consider arbitrary 3-D patient data which can be represented by a series of transverse sectional contours along the patient. This set of 3-D patient data contains target cross-sections and relevant normal tissue outlines or critical points.

Problem Chosen

Case 3-1· The target is assumed to be an elongated cylindrical shape (height=2.0 cm, diameter=0.4 cm) which is represented by a series of contours from three slices. The critical organs are also located at two different positions, $C_3(0,1,1)$ and $C_4(0,-1,-1)$ in the reference BRW coordinate system (Fig. 7-9a).

Case 3-2: The target is assumed to be an elongated cone shape (height= 2.4 cm, diameter= 1.2 cm) which is represented by a series of contours from four slices (Fig 7-9b).

We optimize case 3-1 and case 3-2 using an analytical approach. The isocenter positions and collimator sizes are

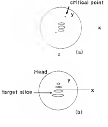

Figure 7-9. The schematic diagram for case 3.

determined to shape the dose to the target using a spherical dose model and rule-based search methods in two cases, and is followed by the search for the best arc parameters (arc spacing or arc weighting) to minimize dose at the critical points chosen in case 3-1.

Optimum isocenter positions and collimator sizes

The isocenter positions and collimator sizes are determined using the spherical dose model and rule-based search methods. Our aim is now to find optimum isocenter positions and collimator sizes with the standard four arcs such that the objective function:

$$\Sigma\ (D_t(\mathbf{x})-D_n(\mathbf{x}))^2 \qquad (7\text{-}1b)$$

is maximized subject to constraint conditions described in Eqs. 7-2 and 3.

$$D^l \le D_t(\mathbf{x}) \le D^u \quad \text{Constraints} \qquad (7\text{-}2)$$

and

$$\mathbf{x}^l \le \quad \mathbf{x} \quad \le \mathbf{x}^u \quad \text{Side constraints} \qquad (7\text{-}3)$$

where

$\mathbf{x}$ = Design vector (isocenter position and collimator size for each four standard arcs)

$D_t(\mathbf{x})$ = Dose to the target at position t

$D_n(x)$ = Dose to the normal structure position n around target boundary

D^l, D^u = Lower and upper limits of the desired dose

x^l, x^u = Lower and upper limits of the design variables

The normal structure positions (n) are selected at a certain distance (e.g. 5mm) away from the target constraint positions (t) located at target contoure on each slice. The sum of the differances of relative dose between two couples is associated with the requirement of steep fall-off around the target region in radiosurgery. The criteria of uniformity of dose to the target region is also defined by lower and upper dose constraints (e.g. relative dose 0.8 to 1.0) at preselected points (t) within the target area. According to the physical limitation of collimator size (e.g. 1.0 to 3.5 cm) and isocenter position, the lower and upper limit for design variables are considered.

Case 3-1 and case 3-2 were solved using eight design variables (i.e. six variables for two isocenter positions and two variables for two collimator sizes) by the rule-based search method developed. For the starting values of design variables, two isocenter positions which are close to the estimated center of each spherical compartment were randomly chosen, as were two collimator sizes, which are less than the estimated sizes of each spherical compartment. The rule-based search method was used for the constrained maximization routine in both case 3-1 and case 3-2. The starting and final design values for the two cases are given in table 7-3.

The values obtained from the computer algorithm represent useful results. The initial variables were unreasonably assigned to undercover the target volume from the desired isodose surface (e.g. 50 to 70 %). The final optimum isocenter positions and collimator sizes were searched to sufficiently cover the target volume within the desired isodose surface while maximizing the dose gradient between target region and surrounding normal structures. The number of iterations depends on the accuracy desired at the cost of time consumed.

As a consequence, the programs required approximately two tminutes to search approximate optimum parameters of two isocenter positions and two collimator sizes for either case 3-1 or 3-2 within one cycle using the rule-based search algorithm and a spherical dose model with the Zenith 386/16 computer with a math coprocessor.

Figure 7-10a and d show montages of spatial contours of dose distribution on the plane along two isocenters and on the vertical plane from a exact dose model and the optimum isocenters and collimator sizes searched by the rule-based search algorithm for case 3-1 and 3-2. The search may not be the same as the optimum values experimentally determined in Fig.6-11 because of initial guesses, iteration numbers, and the approximate dose model used. When we get

Table 7-3 Optimum Variable Values

Case	Variable	Initial	Method	
		(cm)	Rule-based	Powell
Case 3-1	x_1	0.1	0.13	
	y_1	-0.1	-0.13	
	z_1	-0.4	-0.66	
	C_1	1.0	1.4	
	x_2	-0.1	-0.03	
	y_2	0.2	0.03	
	z_2	0.5	0.62	
	C_2	1.0	1.2	
	ϕ_1	-86°		-89°
	ϕ_2	-40°		-59°
	ϕ_3	2°		-29°
	ϕ_4	44°		36°
	ϕ_5	-86°		-84°
	ϕ_6	-40°		-53°
	ϕ_7	2°		-18°
	ϕ_8	44°		36°
Case 3-2	x_1	0.1	0.13	
	y_1	-0.1	-0.13	
	z_1	-0.4	-0.58	
	C_1	1.0	1.0	
	x_2	-0.1	-0.17	
	y_2	0.2	0.17	
	z_2	0.5	1.06	
	C_2	1.0	2.4	

Figure 7-10. Isodose distributions on the plane along two isocenters (a,c) and on the vertical plane (b,d) from a exact dose model with the optimum isocenters and collimator sizes searched by the rule-based search algorithms for case 3-1 (a,b) and case 3-2 (c,d). The isodose lines displayed are from 90 to 10 in decrement 10 and normalized by maximum.

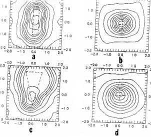
a
b
c
d
-2.0
-1.0
0.0
1.0
2.0

approximate optimum values using computer search methods and approximate dose models, it is useful to check the final dose distribution visually using the exact dose model with final tuning of optimum variables.

The isodose shape in figures 7-10a and d shows a comparable result with that obtained from the spherical dose model near target area in the high isodose lines (Figure 7-11a and d). The dose distribution with the final search values in Fig. 7-10a and d give a more optimum distribution than that obtained with the starting design values in Fig. 7-12a and d, while keeping the target margin and maximizing dose gradient. It is known that the dose distribution with a two isocenter approach in Fig. 7-10a and d gives a better distribution than that obtained with a single isocenter approach in Fig. 7-13a and d, while confining the target margin within the 70% isodose surface saving the dose to the normal structure area.

It is concluded that the spherical dose model is useful in calculating dose quickly for equally spaced arcs, which are generally used in standard stereotactic radiosurgery, and gives dose distributions similar to those of the exact dose model except at low isodose lines, which makes this approximate dose model an attractive alternative to the exact dose model and much more efficient in finding optimum isocenter positions and collimator sizes to fit the target shape within high isodose surface while maximizing dose

Figure 7-11. Isodose distributions on the planes along two isocenters (a,c) and on the vertical plane (b,d) from a spherical dose model with the optimum isocenters and collimator sizes searched by the rule-based search algorithms for case 3-1 (a,b) and case 3-2 (c,d). The isodose lines displayed are from 90 to 10 in decrement 10 and normalized by maximum.

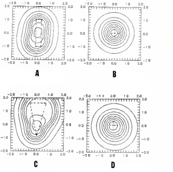
-2.0
-1.0
0.0
1.0
2.0
A
B
C
D

Figure 7-12. Isodose distributions on the plane along two isocenters (a,c) and on the vertical plane (b,d) form a exact dose model with the starting design variables (isocenter position and collimator size) with standard arc system for case 3-1 (a,b) and case 3-2 (c,d). The isodose lines displayed are from 90 to 10 in decrement 10 and normalized by maximum.

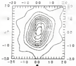
-2.0 -1.0 0.0 1.0 2.0
2.0
1.0
0.0
-1.0
-2.0

A

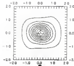
-2.0 -1.0 0.0 1.0 2.0
2.0
1.0
0.0
-1.0
-2.0

B

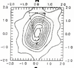
-2.0 -1.0 0.0 1.0 2.0
2.0
1.0
0.0
-1.0
-2.0

C

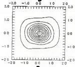
-2.0 -1.0 0.0 1.0 2.0
2.0
1.0
0.0
-1.0
-2.0

D

Figure 7-13. Isodose distributions for single isocenter technique with a cylindrical target (a,b), and cone-shaped target (c,d) covered by 80% isodose surface. The isodose lines displayed are from 90 to 10 in decrement 10 and normalized by maximum.

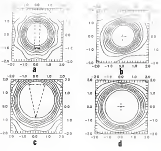
a
b
c
d
−2.0
−1.0
0.0
1.0
2.0

gradient near the target area through computer-aided design optimization.

Optimum arc parameters

The isocenter positions and collimator sizes were determined to shape the dose distribution to the target using a spherical dose model and rule-based search methods in case 3-1 and case 3-2. The next step is the search for the best arc parameters (arc spacing or arc weighting) to further minimize dose at the critical points chosen in case 3-1.

Our aim is now to find optimum arc positions (turntable orientation) and arc weightings for the individual standard arcs (100 deg arc length) such that the objective function:

$$\Sigma\ W_c\ D_c(\mathbf{x}) \qquad (7\text{-}1a)$$

is minimized subject to the constraint conditions described in Eq. 7-2 and 7-3.

$$D^l \le D_c(\mathbf{x}) \le D_c^u \quad \text{Constraints} \qquad (7\text{-}2)$$

and

$$\mathbf{x}^l \le \mathbf{x} \le \mathbf{x}^u \quad \text{Side constraints} \qquad (7\text{-}3)$$

where

$\mathbf{x}$ = Design vector (turntable orientations and arc weightings)

$D_c(x)$ = Dose to the critical organ at position c

W_c = weighting factor to evaluate importance of critical organ at position c

D^l, D^u = Lower and upper limits of the desired dose

x^l, x^u = Lower and upper limits of the design variables

The c's represent positions of critical organs designated for case 3-1. D_c is relative dose to the critical organ located at position c, and is represented by the approximate dose model given by Eq. 5-91. All the arc weights are assumed to be one, and the critical organ weights W_c are assumed to be one. The criteria of uniformity of dose to the target region is also defined by lower and upper dose constraints (e.g. relative dose 0.8 to 1.0) at preselected points t's within the target area. According to the physical limitation of turntable orientation (e.g. -90 to 90), the lower and upper limit for design variables are considered.

Case 3-1 could be solved using eight design variables (i.e. eight turntable orientations) by the penalty function approach described in case 2-2. The another simple alternative might be to utilize a step search method with constraint conditions described in Eqs. 7-2 and 3 even though it is not efficient in the case of many arc variables.

Figures 7-14 give montages of spatial contours of dose distribution on the plane along from an exact dose model and

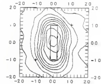

Figure 7-14. Isodose distribution on the coronal plane along two isocenters from a exact dose model. The optimum isocenter positions and collimator sizes were searched by the rule-based search algorithm, and optimum arc positions were searched by conjugated direction search algorithm.

optimum parameters (optimum isocenters, collimator sizes and turntable orientations) searched by the rule-based search algorithm and penalty function method for case 3-1. The starting and final design values are given in table 7-3.

The dose distribution with the final search values in Fig. 7-14 gives a better distribution than that obtained with the starting design values in Fig. 7-12a or 7-10a, while keeping the target margin and minimizing dose near the critical points.

It is concluded that approximate dose models (spherical and cylindrical) are useful in calculating dose quickly for standard one arc or multiple equal spaced arcs, which are generally used in standard stereotactic radiosurgery. These approximate dose models give dose distributions similar to those of the exact dose model, which makes this approximate dose model an attractive alternative to the exact dose model. These models are efficient in finding optimum parameters to fit the target shape within a high isodose surface while maximizing dose gradient near target area and minimizing dose near critical organs through computer-aided design optimization. Figure 7-15 shows the procedure for optimization using computer-aided design optimization and approximate dose model.

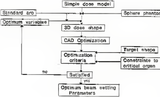

Figure 7-15. The procedure for optimization using computer aided design optimization

CHAPTER 8
CONCLUSION

We discussed two approaches to optimize dose distribution for arc-based radiosurgery. The experimental approach with multiple isocenters is a suitable treatment technique for elongated target shapes. Potential studies for shaping 2-D (thin plate) or 3-D (arbitrary) targets are expected in the future. The simple spherical dose model will be a useful tool to test these problems. However, the use of too many isocenters may not be desirable to shape the complicated target exactly, since it gives little benefit with much increased effort. A conformal therapy using beam's eye view might be a better approach to shape the more complicated targets with an computer-aided design optimization in a future study.

We conclude that in optimal dose distribution for arc-based radiosurgery, it is important to use approximate forms for dose calculation in 3-D space. In the current work we use a spherical or cylindrical dose model to simulate the exact dose distribution for a standard arc, and optimize through computer-aided design optimization. Since the dose distribution from the simple dose model is similar to that from the exact dose model, we conclude that computer-aided design optimization with a simple dose model is an efficient and practical alternative to the trial and error method using the exact dose model. Several improvements are expected in the future. One is finding an arc correction factor for any length of arc in addition to the standard arcs (100° and 180°). This modification makes it possible to use the start and stop positions of gantry angle as variables in CAD optimization. Since the dose distributions are not changed much as target position or head contour vary, it may not be necessary to correct for different target positions and head contours. In the present work only single target in the head was considered. It must be interesting points to consider multiple targets in future study even though those cases are rare in clinical situations. Another task is finding better approximate forms using a different analytical form.

We may consider the possibility of using computer-aided design optimization to find all the optimum parameters using rule-based or step search method. However, the use of too many variables is not efficient and may be ill-conditioned with the CAD optimization technique. The most important and difficult problem is how to find efficient optimization criteria and that of specifying the optimization criteria in the form of simple mathematical formalisms. It may be desirable to develop a few standard plans to use as starting points and then search for an optimal result by varying some parameters using multiple steps. The CAD optimization technique should be initiated on an expert system that will interface between the treatment planner and the three-dimensional treatment planning system. Another task is to develop a method which simulates a real patient treatment with a reference patient model.

Our two approaches are based on physical optimization criteria other than complicated biologic optimization criteria. The statistical approach to optimization including the dose-response model, tumor control probabilities, and normal tissue complication probabilities may be appropriately applied to radiosurgery optimization if all major factors or statistical information can be accounted for. At the simplest level, the physical optimization criteria might be good to implement CAD optimization techniques, and could be used until all the biologic information are obtained. The selection criteria and the cost of the function evaluation for the objective function and constraints are very important to the success of the computer analytic optimization. The simplified dose model and simple selection criteria are essential in analytical optimization techniques.

In the present work, the popular nonlinear programming, "Hooke and Jeeves method" and "Powell method" were used with an interior penalty function approach. Although these methods showed some good results in simple examples, this method may not be the best choice. After testing some other optimization methods (zero order, first order, or second order with penalty approach or direct search method), the most reliable method may be applied to practical optimization problems.

REFERENCES

Ahnesjo, A., "Application of Transform Algorithms for Calculation of Absorbed Dose in Photon Beams," Proc. 8th Int. Conf. on the Use of Computers in Radiotherapy, pp. 17 (1984)

Ammeraal, L., Programming Principles in Computer Graphics, John Wiley & Sons Press, Chichester (1987)

Aoki, Y., Akanuma, A., Sakata, K., Karasawa, K., Nakagawa, K., Muta, N., Hosoi, Y., Onogi, Y., Kojima, K., and Iio, M., "Multiaxial Treatment Technique," Proc. 9th Int. Conf. on the Use of Computers in Radiotherapy, pp. 345 (1987)

Bahr, G.K., Kereiakes, J.G., Horwitz, H., Finney, R., Galvin, J., and Goode, K., "The Method of Linear Programming Applied to Radiation Treatment Planning," Radiology, 91:686 (1968)

Batho, M.F., "Lung Correction in Co-60 Beam Therapy," Canad. Assoc. Radiol. J., 15:79 (1964)

Bauer-Kirpes, B., Schlegel, W., Boesecke, R., and Lorenz, W.J., "Display of Organs and Isodoses as Shaded 3-D Objects for 3-D Therapy Planning," Int. J. Radiat. Oncol. Biol. Phys., 13:135 (1987)

Ben-Israel A., Ben-tal, A., and Zlobec, S., Optimality in Nonlinear Programming: A Feasable Directions Approach, Wiley-interscience NY (1981)

Bentley, R.E., and Milan, J., "An Interactive Digital Computer System for Radiotherapy Treatment Planning," Brit. J. Radiol., 44:826 (1971)

Bjarngard, B.E., and Siddon, R.L., "A Note on Equivalent Circles, Squares, and Rectangles," Med. Phys., 9:258 (1982)

Bower, B., Schlegel, W., Roesecke, R., Doll, J., Hartmann, G., and Lorenz, W.J., "Three-Dimensional Planning of Conformation Therapy," Proc. Int. Symp. CAR'85, pp. 388 (1985)

Boyer, A.L., and Mok, E.C., "Photon Beam Model Using Fourier Transform Techniques," Proc. 8th Int. Conf. on the Use of Computers in Radiotherapy, pp. 14 (1984)

Brahme, A., Roos, J.E., and Laix, I., "Solution of an Integral Equation Encountered in Rotation Therapy," Phys. Med. Biol. 27:1221 (1982)

Cassel, J.K., Hobody, A.P., and Parker, P.R., "The Implementation of a Generalized Batho Inhomogeneity Correction for Radiotherapy Planning with Direct Use of CT Numbers," Phys. Med. Biol., 26:825 (1981)

Chin, L.M., Kijewski, P.K., Svensson, G.K., and Bjarngard, B.E., "Dose Optimization with Computer-Controlled Gantry Rotation, Collimator Motion and Dose-Rate Variation," Int. J. Rad. Oncol. Biol. Phys., 9:723 (1983)

Chin, L.M., Kijewski, P.K., Svensson, G.K., Chaffey, J.T., Levene, M.B., and Bjarngard, B.E., "A Computer-Controlled Radiation Therapy Machine for Pelvic and Para-Aortic Nodal Areas," Int. J. Rad. Oncol. Biol. Phys., 7:61 (1981)

Chin, L.M., Sidden, R.L., Svensson, G.K., and Rose, C., "Progress in 3-D Treatment Planning for Photon Beam Therapy," Int. J. Radiat. Oncol. Biol. Phys., 11:2011 (1985)

Chung-bin, A., and Melyala, R., "Optimization of Conformation Therapy by Variation of Dose Rate," Proc. 9th Int. Conf. on the Use of Computers in Radiotherapy, pp. 223 (1987)

Colombo, F., Benedetti, A., Pozza, F., Avenzo, R.C., Marchetti, C., Chierego, G., and Zanardo, A., "External Stereotactic Irradiation by Linear Accelerator," Neurosurgery, 16:154 (1985)

Cunningham, J.R., "Scatter-Air Ratio," Phys. Med. Biol., 17:42 (1972)

Dahlin, H., and Sarby, B., "Destruction of Small Intracranial Tumors with Co-60 gamma radiation," Acta Radiol., 14:209 (1975)

Dixon, R.L., Ekstrand, K.E., and Huff, W.J., "Beam Characteristics of the Varian 6 MV Clinac 6X Accelerator," Int. J. Radiat. Oncol. Biol. Phys., 2:585 (1977)

Fiacco, A.V., and McComick, G.P., Nonlinear Programming: Sequential Unconstrained Minimization Techniques, John Wiley and Sons Press, New York (1968)

Fraass, B.A., McShan, D.L., and Weeks, K.L. "3-D Treatment Planning: III. Complete Beam's Eye View Planning Capabilities," Proc. 9th Int. Conf. on the Use of Computers in Radiotherapy, pp. 193 (1987)

Friedman, W.A., and Bova, F.J., "The University of Florida Radiosurgery System," Surg. Neurol., 32:334 (1989)

Goitein, M., Abrams, M., Rowell, D., Pollari, H., and Wiles, J., "Multi-Dimensional Treatment Planning: II. Beam's Eye View, Back Projection through CT Sections," Int. J. Radiat. Oncol. Biol. Phys., 9:789 (1983)

Gupta, S.K., and Cunningham, J.R., "Measurement of Tissue Air Ratio and Scatter Functions for Large Field Sizes for Cobalt-60 Gamma Radiation," Brit. J. Radiol., 30:7 (1966)

Hartmann, G.H., Schlegel, W., Strum, V., Lorenz,W.J., "A Fast Algorithm to Calculate Three Dimensional Dose Distributions for Radiosurgery," Proc. 8th Int. Conf. on the Use of Computers in Radiotherapy, pp. 99 (1984)

Hartmann, G.H., Schlegel, W., Sturm, V., Kober, B., Pastyr, O., and Lorenz, W.J., "Cerebral Radiation Surgery Using Moving Field Irradiation at a Linear Accelerator Facility," Int. J. Radiat. Oncol. Biol. Phys., 11:1185 (1985)

Haywood, J,K., Bomford, C.K., Phil, M., Inst, P., and Hatton, J.A., "A Less Empirical Method of Representing Megavoltage Beams for Use in Rapid Radiotherapy Dose Calculations," Brit. J. Radiol., 52:709 (1979)

Heiftz, M.D., Wexler, M., and Thompson, R., "Single Beam Radiotherapy Knife: A Practical Theoretical Model," J. Neurosurg, 60:814 (1984)

Heilbrun, M.P., Roberts, T.S., Wells, T.H., Ball, R.D., and Cosman,E.R., *Instruction Manual for the BRW Brown-Robert-Wells CT Stereotactic System*, Radionics Burlington MA (1983)

Hodes, L., "Semiautomatic Optimization of External Beam Radiation Treatment Planning," Radiology, 110:191 (1974)

Holmes, W.F., "External Beam Treatment Planning with the Programmed Console," Radiology, 94:391 (1970)

Hooke, R., and Jeeves, T.A., "Direct Search Solution of Numerical and Statistical Problems," Journal of the Association for Computing Machinery, 8:212 (1961)

Hope, C.S., Laurie, J., and Halnan K.E., "A Computer Program for Optimized Stationary Beam Treatment Planning Using Score Functions," Comput. Progr. Biomed., 2:221 (1972)

Hope, C.S., Laurie, J., Orr, J.S., and Halnan, K.E., "Optimization of X-Ray Treatment Planning by Computer Judgement," Phys. Med. Biol., 12:531 (1967)

Hosoi, Y., Onogi, Y., Muta, N., Nakagawa, K., Karasawa, K., Sakata, K., Apki, Y., Akanuma, A., Iio, M., Kikuchi, H., and Fujita, R., "Dose Corresponding Technique with Categorized Target Shape," Proc. 9th Int. Conf. on the Use of Computers in Radiotherapy, pp. 157 (1987)

Houdek, P.V., Vanburen, J., and Fayos,J.V., "Dosimetry of Small Radiation Fields for 10 MV X rays," Med. Phys., 4:333 (1983)

Houdek, P.V., Fayos, J.V., Vanburen, J.H., and Ginsberg, M.S., "Stereotactic Radiotherapy Technique for Small Intracranial Lesions," Med. Phys., 12:469 (1985)

Houlard, J.P., and Dutreix, A., "3D Display of Radiotherapy Treatment Plans," Proc. 8th Int. Conf. on the Use of Computers in Radiotherapy, pp. 219 (1984)

Jacoby, S.L.S., Kovelick, J.S., and Pizzo, J.T., Iterative Methods for Nonlinear Optimization Problem, Prentice-hall, Englewood Cliffs NJ (1972)

Johns, H.E., and Cunningham, J.R., The Physics of Radiology, Chrles, C. Thomas Springfield IL, pp 416-419 (1983)

Kalnaes, O., "Computer Program for Dose Planning with Analytical Representation of Radiation Fields," Acta Radiol. Ther. Phys. Biol., 4:449 (1966)

Khan, F.M., Sewchand, W., Lee, J., and Williamson, J.F., "Revision of Tissue-Maximum Ratio and Scatter-Maximum Ratio Concepts for Cobalt 60 and Higher Energy X-Ray Beams," Med. Phys., 7:230 (1980)

Kornelson, R.O., and Young, M.E.J., "Empirical Equations for the Representation of Depth Dose Data for Computerized Treatment Planning," Brit. J. Radiol., 48:739 (1975)

Larsson, B., Liden, K., and Sarby, B., "Irradiation of Small Structures Through Intact Skull," Acta Radiol. 13:512 (1974)

Leksell, L., "Occasional Review: Stereotactic radiosurgery," J. Neurosurg, 46:797 (1983)

Levene, M.E., Kijewski, P.K., Chin, L.M., Bengt, S.M., Bjarngard, E., and Hellman, S. "Computer-Controlled Radiation Therapy," Radiology, 129:769 (1978)

Lind, B.K., and Brahme, A., "Optimization of Radiation Therapy Dose Distributions Using Scanned Electron and Photon Beams and Multileaf Collimators," Proc. 9th Int. Conf. on the Use of Computers in Radiotherapy, pp. 235 (1987)

Lyman, J.T., and Howard, J., "Dosimetry and Instrumentation for Helium and Heavy Ions," Int. J. Radiat. Oncol. Biol. Phys., 3:81 (1977)

Lyman, J.T., Kanstein, L., Yeater, F., Fabrikant, J.I., and Frankel, K.A., "A Helium Ion Beam for Stereotactic Radiosurgery of Central Nervous System Disorders." Med. Phys., 3:695 (1986)

Lutz, W., Winston, K.R., and Maleki, N., "A System for Stereotactic Radiosurgery with a Linear Accelerator," Int.J. Radiat. Oncol. Biol. Phys., 14:373 (1988)

Mackie, T.R., and Scrimger, J.W., "Computing Radiation Dose for High Energy X-Rays Using A Convolution Method," Proc. 8th Int. Conf. on the Use of Computers in Radiotherapy, pp. 36 (1984)

Manglos, S.H., Floyd, C.E., Jaszczak, R.J., Greer, K.L., Harris, C.C., and Coleman, R.E., "Experimentally Measured Scatter Fractions and Energy Spectra as a Test of Monte Carlo Simulations," Phys. Med. Biol., 32:335 (1987)

Mantel J., Perry R, and Weinham, J.J., "Automatic Variation of Field Size and Dose Rate in Rotation Therapy," Int. J. Rad. Oncol. Biol. Phys., 2:697 (1977)

McDonald, S.C., and Rubin, P., "Optimization of External Beam Radiation Therapy," Int. J. Rad. Oncol. Biol. Phys., 2:307 (1977)

Milan, J., and Bentley, R.E., "The Storage and Manipulation of Radiation Dose Data in a Small Digital Computer," Brit. J. Radiol., 47:115 (1974)

Mohan, R., Barest, G., Brewster, L.J., Chui, C.S., Kutcher, G.J., Laughlin, J.S., and Fuks, Z., "A Comprehensive Three-Dimensional Radiation Treatment Planning System," Int. J. Radiat. Oncol. Biol. Phys., 15:481 (1988)

Mohan, R.M., Brewster, L.J., and Barest, G.D., "A Technique for Computing Dose Volume Histrogram for Structure Combinations," Med.Phys., 14:1048 (1987)

Myrianthopoulos, L.C., Chan, G.T.Y., Spelbring, D.R., Pelizzari, C.A., Rosenberg, I., Vijayakumar, S., and Halpern, H.J., "Beam's Eye View Volumetrics: An Aid in Rapid Treatment Plan Optimization," The 30th Annual Meeting of the American Society for Therapeutic Radiology and Oncology, (1988)

Orchard, P.G., "A New Presentation of Data in Cobalt-60 Beam Dosimetry," Brit. J. Radiol., 37:756 (1964)

Orr, J.S., "Optimization of Radiotherapy Treatment Planning," Comput. Progr. Biomed., 2:216 (1972)

Pike, B., Podgorsak, E.B., Peters, T.M., and Pla, C., "Dose Distributions in Dynamic Stereotactic Radiosurgery," Med. Phys., 14:780 (1987)

Powell, M.J.D., "An Efficient Method for Finding the Minimum of a Function of Several Variables without Calculating Derivatives," Comput J., 7:303 (1964)

Purdy, J.A., Wong, J.W., Harms, W.B., Drzymala, R.E., Emami, B., Matthews, J.W., Krippner, K., and Ramchander, P.K., "Three Dimensional Radiation Treatment Planning System," Proc. 9th Int. Conf. on the Use of Computers in Radiotherapy, pp. 277 (1987)

Redpath, A.T., Vickery, B.L., and Wright, D.H., "A New Technique for Radiotherapy Planning Using Quadratic Programming," Phys. Med. Biol., 21.781 (1976)

Reynolds, R.A., Sontag, M.R., and Chen, L.S., "An Algorithm for Three-Dimensional Visualization of Radiation Therapy Beams," Med. Phys., 15:24 (1988)

Rice, R.K., Hansen, J.L., Svensson, G.K., and Siddon, R.L., "Measurement of Dose Distribution in Small Beams of 6 MV X-rays," Phys. Med. Biol., 32:1087 (1987)

Saw, C.B., Ayyangar, K., and Suntharalingam, N., "Coordinate Transformations and Calculations of the Angular and Depth Parameters for a Stereotactic System," Med. Phys., 14:1042 (1987)

Schlegel, W., Boesecke, R., Bauer, B., Alandt, K., and Lorenz, W.J., "Dynamic Therapy Planning" Proc. 9th Int Conf. on the Use of Computers in Radiotherapy, pp. 361 (1987)

Shoup, T.E., and Mistree, F., Optimization Methods with Applications for Personal Computers, Prentice-Hall, Englewood Cliffs NJ (1987)

Siddon, R.L., "Solution to Treatment Planning Problems Using Coordinate Transformations," Med. Phys., 8:766 (1981)

Siddon, R.L., "A 3D Ray-Tracing Algorithm for Radiotherapy Applications," Phys. Med. Biol. 30:817 (1985)

Siddon, R.L., and Barth, N.H., "Stereotaxic Localization of Intracranial Targets," Int. J. Radiat. Oncol. Biol. Phys., 13:1241 (1987)

Sontag, M.R., and Cunningham, J.R., "Correction to Absorbed Dose Calculations for Tissue Inhomogeneities," Med. Phys., 4:431 (1977)

Sontag, M.R., and Cunningham, J.R., "The Equivalent Tissue Air Ratio Method for Making Absorbed Dose Calculations in a Heterogeneous Medium," Radiology, 129:787 (1978)

Starkschall, G., "A Constrained Least-Squares Optimization Method for External Beam Radiation Therapy Treatment Planning," Med. Phys., 11:659 (1984)

Sterling, T.D., Perry, H., and Katz, K., "Automation of Radiation Treatment Planning IV. Derivation of Mathematical Expression for the Percent Depth Dose Surface of Cobalt-60 Beams and Visualization of Multiple Field Dose Distributions," Brit. J. Radiol., 37:544 (1964)

Sterling, T.D., and Weinkam, J., "Automation of Radiation Treatment Planning. VI. A General Field Equation to Calculate Percent Depth Dose in the Irradiated Volumes of Cobalt 60 Beams," Brit. J. Radiol., 40:463 (1967)

Tabushi, K., Itoh, S., Sakura, M, Kutsutani-Nakamura, Y., Iinuma, T., and Arai, T., "A Method for Calculating the Optimum Irradiation Condition for Intracavitary Radiotherapy Using Quadratic Programming," Phys. Med. Biol., 33:515 (1988)

Takahashi, S., "Conformation Radiotherapy Rotation Techniques as Applied to Radiography and Radiotherapy of Cancer," Acta Radiol (Suppl), 242:57 (1962)

Takai, M., Nishimura, T., and Kaneko, M., "Optimization of the Conformation Radiotherapy," Proc. 9th Int. Conf. on the Use of Computers in Radiotherapy, pp. 231 (1987)

Thomas, R.L., and Haybittle, J.L., "A Widely Applicable Method for Computing Dose Distributions Form External Megavoltage Beams," Brit. J. Radiol., 48:749 (1975)

Tolli, H., and Ragnhult, I., "An Analytical Method to Solve an Optimization Problem in Brachytherapy." Proc. 9th Int. Conf. on the Use of Computers in Radiotherapy, pp. 123 (1987)

Trump, J.G., Wright, K.A., and Smedal, M.I., "Synchronous Field Shaping and Protection in 2-Million-volt Rotational Therapy," Radiology, 76:275 (1961)

Tsien, K C., "The Application of Automatic Computing Machines to Radiation Treatment Planning," Brit. J. Radiol., 28:432 (1955)

Van de Geijn, J., "The Computation of Two and Three Dimensional Dose Distributions in Cobalt 60 Teletherapy," Brit. J. Radiol., 38:369 (1965)

Van de Geijn, J , "A New Description of the Photon Beam Peak-Depth Profile as a Function of Field Size," Med. Phys., 13(6):904 (1986)

Van de Geijn, J., Fraas, B.A., Miller, R.W., and Creecy, R.H, "The Projective Beam Model: An Updated on Model and Characteristic Data," Proc. 8th Int. Conf. on the Use of Computers in Radiotherapy, pp. 94 (1984)

Van Dyk, J., "Practical Dosimetric Considerations of a 10 MV Photon Beam," Med. Phys., 4:145 (1977)

Van Panthalean, R.B., Three Dimensional Teletherapy Treatment Planning, (1986)

Webb, S., Fox, R.A., "Verification by Monte Carlo Methods of a Power Law Tissue-Air Ratio Algorithm for Inhomogeneity Corrections in Photon Beam Dose Calculations," Phys. Med. Biol., 25:225 (1980)

Wong, J.W., Slessinger, E.D., Rosenberger, F.U., Krippner, K., and Purdy, J.A., "The Delta-Volume Method For 3-Dimensional Photon Dose Calculation," Proc. 8th Int. Conf. on the Use of Computers in Radiotherapy, pp. 26 (1984)

Wong, J.W., and Henkelman, R.M., "A New Approach to CT Pixel-based Photon Dose Calculations in Heterogeneous Media," Med. Phys., 10:199 (1983)

Worthley, B., and Cooper, R.E.M., "Empirical Formulae for Calculation of Depth Dose," Phys. Med. Biol., 12:229 (1967)

Yuen K., McParland, B.J., and Kornelson, R.O., "A Differential Method for Inhomogeneity Correction on Dose in a Photon Beam," Med. Phys., 11:15 (1984)

BIOGRAPHICAL SKETCH

Tae-suk Suh was born on March 13, 1957, in Seoul, the capital of Republic of Korea. He graduated from Kyunggi High School and Seoul National University in Korea. He received a Bachelor of Science in Nuclear Engineering from the Seoul National University in 1980. After graduation, he served in the Korean Army for two years as a citizen duty. In August 1984 he emigrated to United States as a permanent resident. Since August 1984, he has been involved in the graduate program in the Nuclear Engineering Sciences Department at University of Florida. He received the degree of Master of Science in the field of health physics in August 1986. Since August 1986, he has been involved in the medical physics program, studying for the Ph.D. From 1987 until 1990, he held graduate assistantships in the Radiology Department and has worked on projects involving the development of the University of Florida stereotactic radiosurgery system.

He is a student member of the American Association of Physicists in Medicine.

I certify that I have read this study and that in my opinion it conforms to acceptable standards of scholarly presentation and is fully adequate, in scope and quality, as a dissertation for the degree of Doctor of Philosophy.

Frank J. Bova

Frank J. Bova, Chair
Associate Professor of
Nuclear Engineering Sciences

I certify that I have read this study and that in my opinion it conforms to acceptable standards of scholarly presentation and is fully adequate, in scope and quality, as a dissertation for the degree of Doctor of Philosophy.

Lawrence T. Fitzgerald

Lawrence T. Fitzgerald
Associate Professor of
Nuclear Engineering Sciences

I certify that I have read this study and that in my opinion it conforms to acceptable standards of scholarly presentation and is fully adequate, in scope and quality, as a dissertation for the degree of Doctor of Philosophy.

Genevieve Roessler

Genevieve Roessler
Associate Professor of
Nuclear Engineering Sciences

I certify that I have read this study and that in my opinion it conforms to acceptable standards of scholarly presentation and is fully adequate, in scope and quality, as a dissertation for the degree of Doctor of Philosophy.

David Hintenlang

David Hintenlang
Assistant Professor of
Nuclear Engineering Sciences

I certify that I have read this study and that in my opinion it conforms to acceptable standards of scholarly presentation and is fully adequate, in scope and quality, as a dissertation for the degree of Doctor of Philosophy.

George N. Sandor

George N. Sandor
Research Professor of
Mechanical Engineering

I certify that I have read this study and that in my opinion it conforms to acceptable standards of scholarly presentation and is fully adequate, in scope and quality, as a dissertation for the degree of Doctor of Philosophy.

Rodney R. Million

Rodney R. Million
Professor of Radiology

This dissertation was submitted to the Graduate Faculty of the College of Engineering and to the Graduate School and was accepted as partial fulfillment of the requirements for the degree of Doctor of Philosophy.

August 1990

W S Shafer

~~Winfred M. Phillips~~
Dean, College of Engineering

Madelyn M. Lockhart
Dean, Graduate School